Active, phoretic motion

Von der Fakultät Mathematik und Physik der Universität Stuttgart
zur Erlangung der Würde eines Doktors der

Naturwissenschaften (Dr. rer. nat.) genehmigte Abhandlung

Vorgelegt von
Benedikt C. Sabaß
aus
München

Hauptberichter: Prof. Dr. Udo Seifert
Mitberichter: Prof. Dr. Christian Holm

Tag der mündlichen Prüfung: 01.08.2012

II. Institut für Theoretische Physik der Universität Stuttgart
2012

Contents

List of important symbols

Dimensional variables carry a tilde ($\sim$) throughout the thesis. Nondimensional variables and constants carry no tilde.

α	Chemical reaction rates
a	Radius of fluid constituents
b	Hydrodynamic slip length
c_i	Molecular concentration of i-type fluid constituents
c_i^∞	Concentration of i-type molecules at the outer periphery of the boundary layer
$\mathcal{C}_\mathrm{i}$	Concentration scale for ionic solutes in Chap. 2
$\mathcal{C}$	Concentration scale for nonionic solutes in Chap. 3
δ	Relative bulk concentration of free protons and salt ions in Chap. 2
D	Diffusion constant of solutes
D_S	Diffusion constant of the swimming particle
D_rot	Rotational diffusion constant of the swimming particle
$\mathbf{D}_{mn}$	Diffusion matrix
ϵ	Overall efficiency
ϵ_h	Hydrodynamic efficiency
ϵ_h^*	Hydrodynamic efficiency at maximum power
ϵ_i	Internal chemical energy of i-type molecules
ε	Absolute electric permittivity of the solution
η	Viscosity of the Newtonian fluid
$\mathbf{E}$	Hydrodynamic strain rate tensor
$\mathbf{F}$	Force acting on the swimming particle
$\mathbf{F}_\mathrm{m}$	Externally applied force acting on the swimming particle
$\mathbf{j}_i$	Flux of molecules of type i relative to the center of mass
$\mathbf{j}_\Theta$	Flux of entropy relative to the center of mass
$\mathbf{j}_\mathrm{q}$	Heat flux
$\mathbf{J}_i$	Flux of molecules of type i
kT	Thermal energy scale at room temperature
k, κ	Reaction rate constants
K_m	Unnormalized moments of excess solute concentration; see Eq. (1.46)
λ	Dimensionless lengthscale of the solute-swimmer interaction
λ_s	Dimensionless thickness of the Stern layer
L	Lengthscale of the solute-swimmer interaction potential

L_{D}	Dissipation length
L_{ik}	Phenomenological constants
μ_i	Chemical potential of molecules of type i
m_i	Mass of molecules of type i
ϖ	Nondimensional surface reaction rate
ψ	Solute-swimmer interaction potential
Ψ	Equilibrium solute-swimmer interaction potential
ϕ	Electric potential
$\Delta\phi_s$	Voltage change across the Stern layer
$\delta\dot{Q}$	Heat exchange rate of a closed system
p	Hydrodynamic pressure
p_{H}	Hydrostatic pressure
P_{in}	Power consumed by the external apparatus
$P_{\mathrm{h,in}}$	Overall hydrodynamic dissipation rate
P_{out}	Power output of the system
Pe	Peclét number
ρ	Local mass density
r	Radial distance from the center of the swimming particle
R	Radius of the swimming particle
$\mathbf{r}$	Spatial coordinate; origin is at the center of the swimming particle
σ	Hydrodynamic stress tensor
s	Local entropy density
S	Stream function
θ	Polar angle in the spherical coordinate system fixed at the center of the swimmer
Θ	Local entropy production rate
τ_{rot}	Timescale of the particle's rotational diffusion
τ_{h}	Timescale of hydrodynamic fluctuations
$\mathbf{T}$	Hydrodynamic resistance tensor of translation
$\mathbf{u}$	Local fluid velocity
$\mathbf{u}_{\mathrm{S}}$	"Slip" velocity at outer periphery of the hydrodynamic boundary layer
$\mathbf{U}$	Velocity of the swimming particle
$\mathcal{U}$	Velocity scale of hydrodynamic flow and particle speed
v_i	Molecular volume of molecules of type i
V	Electric potential a the surface of the swimming particle
ξ	Relative equilibrium concentration perturbation in Chap. 3
$\tilde{\Xi}$	Legendre transform of divergence of $\mathbf{u}_{\mathrm{S}}$; see Eq. (1.47)
y	Stretched radial variable in the hydrodynamic boundary layer
Ze	Single unit charge ($Z = 1$)

Zusammenfassung

In der vorliegenden, theoretischen Arbeit werden verschiedene Facetten einer von Konzentrationsgradienten getriebenen Bewegung untersucht. Befinden sich die Mikro- oder Nanopartikel in einer nichtionischen Lösung, so spricht man von Diffusiophorese. Von Konzentrationsgradienten getriebenes Schwimmen in ionischen Lösungen wird Chemiphorese oder auch Elektrophorese genannt, wenn ein elektrisches Feld zur Bewegung beiträgt. Wegweisende Arbeiten zu diesen phoretischen Effekten wurden schon von Smoluchowsky [117] und Derjaguin [34] publiziert. Es ist hingegen ein recht neues Konzept, den Konzentrationsgradienten von aktiven Partikeln selbst erzeugen zu lassen. Dabei katalysieren die Partikel zumeist eine chemische Reaktion asymmetrisch an ihrer Oberfläche. Die Herstellung dieser Schwimmer ist seit einigen Jahren, in verschiedener Form, im Labor möglich. Deshalb werden sie zur Zeit intensiv von experimenteller und theoretischer Seite her untersucht. Man verfügt mit ihnen über ein künstliches Modellsystem zur Erforschung von Nichtgleichgewichtsphänomenen im Mikrobereich. Die Größenordung der Schwimmer ist vergleichbar mit der von biologischen Zellen. Daher liegt auch eine Wechselwirkung mit der mikrobiologischen Forschung auf der Hand. Des Weiteren erhofft man sich auch technische Anwendungen. Beispielsweise ließen sich Suspensionen von Mikroschwimmern zur Veränderung der effektiven Viskosität einer zähen Flüssigkeit einsetzen.
Diese Arbeit soll durch eine verbesserte theoretische Beschreibung zum Verständnis der aktiven, phoretischen Fortbewegung beitragen. Darüber hinaus werden hier auch energetische Aspekte zum ersten Mal eingehend untersucht.

Kapitel 1: Einführung und theoretisches Grundgerüst.– Nach einer kurzen Vorstellung der wichtigsten experimentellen Befunde werden im ersten Kapitel die der Arbeit zugrunde liegenden theoretische Konzepte erläutert. Phoretische Effekte werden auf einer mittleren Zeitskala betrachtet, auf der ein stationärer Zustand eintritt. Auf sehr kurzer Zeitskala treten Fluktuationen in den Vordergrund. Die Hydrodynamik und die Stofftransporte in der Umgebung des Partikels werden durch eine mesoskopische, grobkörnige Beschreibung dargestellt. Dabei beschränken wir uns von vorne herein auf stark verdünnte Lösungen. Diese Annahme erlaubt es, nur lokale Mittelwerte zu betrachten und ortsunabhängige Diffusionskonstanten und Viskositäten zu verwenden. Es ergeben sich Diffusionsgleichungen, welche auch die Wechselwirkungen der gelösten Stoffe mit dem Schwimmer berücksichtigen. Der hydrodynamische Fluß wird durch die stokessche Gleichung beschrieben. Im Rahmen der grobkörnigen Beschreibung entsteht durch die Wechselwirkung von Konzentrationsgradienten mit dem Schwimmer eine Volumenkraft, welche für eine Bewegung der Flüssigkeit sorgt. Aus der Kenntnis der Konzentrationen lässt sich also die Geschwindigkeit des Schwimmers berechnen. Allerdings lassen sich die Diffusionsgleichungen mit Wechselwirkungspotential in drei Dimensionen zumeist nicht analytisch lösen. Hier muss auf Störungsrechnung zurückgegriffen werden. Häufig existiert eine Skalenseparation zwischen Transportprozessen auf der Längenskala der Partikelgröße R und auf der Längenskala L der Wechselwirkung mit den gelösten Stoffen. Diese Separation ermöglicht die Verwendung einer etablierten Grenzschichttheorie. Für $L \ll R$ entkoppeln die räumlichen Komponenten der Transportgleichungen nahe der Oberfläche des Partikels. Die effektiv eindimensionalen Gleichungen lassen sich analytisch lösen. In größerer Entfernung vom Partikel lassen sich die Transportgleichungen ebenfalls analytisch lösen, da hier die Wechselwirkung keine Rolle mehr spielt. Die Balance der Kräfte am Schwimmer, und damit auch seine Geschwindigkeit U, ist durch das hydrodynamische Fernfeld festgelegt. U ist proportional zu L^2, also stark von der Reichweite der Wechselwirkung abhängig. Auch mit der Grenzschichttheorie lassen sich zumeist nur dann analytische Lösungen finden, wenn die Grundgleichungen für kleine Störungen eines gegebenen Zustandes linearisiert wurden.

Kapitel 2: Elektrophoretische Bewegung.– Hier widmen wir uns einem Modell für die Bewegung von elektrokatalytisch aktiven Partikeln. Letztere sind etwa einen Mikrometer lang und bestehen in beiden Hälften aus unterschiedlichen Metallen. Die Partikel werden in eine Wasserstoffperoxidlösung gebracht. Eine Dissoziation der Reagenzie an den Partikeloberflächen führt zur Bewegung. Es wird angenommen, dass die Bewegung von elektrophoretischer Natur ist. Durch Redoxreaktionen auf den unterschiedlichen Metallen entsteht ein elektrischer Strom durch das Partikel. Dieser wird durch einen Kationenfluß in

der Lösung kompensiert. Somit entsteht auch ein hydrodynamischen Fluß, der das Partikel antreibt. Für bimetallische Schwimmer sind verhältnismäßig viele experimentelle Daten zugänglich [90, 130]. Daher bietet sich hier die Validierung eines Modells des phoretischen Schwimmens anhand experimenteller Befunde an. Dies setzt jedoch eine vollständige Beschreibung aller Prozesse, inklusive der chemischen Reaktion, voraus. Bisherige Arbeiten [119, 79, 134] sind im Hinblick auf die Modellierung der Reaktion unvollständig oder liefern mit dem Experiment unverträgliche Vorhersagen [78]. Auch Adsorbtion von Salzionen auf der Oberfläche der Schwimmer wurde bisher nicht untersucht. Die hier vorgestellte Arbeit schließt diese Lücken.

Beim betrachteten Modell liegt eine geringe Konzentration von Elektrolyten in der Lösung vor. Das elektrische Feld wird aus der Poisson-Bolzmann Gleichung bestimmt. Dabei wird adsorbierten Ionen auf der Oberfläche des Partikels durch eine sternsche Schicht Rechnung getragen. Die sternsche Schicht verändert die Randbedingungen und damit das elektrische Potential des Partikels. Der Redoxprozess an der Oberfläche wird durch eine Ratengleichung des Butler-Volmer Typs beschrieben. Die Konzentrationen von Wasserstoffperoxid und verfügbaren Protonen gehen linear in die Reaktionsrate ein. Der Einfluss der sternschen Schicht auf den Ladungstransport wird phänomenologisch durch eine Korrektur der Ratenkonstanten beschrieben. Die elektrostatische Abschirmlänge in der Lösung ist viel geringer als der Radius des schwimmenden Partikels. Somit ist eine Grenzschichttheorie anwendbar. Das Rechenverfahren ergibt sich aus einer Verallgemeinerung der im ersten Kapitel vorgestellten Theorie. Im betrachteten Fall, fern des Gleichgewichtes, liefert die klassische Grenzschichttheorie keine analytische Lösung. Sie kann jedoch trotzdem zur Vereinfachung des Gleichungssystems verwendet werden und stellt einen ganz beträchtlichen Gewinn für die Lösung des Zwei-Skalen-Problems dar. Nahe der Oberfläche erhält man, wie zuvor, eindimensionale Transportgleichungen, welche analytisch lösbar sind. Außerhalb des elektrostatisch abgeschirmten Bereichs um das Partikel sind die Konzentrationen nun durch einen Satz numerisch gelöster, nichtlinearer Differentialgleichungen vorgegeben. Die Geschwindigkeit ergibt sich schließlich durch eine einfache Formel aus den numerischen Ergebnissen für die Konzentrationen und das Potential. Für die Numerik wird ein pseudospektrales Verfahren zusammen mit einer Newton-Raphson Iteration verwendet. Neben der numerischen Lösung wird auch eine analytische Näherung für die Geschwindigkeit hergeleitet. Sie gilt für den Fall, dass der Unterschied in den Redoxpotentialen der beiden Metalle klein ist. Somit kann die relative Variation der Ratenkonstanten als Entwicklungsparameter verwendet werden. Mit dieser Näherung wird also angenommen, dass das Wasserstoffperoxid überwiegend gleichmäßig auf der Oberfläche des Schwimmers zersetzt wird, ohne zu einem elektrischen Strom zu führen.
Eine weitestmögliche Anpassung der Konstanten des Modells an experimentell zugängliche

Werte liefert Geschwindigkeiten, welche den gemessenen ähnlich sind. Anfänglich steigt die Geschwindigkeit linear mit der Wasserstoffperoxidkonzentration an. In einer Flüssigkeit mit einem neutralen pH-Wert limitiert die Diffusion von Protonen von der Anode zur Kathode die Reaktionsrate. Dies führt im Modell zu einer Abflachung der Kurve von Geschwindigkeit vs. Wasserstoffperoxidkonzentration. Dieser Effekt wird in sauren Lösungen durch die größere Verfügbarkeit von freien Protonen unterdrückt. Da Wasserstoffperoxid durch seine natürliche Dissoziation den pH-Wert senkt, ist die Abflachung der Geschwindigkeit also nur bedingt beobachtbar. Das elektrische Potential des Metallpartikels wird durch die Ladungserhaltung im stationären Zustand bestimmt. In früheren theoretischen und experimentellen Arbeiten [79, 89] wurde zumeist angenommen, dass das Potential auf dem Partikel in Gegenwart von Wasserstoffperoxid dem Gleichgewichtspotential in einer ionischen Lösung entspricht. Im hier betrachteten Modell ist dies nicht der Fall. Das elektrische Potential auf Metall in Wasserstoffperoxidlösungen unterscheidet sich deutlich vom Gleichgewichtspotential.
Im einfachen Grenzschichtmodell für passive Elektrophorese skaliert die Geschwindigkeit wie das Inverse der Ionenkonzentration. Bei aktiver, phoretische Bewegung beeinflusst die Ionenkonzentration jedoch auch die Reaktionsrate. Durch die Verwendung von Raten des Butler-Volmer Typs spielt im vorliegenden Modell insbesondere die sternsche Schicht eine Rolle. Im Ergebnis skaliert die Geschwindigkeit nicht mehr genau wie eins durch die Ionenkonzentration. Eine Abweichung von der einfachen Grenzschichttheorie wurde auch im Experiment in qualitativer Form beobachtet [89].

Kapitel 3: Diffusiophoretische Bewegung.– Hier wird ein stark idealisiertes Modell für aktives, phoretisches Schwimmen in elektrisch neutralen Lösungen betrachtet. Solch ein Modell lässt sich wohl am ehesten auf die von Howse und Koautoren [54] experimentell untersuchten Kunststoffpartikel in einer Wasserstoffperoxidlösung anwenden. Die Partikel sind auf einer Hälfte mit Platin bedampft und katalysieren dort die Dissoziation des Wasserstoffperoxids. Da die Partikel elektrische Nichtleiter sind, spielen elektrophoretische Effekte wohl keine Rolle. Diffusiophoretische Bewegung basiert hier etwa auf einer van der Waals Wechselwirkung mit dem entstehenden Sauerstoff. Mit einem vorgegebenen, radialsymmetrischen Wechselwirkungpotential ist die Modellierung einfacher als im elektrokatalyischen Fall, denn hier muss keine Poisson-Bolzmann Gleichung gelöst werden. In analytischen Arbeiten zur aktiven Diffusiophorese wird bisher nur die Grenzschichtteorie niedrigster Ordnung in der Reichweite des Potentials betrachtet. Außerdem wird zumeist angenommen, dass die Reaktionsrate von der lokalen Konzentration der Reaktanden unabhängig ist [47, 12]. Das hier vorgestellte Modell dient einerseits dazu, Korrekturen der einfachen Grenzschichtmodelle zu berechnen und soll andererseits als Basis für Betrach-

tungen der Energetik in Folgekapiteln dienen.

Wir modellieren eine inhomogen ablaufende Oberflächenreaktion der Form $a \leftrightarrow b$. Die Moleküle der Sorte a und b liegen stark verdünnt vor. Moleküle der Sorte b wechselwirken mit dem Schwimmer durch ein Potential mit der Reichweite L. Die chemischen Potentiale der Reaktanden werden am Rand des Systems festgelegt, welcher vom Schwimmer unendlich weit entfernt ist. Alle Gleichungen werden systematisch für kleine Abweichungen vom Gleichgewicht linearisiert. Die Transportgleichungen beinhalten so eine näherungsweise Beschreibung der Konvektion von gelösten Stoffen im hydrodynamischen Fluss.
Zunächst wird angenommen, dass Edukte der Reaktion im Überschuss vorhanden sind, so dass die Diffusion der Reaktanden für die Reaktionsrate keine Rolle spielt. Dann entspricht die Emissionsrate von Produkten nur der lokalen, katalytischen Aktivität der Oberfläche. Die einfache Grenzschichttheorie aus Kapitel 1 wird durch eine systematische Entwicklung für $L/R \ll 1$ untermauert und Korrekturen zur Geschwindigkeit berechnet. Korrekturen höherer Ordnung in L/R zeigen sich vor allem bei Wechselwirkungspotentialen sinnvoll, deren Betrag größer als die thermische Energie bei Raumtemperatur kT ist. Von besonderem Interesse ist darüber hinaus ein Korrekturterm, welcher direkt aus der chemischen Umwandlung der Moleküle an der Oberfläche folgt. Bei einem überwiegend repulsiven Wechselwirkungspotential erhöht diese Korrektur die Geschwindigkeit. Zum Vergleich wird die Geschwindigkeit auch numerisch für beliebige Reichweiten der Wechselwirkung ermittelt.
Als Nächstes wird die Oberflächenreaktion durch eine Ratengleichung erster Ordnung beschrieben. Sowohl die Hinreaktion, als auch die Rückreaktion hängen von der Konzentration der gelösten Stoffe an der Oberfläche des Partikels ab. Somit koppelt die Reaktionsrate verschiedene räumliche Momente der Konzentrationsverteilungen. Die Felder werden mit einer Reihendarstellung in Legendre Polynomen berechnet. Es ergibt sich ein rekursives System für die Koeffizienten der Reihe, welches näherungsweise gelöst werden kann. Dieses Vorgehen ist im Rahmen der Grenzschichttheorie ebenso wie für den allgemeinen Fall möglich. Die Geschwindigkeit wird analytisch in niedrigster Ordnung der Grenzschichttheorie und numerisch für beliebige Werte von L/R berechnet. Es zeigt sich, dass die Kopplung der räumlichen Momente der Konzentrationsverteilung eine erhebliche Reduktion der Geschwindigkeit zur Folge haben kann.

Kapitel 4: Irreversible Thermodynamik.– In diesem kurzen Kapitel wird ein knapper Abriss eines etablierten Formalismus für die Thermodynamik nahe beim Gleichgewicht gegeben. Anschliessend wird erklärt, wie diese Theorie des lokalen Gleichgewichtes zur Beschreibung der Energetik von aktiver Diffusiophorese verwendet werden kann. Abweichend von der klassischen Thermodynamik wird keine Ungleichung für die Entropieän-

derung aufgestellt, sondern die Entropieänderung wird direkt aus einem mesoskopischen Modell berechnet und mit dem ersten Hauptsatz verknüpft. In die Formel für die lokale Entropieproduktion gehen grobkörnig gemittelte Flüsse und thermodynamische Kräfte ein. Es wird auch ein Entropiefluß definiert und eine entsprechende Erhaltungsgleichung formuliert. Daran anknüpfend lässt sich für ein System ohne Teilchenaustausch mit der Umwelt ein Wärmestrom definieren. Für eine energetische Betrachtung des diffusiophoretischen Schwimmens soll zunächst der gesamte Energiedurchsatz des Systems ermittelt werden. Zur Erhaltung des stationären Zustandes, werden am Rand des Systems laufend Moleküle ausgetauscht. Damit ist jedoch im Rahmen des verwendeten Formalismus kein Wärmestrom definierbar und also auch keine Energiebilanz möglich. Als Ausweg wird ein zusätzlicher Apparat angenommen, welcher Moleküle durch einen reversiblen Prozess ineinander umwandelt und dafür nur Energie aufnimmt. Dieser Apparat sorgt nun für konstante chemische Potentiale am Rand des Systems. Die Gesamtheit aus System und Apparat tauscht keine Teilchen mit der Umwelt aus, womit die Energiebilanz berechenbar wird. Die dargestellte Hilfskonstruktion zeigt, dass die Entropieproduktion der Diffusion der Moleküle an der Energiebilanz des Systems teilhat. Dies ist zunächst erstaunlich, weil statistisch diffundierende Moleküle im thermischen Gleichgewicht mit der Lösung sind und im Mittel keine Energie dissipieren. Jedoch findet der eigentliche Energieverlust hier im externen Apparat statt.

Kapitel 5: Effizienz von Diffusiophorese.– Hier wird die Effizienz der aktiven, diffusiophoretischen Bewegung eines freien Teilchens berechnet. Dabei wird auf das Modell aus Kapitel 3 zurückgegriffen. Die Effizienz is definiert als Quotient aus der Leistung beim Ziehen eines passiven Partikels in Wasser und dem Leistungsaufwand für das aktive Schwimmen mit derselben Geschwindigkeit. Die vom System aufgenommene Leistung wird mit dem Formalismus aus Kap. 4 berechnet. Für das betrachtete Fluid aus Molekülen mit ähnlichen Massen und Volumina wird gezeigt, dass die Leistungsaufnahme des externen Apparates gleich der Rate der vom System aufgenommenen freien Energie ist. Die Berechnung dieser Größe setzt die vollständige Beschreibung aller Prozesse im System voraus. Hydrodynamische Dissipation kann dabei als Folge der Konvektion gelöster Stoffe im Potentialgradienten interpretiert werden. Daher führt eine Vernachlässigung der Konvektion zu einem energetisch unvollständigen Bild des autonomen Schwimmens. Im Fall von Mikroschwimmern mit $L \ll R$ lässt sich die Effizienz näherungsweise analytisch berechnen. Bei Nanoschwimmern mit $L \gtrsim R$ werden numerische Berechnungen angestellt. Dabei verwenden wir, wie zuvor, für kleine Abweichungen vom Gleichgewicht linearisierte Gleichungen. Daher ist die Effizienz nicht direkt von der treibenden Kraft, der Differenz der chemischen Potentiale am äußeren Rand des Systems, abhängig.

Die Effizienz skaliert mit dem Produkt dreier dimensionsloser Größen. Der erste Beitrag ist ein Quotient aus dem Wechselwirkungsreichweite L und dem Radius des Schwimmers R. Für Mikroschwimmer bedeutet dieser Faktor eine Beschränkung der Effizienz auf weniger als $\sim 10^{-3}$. Der zweite Beitrag ist die Diffusionskonstante des Schwimmers geteilt durch die Diffusionskonstante der gelösten Moleküle. Dies reduziert die Effizienz auf jeden Fall um einen Faktor $\lesssim 10^{-3}$. Der dritte Beitrag ist eine typische Konzentration der gelösten Stoffe im Volumen L^3. Dieser Faktor legt nahe, dass die Effizienz mit der absoluten Konzentration von gelösten Stoffen zunimmt. Insgesamt ergeben sich maximal mögliche Effizienzen von $\sim 10^{-3}$ im Fall von Nanoschwimmern. Typische Effizienzen von Mikroschwimmern liegen jedoch weit darunter, bei $\sim 10^{-9}$. Für ein verschwindendes Wechselwirkungspotential wird die Effizienz null, da der Schwimmer sich nicht bewegt. Für anziehende, wie auch für abstoßende Potentiale existiert jeweils ein Maximum der Effizienz. Auch die Abhängigkeit der Effizienz von den Ratenkonstanten ist nicht monoton.

Kapitel 6: Obere Grenzen für die Effizienz.– Hier werden allgemeine, über die Analyse eines detaillierten Modells hinaus gehende Überlegungen zur Energetik von kleinen Schwimmern dargestellt. Ein wichtiges Konzept ist dabei die hydrodynamische Effizienz, bei deren Berechnung von den Details der Dissipation im Antriebsmechanismus abgesehen wird. Lediglich der Energieverlust in der Hydrodynamik wird betrachtet. Die hydrodynamisch dissipierte Energie ist geringer als der gesamte Energieverlust. Damit stellt die hydrodynamische Effizienz eine obere Schranke für die Gesamteffizienz dar. Das Konzept lässt sich sowohl auf phoretische Fortbewegung wie auch zum Beispiel auf das autonome Schwimmen von Mikroorganismen mit Zilien anwenden.
Wir betrachten den Fall, in dem eine äußere Kraft auf den Mikroschwimmer wirkt. Die hydrodynamische Effizienz setzt die gegen die Kraft geleistete Arbeit zu der gesamten hydrodynamischen Arbeit ins Verhältnis. Um die Abhängigkeit dieser Größe von der externen Kraft zu eliminieren wird die Effizienz bei maximaler Leistung betrachtet. Für die überdämpfte Bewegung eines beliebigen Schwimmers wird gezeigt, dass die hydrodynamische Effizienz bei maximaler Leistung kleiner als $1/2$ ist. Dies ist eine direkte Konsequenz der Linearität der Gleichung von Stokes.
Wird das Fluid in einer dünnen Schicht nahe der Oberfläche des Schwimmers angetrieben, so entsteht in der Grenzschicht ein starker Geschwindigkeitsgradient mit naturgemäß großer Dissipation. Die hydrodynamische Effizienz skaliert nun mit der Dicke der Grenzschicht geteilt durch den Partikelradius R. Dieser limitierender Faktor für die Effizienz wurde auch im Modell von Kapitel 5 identifiziert. Nun ist klar, dass er von der Hydrodynamik in der Grenzschicht herrührt und eine modellunabhängige, obere Schranke für die Effizienz darstellt.

Um die Skalenargumente zu konkretisieren wird beispielhaft die hydrodynamische Effizienz von passiver Bewegung in extern angelegten Konzentrationsgradienten betrachtet. Ionische und nichtionische Lösungen werden dabei gemeinsam behandelt. Zunächst wird die Grenzschichttheorie herangezogen. Es stellt sich heraus, dass die Längenskala der hydrodynamischen Dissipation nur für sehr spezielle, einfache Modelle genau der Reichweite des Oberflächenpotentials L entspricht. Die aus der Grenzschichttheorie berechnete, hydrodynamische Effizienz erlaubt jedoch die Definition einer neuen Längenskala die $\sim L$ ist. Damit ist die einfache Skalenabschätzung gültig.
Als Nächstes werden die hydrodynamischen Effizienzen numerisch berechnet. Im Fall von Diffusiophorese in nichtionischen Lösungen beschränkt sich hier der Aufwand auf die Lösung von separablen Differentialgleichungen. Die Differentialgleichungen für Felder in ionische Lösungen werden in Potenzen der Oberflächenladung des Partikels entwickelt. So entsteht eine "Debye-Hückel" Theorie, die semi-analytisch zugänglich ist [63]. Für ionische und nichtionische Systeme ergeben sich qualitativ übereinstimmende Ergebnisse bezüglich der hydrodynamischen Effizienz bei maximaler Leistung. Bei Mikropartikeln ist die Effizienz verschwindend gering. Bei Nanopartikeln, mit $L > R$, erreicht die hydrodynamischen Effizienz bei maximaler Leistung nahezu ihr Optimum von $1/2$. Phoretische Bewegung von Nanopartikeln ist also viel effizienter als die von Mikropartikeln.
Bei einer Anwendung autonomer Schwimmer für den gerichteten Transport ist nicht nur die Rate der Energiedissipation wichtig. Interessant ist auch wie viel Energie pro Transportvorgang dissipiert wird. Letztere Größe ergibt sich aufgrund der Mischung aus gerichteter und diffusiver Bewegung des Schwimmers nicht direkt aus der Rate der Energiedissipation. Dies verlangt nach einer neuen Größe, die wir Transporteffizienz nennen. Die Transporteffizienz ist der Quotient aus der Energiedissipation beim gerichteten Transport eines passiven Teilchens und der Energiemenge, die beim aktiven Transport durch einen Schwimmer verbraucht wird. Bei einem Transportweg, der viel größer als eine typische Persistenzlänge der Bewegung des Partikels ist, ergibt sich eine einfache Formel für die Transporteffizienz. Diese ist dann proportional zu einer Persistenzlänge geteilt durch die Länge des Transportweges. Die Transporteffizienz ist nochmals kleiner als die in den vorigen Kapiteln studierte Effizienz des Schwimmens. Sehr allgemein stellt die geringe Transporteffizienz eine inhärente Schwäche des ungerichteten, aktiven Transports auf der Mikroskala dar.

Summary

This work is dedicated to different aspects of the motion of micro- and nanoparticles that are driven by interaction with a concentration gradient. The swimming of particles in a solution is called diffusiophoresis if it results from the interaction with nonionic solvent gradients. Motion driven by ionic concentration gradients is called electrophoresis or chemiphoresis, depending on whether or not an electric field moves the particle. Theoretical investigation of electrophoresis and diffusiophoresis have their origin in seminal works of Smoluchowsky [117] and Derjaguin [34]. Recently, the concept of active phoresis has emerged. The new idea is here that the swimming particle produces the concentration gradient by itself. In corresponding experiments, the particle mostly catalyzes a chemical reaction in an asymmetric way on its surface. Various realizations of such systems have been explored experimentally during the last years. These swimmers are a unique model system for the investigation of microscale non-equilibrium phenomena. Also, the size of phoretic swimmers is comparable to the size of bacteria, which makes them an attractive subject of biophysical and biological research. Finally, there also is hope for technological applications. A most prominent example is here the control of the effective viscosity by microswimmers in complex mixtures.

For the above reasons, the theoretical investigation of active phoresis is a very timely subject. The aim of the thesis is to contribute to an improved understanding of active, phoretic motion. In particular energetic aspects of this type of swimming are investigated for the first time.

Chapter 1: Introduction to active, phoretic transport.– Following a brief discussion of important experimental findings, we explain here the theoretical concepts that constitute the foundation of this work. We focus on a steady-state description of swimming for timescales where the fluctuations in the system average out. The multicomponent fluid around the swimmer is modeled on a coarse-grained, hydrodynamic level. The fluid is to be a very dilute solution. Solutes and solvent interact differently with the swimming particle. These assumptions result in standard diffusion equations for the solutes. The hydrodynamic flow is described with the Stokes equation. Within the coarse grained model, the concentration gradients lead to a body force that drives fluid flow. The flow, in turn, results in motion of the swimmer. The knowledge of the concentration field therefore allows for the computation of the swimming speed. However, the three-dimensional diffusion equations cannot be solved analytically and perturbation techniques are called for. Frequently, we have a scale separation between transport processes on a lengthscale of the size of the swimmer R and processes near the swimmer's surface on the lengthscale of the solute-swimmer interaction L. This scale separation allows to employ an established boundary layer theory for $L \ll R$. Calculation of the swimming speed in the boundary layer theory mostly requires a linearization of the pertaining equations for small deviations from a given state. Near the particle surface, the transport equations become quasi one-dimensional and can be solved analytically. The transport equations outside the range of the solute-swimmer interactions can also be solved analytically. The boundary layer theory predicts that the swimming speed U is proportional to L^2.

Chapter 2: Self-electrophoretic motion.– We model here the phoretic motion of electrocatalytically active particles. These are about one micrometer long and consist of two different metals that are joined together. The particles are immersed in a hydrogen peroxide solution. Dissociation of the hydrogen peroxide on the surface of the swimmer leads to a directed motion. Most probably, the motion is of electrophoretic nature. Redox reactions on the different metals lead to an electric current through the swimmer. This current is compensated by a flux of cations around the swimmer. The particle moves since the charge imbalance results in hydrodynamic flow around it. A comparably large amount of experimental data is available for these bimetallic swimmers [90, 130]. Therefore, a theoretical model of phoretic motion can be validated here. Such an undertaking demands a complete modeling of all involved processes, including the chemical surface reactions. Currently available models of self-electrophoresis are either incomplete [119, 79, 134] or yield results which are inconsistent with the experimental findings [78]. In this chapter we improve on these shortcomings.

The electric field, calculated from the Poisson-Boltzmann equation, mediates the inter-

action between swimmer and solutes. We assume the presence of a low concentration of electrolytes in the solution around the swimmer. Salt that is adsorbed at the surface of the swimmer is modeled with a Stern layer. A Stern layer modifies the boundary conditions and thereby affects the electric potential of the particle. The redox processes on the surface are modeled by linear rate equations of the Butler-Volmer type. Here, the influence of the Stern layer on the redox reactions is modeled with a phenomenological modification of the rate constants. Surrounding the swimmer, we have a charged, diffuse layer. The Debye screening length, which is a measure for the thickness of the charged layer, is much shorter than the particle Radius R. Therefore, a boundary layer theory can be employed. We extend the theory introduced in the first chapter to cover transport equations which are nonlinear in the fields. In this case, an analytical calculation is no longer possible, but the boundary layer theory still constitutes a considerable simplification of the two-scale problem. Near the surface, the transport equations are one-dimensional and can be solved analytically. The concentrations outside the electrically screened region are determined by numerical solution of coupled differential equations. For this purpose we implement a pseudospectral method in conjunction with a Newton-Raphson iteration. The swimming speed can eventually be calculated with a simple formula from the numerical results. We also derive an analytical approximation for the speed. Here, it is assumed that the relative spatial variation of the reaction rate constants is small. This amounts to a perturbation theory for a steady state where the hydrogen peroxide decomposes homogenously on the surface of the swimmer.

After adjusting the model constants as far as possible to values that are known from the experiment, our theory yields swimming speeds that are similar to the measured results. Initially, the speed increases linearly with the concentration of hydrogen peroxide. We find that the diffusion of cations around the swimmer can limit the reaction rate when the pH value of the solution is neutral. This limitation of the rate leads to a saturation of the swimming speed for hydrogen peroxide concentrations above a certain threshold. However, the excess of available protons in a acidic solution suppresses this effect. A low pH value can result, for example, from the natural dissociation of hydrogen peroxide in the bulk. The electric potential of the metal particle is determined by charge conservation. It has been assumed in previous theoretical and experimental works that the electric potential of the swimmer is similar to its equilibrium potential in water, even in the presence of hydrogen peroxide [134, 89]. Our model demonstrates that this assumption is not valid. The standard boundary layer theory for passive electrophoresis predicts that the speed is proportional to the inverse of the ion concentration. In our model, the ion concentration also affects the reaction rate at the active particle. Furthermore, the voltage drop across the Stern layer depends also on the ion concentrations. As a result, the model

predicts deviations from the standard scaling of the swimming speed. These deviations are qualitatively confirmed by experimental results [89].

Chapter 3: Self-diffusiophoretic motion.– We consider here idealized models of active, diffusiophoretic motion in neutral solutions. This class of models might be used to describe experimentally investigated polysterene microspheres in a hydrogen peroxide solution [54]. The spheres are half-coated with platinum and catalyze the decomposition of hydrogen peroxide. Electrophoretic effects are thought to be negligible since the particles do not conduct electric current. Diffusiophoresis could occur, e.g., through van der Waals interaction with the produced oxygen. We model diffusiophoresis with a prescribed, radially symmetric solute-swimmer interaction potential with lengthscale L. Analytical theories to date only consider the boundary layer theory to lowest order in L/R. Also, it is mostly assumed that the reaction rate is independent of the local concentration of educts and products [47, 12]. We calculate here corrections to the simple boundary layer theory and investigate how the form of the reaction rate influences the swimming speed. Our model also permits us to study the energetics of diffusiophoresis in later chapters.
The solution around the particle contains dilute a- and b-type solutes. The particle inhomogeneously catalyzes a surface reaction of the form $a \leftrightarrow b$. The b-type molecules interact with the swimmer through a potential. The chemical potentials are maintained constant at the outer boundaries of the system that are infinitely far away from the swimmer. All equations are systematically linearized for small deviations from equilibrium. The transport equations incorporate convection of solutes in an approximate way.
We first consider a reaction-limited surface process. Here, the reaction rate is solely determined by the local catalytic activity on the swimmer's surface. We systematically calculate the swimming speed in orders of $L/R \ll 1$. Corrections to the lowest order results are seen to become important when the magnitude of the solute-swimmer interaction potential exceeds the thermal energy. A particularly interesting correction results from the chemical transformation of molecules within the range of the surface potentials. This correction increases the swimming speed for repulsive potentials. We also calculate the swimming speed numerically for arbitrary interaction lengths.
Next, we consider first order rate equations for the surface reaction. The forward and backward reaction are both linear in the local concentrations, which leads to a coupling of different spatial moments of the concentration fields. A series expansion of the fields in Legendre Polynomials furnishes a recursive system of equations for the series coefficients. This system can be solved in an approximative way. We employ this technique within the boundary layer approximation and for the full numerical solution of the transport equations. We find that the explained coupling of the spatial moments of the concentration

field can strongly reduce the swimming speed.

Chapter 4: Linear, irreversible thermodynamics.– This short chapter provides a brief summary of an established formalism for thermodynamics close to equilibrium. The application of the formalism to our phoretic systems is explained. Unlike in classical thermodynamics, a local equilibrium is assumed. Gradients in state variables lead to an entropy production. The entropy production rate is calculated from a coarse-grained mesoscopic model for average fluxes and thermodynamic forces. Also, an entropy flux and a conservation equation for entropy are defined. These quantities allow to calculate the heat exchange of a system with its environment if no particle exchange occurs. However, in order to assess the energetics of active, diffusiophoretic motion, we need to study systems with particle exchange. Particle exchange happens since the steady state is maintained by constant replenishment of reacting molecules at the outer boundaries of the system. We remedy this situation by assuming an ideal external apparatus that transforms the product molecules back into educts. The apparatus works quasi-reversibly. The ensemble of apparatus and system do not exchange particles with the environment. Heat flux and energy consumption can be calculated. The result shows that the diffusion of solute molecules contributes to the overall energy balance. This is somewhat astonishing since the randomly diffusing molecules are in thermal equilibrium with their environment and dissipate no energy. However, the energy is really spent in the external apparatus on maintaining the chemical potential.

Chapter 5: Efficiency of self-diffusiophoretic swimming.– Here we calculate the efficiency of the self-diffusiophoretic swimmer studied in Chap. 3. The efficiency is defined as the power spent on dragging the particle through water divided by the power input that is necessary for phoretic swimming at the same speed. The power input at the diffusiophoretic system is calculated with the formalism presented in Chap. 4. We assume that the constituents of the multi-component fluid have similar molecular masses and volumes. It then follows that the power input of system plus apparatus equals the flux of free energy from the apparatus to the system. Calculation of this quantity requires a complete description of reactions and transport. Particularly the neglect of convection of solutes leads to an incomplete energetic picture.
The efficiency of microswimmers with $L \ll R$ is calculated analytically. We perform numerical calculations for the case of nanoswimmers with $L \gtrsim R$. All equations are linearized for small deviations from equilibrium. Therefore, the efficiency does not directly depend on the driving chemical potential difference that keeps the system out of equilibrium.

The efficiency scales as the product of three dimensionless factors. First, we have the diffusion constant of the swimmer divided by the diffusion constant of the solutes. This quotient generally limits the efficiency to values $\lesssim 10^{-3}$. The second contribution is L/R, the quotient of solute-swimmer interaction length and swimmer radius. This quotient implies for microswimmers a further reduction of the efficiency by a factor $\sim 10^{-3}$. The third factor is a typical concentration of solutes in a volume of L^3. The efficiency therefore should increase with the absolute concentration of solutes. Taken together, we find maximal efficiencies of $\sim 10^{-3}$ for the case of nanoswimmers. We also predict that typical efficiencies for the experimentally investigated microswimmers are $\sim 10^{-9}$. The efficiency tends to zero for vanishing solute-swimmer interactions. Maxima of the efficiency occur for both positive and negative values of the interaction potential. We also demonstrate a nonmonotonous dependence of the efficiency on the rate constants.

Chapter 6: General limits on the efficiency.– This chapter is devoted to general characteristics of the efficiency of small swimmers. In order to go beyond predictions for a detailed model system we employ the concept of hydrodynamic efficiency. For this quantity, only hydrodynamic dissipation is taken into account. The hydrodynamic efficiency is an upper bound for the full efficiency. The concept is general and can be employed not only for phoretic swimming but also, e.g., for biological swimmers.

In the presence of an external force, the swimmer can do work by moving against it. To calculate the hydrodynamic efficiency, we divide this work output by the overall hydrodynamic work. The dependence of our efficiency measure on the external force is eliminated by only considering the hydrodynamic efficiency at maximum power. We show that the hydrodynamic efficiency at maximum power for an arbitrary swimmer in the overdamped regime is always smaller than 1/2. This result is a direct consequence of the linearity of the Stokes equation.

If the fluid motion is driven from within a thin layer on the surface, large dissipation is expected to occur in this boundary layer. The resulting hydrodynamic efficiency scales as the quotient of a thickness L of the boundary layer and the radius R. This factor also appeared in the efficiency of self-diffusiophoresis calculated in Chap. 5. It is now clear that this limitation of the efficiency generally results from the presence of hydrodynamic boundary layers.

To illustrate these results we now consider phoretic motion that is driven by externally applied concentration gradients. We treat the cases of ionic and nonionic solutes together. The boundary layer theory for $L \ll R$ shows that the short lengthscale in the hydrodynamic efficiency in general does not exactly agree with the lengthscale L. However, the magnitude of this new dissipation length is found to be comparable to L. Therefore the

scaling prediction for the hydrodynamic efficiency of microswimmers is satisfied. Next, the hydrodynamic efficiencies are calculated numerically. For the case of diffusiophoresis in nonionic solute gradients, only separable differential equations must be solved. For ionic solutes, we resort to an expansion of the fields in powers of the surface charge density. This approach leads to a Debye-Hückel-like theory which yields semi-analytical solutions. The hydrodynamic efficiency at maximum power is for ionic and nonionic systems qualitatively similar. For nanoswimmers with $L > R$ the hydrodynamic efficiency at maximum power almost attains its optimal value of $1/2$. Phoretic motion of nanoparticles is therefore much more efficient than that of microparticles.

Autonomous microswimmers can be used for the transportation of cargo. Then, the efficiency is not only limited by the rate of energy dissipation. It is also important how much energy is spent for each transport process. This quantity is affected by the randomness of the motion of the swimmer. Therefore, we define a new efficiency measure, termed efficiency of transport. Efficiency of transport is the energy dissipation during directed, passive transportation across a given distance divided by the necessary energy input for the corresponding active transport with a microswimmer. The efficiency of transport is given by a simple formula if the transport distance is much larger than a typical persistence length. Efficiency is now not only limited by the energy dissipation rate but also by the quotient of the persistence length and the transport distance. Therefore, a low efficiency of transport is an inherent weakness of undirected, active transport on the microscale.

Chapter 1

Introduction to active, phoretic transport

The question how it is possible that invisibly small objects can actively move around has puzzled scientists for a long time. Swimming of micrometer-sized biological matter was first demonstrated with the discovery of bacteria by A. van Leewenhoeck (or Leeuwenhoek) around 1680. Using a very basic microscope, he was able to discern actively moving creatures from passive objects in dental plaque. His description of this finding as "very many small living animals, which moved themselves very extravagantly" [72] demonstrates, that active motion was associated with the concept of life. Owing to the rapid advance of microscopy and biochemistry during the last century, many modes of microbiological self-propulsion are now well known. Most notably, these are based on the active motion of even smaller units, namely of flagella or motile cilia [21]. Non-reciprocal shape distortions of the swimmer and lateral streaming of the cell surface have also been discussed [71]. Recently, the quest for a physical understanding of biological micro-motion led to the suggestion of non-living, man-made microswimmers, see e.g. [22, 61, 41, 38]. These can in principle fulfill similar tasks as the biological swimmers. Possible applications of swimmers are, e.g., enhanced mixing of chemicals [65], transportation of micro-cargo [12] and controlling rheological properties of complex fluids [103]. Accordingly, much effort has been spent in recent years to develop artificial self-propellers [38]. Since nanomechanical degrees of freedom are still very hard to control, many models of synthetic swimmers are not driven by mechanical actuation. It is more expedient to employ chemical surface reactions on the swimmers for their propulsion. The predominant opinion is that the physical mechanism underlying this mode of propulsion is of phoretic nature [6]. The following section shall give a brief introduction to this concept.

1.1 Phoretic motion in a nutshell

The ancient Greek suffix "-phoresis" indicates that something is carried or transported. Accordingly, the derived technical term "phoretic motion" refers to a class of transport mechanisms in the domain of colloids. A colloidal particle that is driven by an electric field undergoes electrophoresis. Chemiphoresis means that the particle is carried along by a concentration gradient of ionic solutes. Diffusiophoresis refers to motion that is driven by a nonionic concentration gradient. We do not concern ourselves with motion driven by temperature gradients, but thermophoresis is also mentioned here for completeness.

We briefly focus on diffusiophoresis for illustration of the common physical principle. Picture a micrometer-sized particle immersed in a viscous solution. A concentration gradient of solutes is present. The particle interacts through some distance-dependent force with the solutes and therefore "feels" the concentration imbalance. Since the whole system tries to relax to an equilibrium configuration, the solute molecules and the particle will both start to move. The steady state swimming speed $\tilde{U}$ can be estimated from a simple scaling argument. Let us denote the lengthscale of the solute-particle interaction with L and the particle radius with R. The thermal energy scale is written as kT, η is the viscosity and $\tilde{c}$ is the concentration of solute molecules. The hydrodynamic friction force per volume is proportional to a second spatial derivative of the fluid velocity and we therefore estimate it to be $\sim \eta\tilde{U}/L^2$. The driving force is determined by the gradient of the chemical potential per volume $\sim -kT\nabla\tilde{c}$. The balance of these force estimates yields

$$\tilde{U} \sim -\frac{L^2\, kT}{\eta}\nabla\tilde{c}. \tag{1.1}$$

We have chosen L instead of R as lengthscale in the friction term since the shorter lengthscale dominates in the spatial derivative and we expect $L \ll R$. Conversely, if $L \gg R$, then the dominating lengthscale in the hydrodynamic friction is R. The main message of Eq. (1.1) is that the swimming speed is proportional to the square of the interaction length if $L \ll R$. This scaling is due to the hydrodynamic dissipation and not due to the driving force. It therefore also holds for the other phoretic effects.

The concentration gradient or the electric field can also be generated by the particle itself. Then, we use the terms "self-diffusiophoresis" or "self-electrophoresis". Since the direction of swimming is not fixed in this case, active particles reorient on the timescale of rotational diffusion $\tau_{\mathrm{rot}} = 8\pi\eta R^3/kT$. On timescales much larger than τ_{rot}, swimming of particles merely enhances their diffusion. Self-diffusiophoresis and self-electrophoresis are the mechanisms considered for active motion in this thesis.

1.2 Realizations of autonomous, phoretic swimmers

Active, phoretic motion was originally suggested by Mitchell [77] as a mode of biological self-propulsion. The reported absence of flagella at swimming cyanobacteria [131] led to the speculation that these might be driven by a self-electrophoretic effect. Phoretic swimming of protists and bacteria was investigated theoretically by Anderson [5] and later by Lammert et al. [69]. Self-electrophoresis is in many cases arguably not the mechanism employed by microorganisms since they can mostly swim in the presence of quite high salt concentrations, where the interaction length L becomes negligibly small. Moreover, reported swimming speeds of $\sim 10\,\mu$m/s would require unrealistically high ion currents. For cyanobacteria, the self-electrophoretic mechanism was rejected since it has been found that they do not drift in external electric fields [93].

However, the advance of micro-fabrication techniques in recent year has led to a variety of artificial swimmers whose motion is based on phoretic effects [22, 38]. The employed reactions often involve hydrogen peroxide (H_2O_2) which decomposes on the surface of microparticles. A notable first demonstration of the use of H_2O_2 for micro-propulsion is due to Ismagilov et al. [56]. Millimeter-sized plates with a platinum attachment were placed on the surface of a H_2O_2 solution. It was found that the plates are propelled by the recoil of oxygen bubbles that result from the decomposition of H_2O_2. With a further miniaturization of the swimmers into the μm range, these bubbles are no longer observable and phoretic effects are presumably dominant.

Three-dimensional motion of metallic, micro- and nanoswimmers was first studied in a series of experiments led by Sen and Mallouk [90, 91, 66, 31, 92, 130]. Bimetallic rods (often gold/platinum particles) were immersed in a H_2O_2 solution. The surfaces of the rods catalyze a decomposition of H_2O_2 into oxygen ($O_2\,(g)$) and water. Fig 1.1 shows typical swimming trajectories and a microscopic image of such a swimmer.
It was found that the decomposition of H_2O_2 at the surface of the swimmers occurs at least in two different modes [92, 130]. First, a non-electrochemical decomposition of the form

$$2\,H_2O_2 \rightarrow 2\,H_2O + O_2 \tag{1.2}$$

takes place at the metal surfaces. Second, an electrochemical decomposition has been found for swimmers that are built of a combination of different metals. Different redox potentials of the metals lead to an electric current in the swimmer. The resulting electric field and ion fluxes in the solution cause self-electrophoretic motion of the particle. Fig. 1.2 shows experimental data for the short-time swimming of microswimmers. The swimming speed increases linearly with the concentration of H_2O_2 until it saturates above concentrations of about 5 % wt/v (1 % wt/v corresponds to 10g of H_2O_2 per liter solvent). An

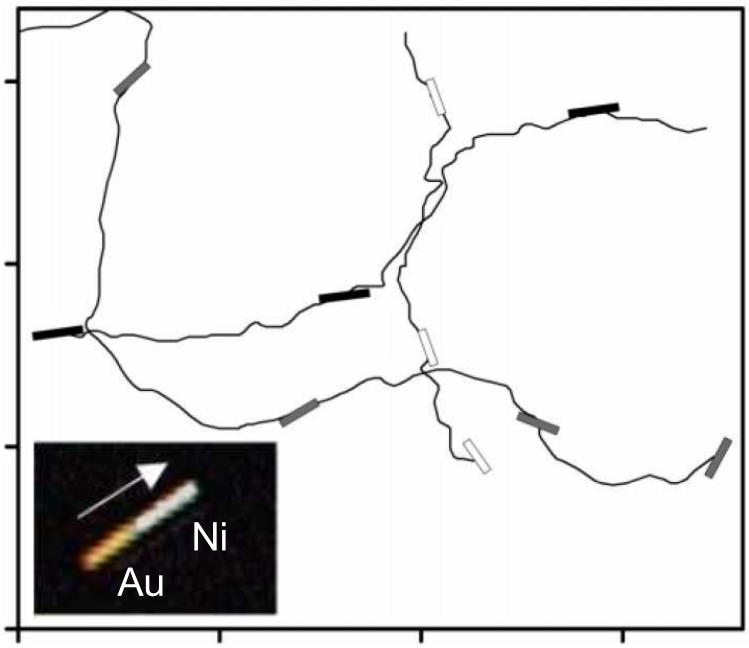

Figure 1.1: Swimming trajectories (5 s) of 2 μm long gold/platinum rods in a 2.5 % wt/v hydrogen peroxide solution. The rods are seen to move in the direction of the platinum end. The inset shows a microscopic image of a gold/nickel swimmer which moves in the direction of the nickel end. Adapted from [90, 130] with permission. Copyright (2004, 2006) American Chemical Society.

interpretation of this saturation can be given in the framework of a Michaelis-Menten like surface kinetics [115]. Wang et al. [130] conducted a comprehensive study using different combinations of metals for bimetallic microswimmers. A clear correlation between the mixed potential differences between the two metals and the swimming speed was found. By choice of optimal materials for the anode, cathode and intermediate part of the swimmer, the speed could be increased to more than 50 μm/s. Addition of exothermically decomposing reagents like Hydrazine (N_2H_4), can even lead to higher speeds [30, 70]. In the long-time average, enhanced diffusive motion is observed in a three dimensional setup [90]. However, the motion of microrods in a Gibbs monolayer was reported to be super-diffusive, Levi-walk-like [31].

A different kind of experiment, with polystyrene spheres instead of metallic rods, was first conducted by Howse et al. [54]. The polystyrene spheres were half coated with platinum as a catalyst and also suspended in an H_2O_2 solution. Fig. 1.3 shows a microscopic recording of a swimming trajectory. Since the spheres are nonconducting, no electric current inside the swimmer is expected here. The fuel decomposes non-electrocatalytically at the platinum-coated side. Fig. 1.4 shows the dependence of swimming speed on H_2O_2. The data was explained with a generic model of diffusiophoresis proposed by Golestanian

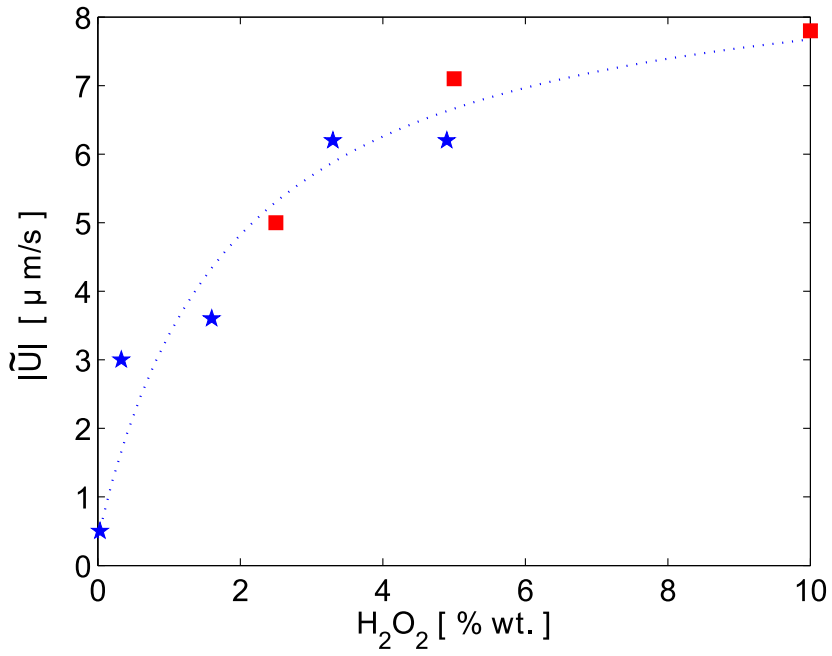

Figure 1.2: Measured swimming speed of 2 μm long gold/platinum rods at different hydrogen peroxide concentrations. (★): data from [91], (■): data from [70], (Dotted line): fit with a rational polynomial of first order.

et al. [47]. An interaction length L was estimated to be about 0.5 nm. The concave shape of the dependence of speed on H_2O_2 concentration was attributed to a Michaelis-Menten-like surface kinetics. A crossover between directed swimming and random diffusion at the timescale of τ_{rot} was confirmed. The rotational diffusion of the swimmers was experimentally analyzed in detail by Ke et al. [62]. An enzyme coating of microswimmers [126] can be used to enhance the reaction rate.

It should be mentioned that the motion of platinum-coated polymer microspheres can also be explained by an emission of so-called nano-bubbles [43, 44]. The latter, however, are not assumed to contribute to a phoretic effect but drive the swimmer through their recoil. Since the bubbles are so small, they may not be resolved under the microscope. A characteristic of bubble propulsion is that motion only occurs towards the non-coated side while phoretic swimming can also occur towards the platinum-coated side. A study by Ebbens and Howse [39] correlated the orientation of the sphere with the direction of motion. The movement was found to occur away from the platinum side of the sphere. This is consistent with both the diffusiophoretic mechanism, and nano-bubble propulsion. Thus, the influence of nano-bubbles on the swimming speed remains somewhat unclear. Pressure waves have also been discussed in the context of autonomous, reaction driven motion [42]. Their contribution to the motion depends on the compressibility of the

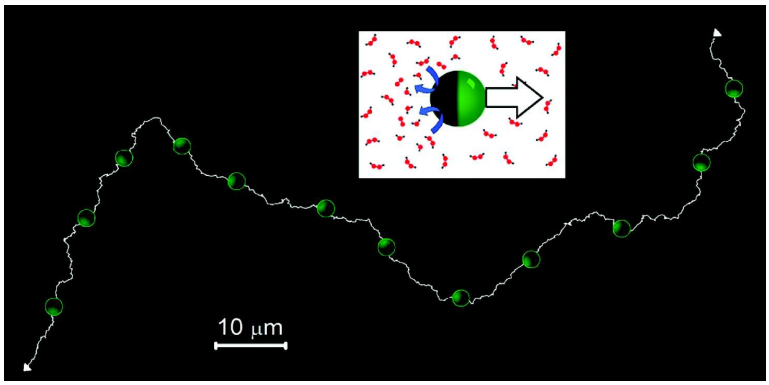

Figure 1.3: Swimming trajectory (45 s) of a green-fluorescent polymer particle in a 5 % vol. hydrogen peroxide solution. The platinum-coated side appears dark. Platinum catalyzes an asymmetric decomposition of hydrogen peroxide. The inset shows the process schematically. Adapted from [39] with permission. Copyright (2011) American Chemical Society.

solvent. Such dynamical effects have not yet found wide appreciation and their importance remains to be experimentally assessed.

The decomposition of H_2O_2 is by no means the only way how swimmers can produce concentration gradients. Mano and Heller [75] have demonstrated the propulsion of microswimmers through asymmetric oxidation and reduction of glucose. A related approach was used to generate H_2O_2 *in situ* from the conversation glucose [87]. The produced H_2O_2 was then directly decomposed by a catalase on the carbon-nanotube swimmer. Finally, thermally induced phase separation of a critical mixture of 2,6 lutidine has also been used to propel microparticles. Heating the particle asymmetrically by a laser leads to strong local concentration gradients and diffusiophoretic swimming [127].

Superficially very similar to diffusiophoresis are propulsion mechanisms based on chemical modification of fluid-fluid interfaces. Examples include asymmetric hydrolyzation [52] or bromination [123] at a droplet surface. The resulting interfacial tension gradient moves the droplet through the so-called Marangoni effect. This motion is however fundamentally different from the phoretic swimming discussed in this thesis. The no-slip boundary condition on solid-fluid interfaces necessitates a very strong velocity gradient near the surface. This gradient is not present at fluid-fluid interfaces. The scaling of the phoretic swimming speed $\tilde{U} \sim L^2$ is replaced by a scaling $\tilde{U} \sim R^2$ for the Marangoni effect [8].

A number of experiments have been carried out in order to demonstrate the practical applicability of microswimmers, some of which are summarized in [85]. Phoretic swimmers can transport other small objects that are chemically bound to them [119, 35, 12]. They can even be employed to to sort and manipulate biological cells if they are functionalized

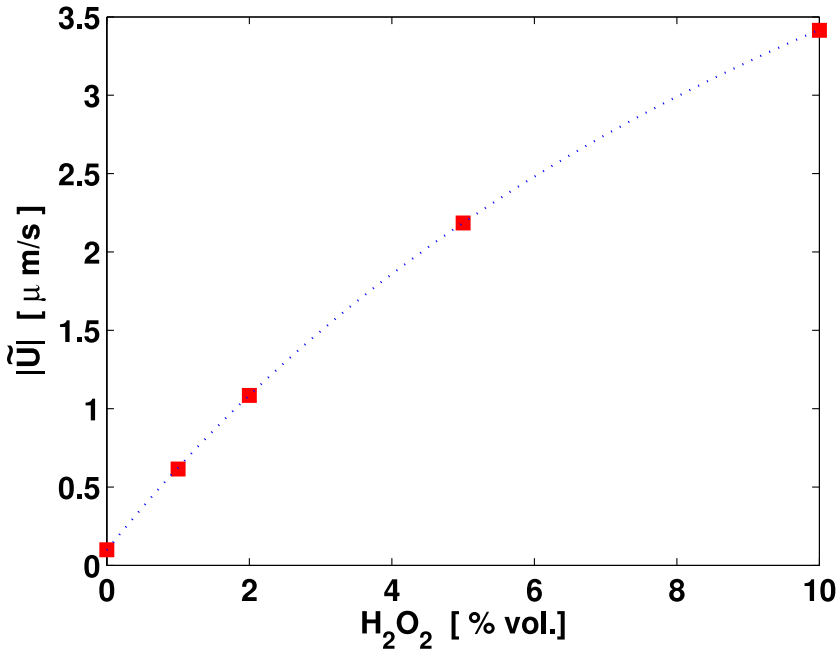

Figure 1.4: Measured swimming speed of platinum-coated polymer particles at different hydrogen peroxide concentrations. (■): data from [54], (Dotted line): fit with a rational polynomial of first order.

with specific receptors [11]. Controlling microswimmers remotely might also be important in this context. Therefore, steering of phoretic transport with externally applied fields has been investigated [66, 36]. Mixing of a solution can be enhanced by diffusiophoresis [2] and possibly also by the motion of microswimmers. Also, active motion of fluid constituents changes the bulk flow behavior [76]. The possibility to tune the effective viscosity of a complex fluid through addition of a chemical fuel may have many applications in the chemical and petrochemical industry. From the point of view of pure research, phoretic microswimmers are a very promising model system to investigate the physical principles of nonequilibrium diffusive motion [46, 86, 104]. A further active field of research are mutual interactions [133, 67, 60, 14] and boundary effects in suspensions with many swimmers [102, 40, 94].

1.3 Previous theoretical work and the aim of this thesis

The theory for electrophoresis of particles with thin charged surface layers, $L \ll R$, dates back to Smoluchowski [117]. Subsequent work put this so-called boundary layer

theory on firm mathematical grounds and extended it (see e.g. [125, 109]). The corresponding theory for diffusiophoretic effects was developed by Derjaguin and Dukhin [34]. Here, the interaction between the solutes and the swimmer is modeled with an effective, phenomenological approach. Anderson and Prieve employed this theory extensively for studies of passive diffusiophoresis in an external gradient [8, 6]. After establishing the basic model equations in Sec. 1.4, we discuss the classic theory of diffusiophoresis in Sec. 1.5. This includes a short calculation of the swimming speed of a diffusiophoretic swimmer. The classic boundary layer theory is the basis for most of our contributions to active, phoretic motion.

Self-electrophoresis.– A major issue for the theoretical explanation of the experimental data on active, phoretic motion is the general lack of knowledge concerning the complex details of the surface decomposition of H_2O_2 on microparticles. In addition, the exact nature of the solute-solute and solute-swimmer interactions is often unknown. The self-electrophoretic swimmers studied by Sen, Mallouk and co-workers [92, 130] are in this respect advantageous since careful experiments have demonstrated the electrokinetic mechanism at work here. A few previous theoretical studies have been conducted in order to understand self-electrophoresis quantitatively. Sundararajan et al. [119] compared experimental data with results from a numerical solution of hydrodynamic equations where the rate of cation exchange was fixed. Yariv [134] conducted a throughout study of the case of a thin diffuse layer of charges surrounding the particle ($L \to 0$). His theory includes surface reaction kinetics explicitly. Although the framework is in principle complete, it leaves a number of effective parameters and is limited to the linear response regime. Moran and Posner [79] investigated a full numerical model for rather thick, diffuse layers of ions around the swimmer ($L \sim R$). Most recently, they included a surface reaction which was second order in H^+ concentration[78]. This provided a closed, quantitative model which could be directly compared to experimental data. However, the results indicated a quadratic increase of the swimming speed with the concentration of H_2O_2, which, as seen in Fig. 1.2, is not consistent with the experimental data. To resolve this unsatisfactory situation, Chap. 2 of this thesis is devoted to a model of self-electrophoresis which can explain the experimental data. After an introduction of our framework in Sec. 2.2 we investigate in Sec. 2.3 the limit of thin diffuse layers. In Sec. 2.5 we present various numerical and analytical model predictions that could partly be tested experimentally.

Self-diffusiophoresis of nonconducting swimmers.– A theoretical description of self-diffusiophoresis can be simpler than in the case of self-electrophoresis since the governing equations are not inherently nonlinear. However, a true theoretical understanding is

here hampered by the fact that both the interaction between solutes and swimmer and the chemical processes are not well understood. Computer simulations of self-diffusiophoresis have been done by Kapral and co-workers [105, 120] with a combination of molecular dynamics and multiparticle collision dynamics. Newer work includes different, reversible reaction schemes at the swimmer surface [122]. However, the *in silico* reconstitution of the real chemical process and interaction forces remains very challenging. Analytical work [47, 94] is based on a hydrodynamic boundary layer theory. The strength and also the weakness of these theories lies in the fact that very generic assumptions are made concerning the solute-particle interactions and the boundary conditions. A further shortcoming of this previous work is the assumption of a spatially fixed distribution of solute emission by the chemical reaction [54]. As the present thesis was completed, a more detailed model was put forth by Ebbens et al. [37], where the above problem was alleviated. In Chap. 3 we revisit the boundary layer theory with a systematic approach and describe how previous analytical theories can be improved. The common limitation to the lowest order boundary layer theories may lead to errors in the swimming speed. In Sec. 3.2 we therefore calculate corrections for nonvanishing L/R. In Sec. 3.3 we investigate a simple, but complete chemical reaction mechanism and calculate the resulting swimming speed in the linear response. The novelty is here that we do not assume that diffusive transport is much faster than the chemical transformation. In this sense, our work presents a first attempt to formulate a complete, albeit simplified model for active, diffusiophoretic motion.

Energetics and efficiency.– Although phoretic effects are known for more than a century their energetic aspects have hardly been explored. This contrasts with the situation for biological molecular motors [88, 58] and other swimming mechanisms at low Reynolds numbers [118, 10]. The assessment of energetics requires a thermodynamical framework. In the case of idealized molecular motors with few degrees of freedom, it is possible to model the processes with stochastic equations and the resulting thermodynamics [111, 101]. This approach even allows the investigation of the far-from equilibrium situation. However, the description of active, phoretic motion involves multiple, spatially dependent degrees of freedom. The transport equations commonly used for this system employ the assumption of local equilibrium to avoid a probabilistic description in favour of describing averaged quantities [27, 59]. It is therefore only consistent to also use this local equilibrium framework for thermodynamical considerations. In Chap. 4 we provide a very brief introduction to the theory of linear, irreversible thermodynamics. The next Chap. 5 then contains an energetic analysis of the model of self-diffusiophoresis explored in Chap. 3. This includes analytical and numerical calculations of the efficiency of a freely

moving swimmer.
In order to go beyond the predictions for concrete models, we study in Chap. 6 generic limits on the efficiency of autonomous swimmers. Hydrodynamic dissipation imposes clear upper bounds on the efficiency of phoretic motion. In Sec. 6.1.2 we propose a widely applicable and simple scaling relation to estimate the hydrodynamic efficiency without detailed knowledge of the system. Finally, we briefly investigate in Sec. 6.2 how the orientational randomness of free swimmers affects their ability to efficiently transport themselves across a given distance.

1.4 Theoretical foundations

1.4.1 The coordinate system

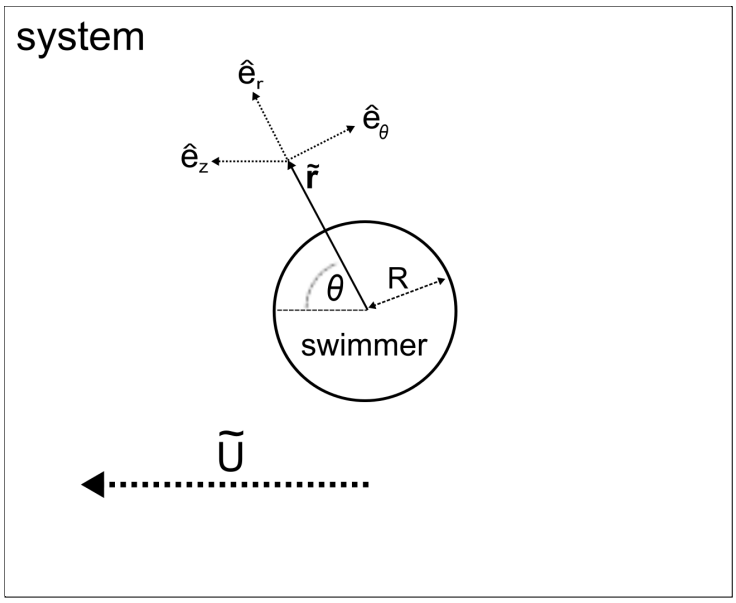

Figure 1.5: The coordinate system employed throughout this thesis. $\tilde{\mathbf{r}}$ is the position vector and θ is the polar angle in a spherical coordinate system. Azimuthal symmetry is assumed. The swimmer has a radius R and moves with speed $\tilde{U}$.

Throughout this thesis, we will designate dimensional variables with a tilde ($\tilde{}$). Constants and nondimensional quantities carry no tilde. Fig. 1.5 depicts the system schematically. The swimming particle is placed in an infinitely large container. We employ a spherical coordinate system aligned in the $\hat{\mathbf{e}}_z$ direction, where $\tilde{r}$ is the distance from the particle center and θ is the inclination angle. The unit vectors of the spherical system are denoted by $\hat{\mathbf{e}}_r$, $\hat{\mathbf{e}}_\theta$, $\hat{\mathbf{e}}_\varphi$. Since all systems considered in this thesis are axially symmetric, no use is made of the azimuthal variable φ. The swimming velocity $\tilde{\mathbf{U}}$ is aligned with the

$\hat{\mathbf{e}}_z$ axis.

1.4.2 Conservation of substance

We describe multicomponent mixtures on a hydrodynamic level, as it is common, e.g., for models of electrophoresis [109]. All position-dependent variables are thought of as local averages. The molecular concentration of the fluid constituent of type i is denoted by $\tilde{c}_i$. For the solvent, we write the index s. Molecular volumes are constants, denoted by v_i. A flow of molecules is denoted by $\tilde{\mathbf{J}}_i = \tilde{c}_i \tilde{\mathbf{u}}_i$ with $\tilde{\mathbf{u}}_i$ being the velocity of the molecules of type i. The conservation of the amount of substance is written as

$$\partial_t \tilde{c}_i + \nabla \cdot \tilde{\mathbf{J}}_i = \partial_t \tilde{c}_i + \nabla \cdot (\tilde{c}_i \tilde{\mathbf{u}}_i) = \sum_r \tilde{\alpha}_{ir}, \tag{1.3}$$

where $\tilde{\alpha}_{ir}$ is the rate at which the reaction with index r changes the concentration of species i inside the volume. Assigning a mass per molecule m_i to the fluid constituents, we can define a mass density as

$$\tilde{\rho} \equiv \sum_i m_i \tilde{c}_i. \tag{1.4}$$

The center of mass flow velocity is accordingly given by

$$\tilde{\mathbf{u}} \equiv \sum_i \frac{m_i \tilde{c}_i \tilde{\mathbf{u}}_i}{\tilde{\rho}}. \tag{1.5}$$

Conservation of mass follows from Eq. (1.3) by multiplication with m_i and subsequent summation. Since the overall mass is not affected by the chemical transformations we have

$$\partial_t \tilde{\rho} + \nabla \cdot (\tilde{\mathbf{u}}\, \tilde{\rho}) = 0. \tag{1.6}$$

It is now possible to define a flux of solution constituent of type i relative to the center of mass as

$$\tilde{\mathbf{j}}_i \equiv \tilde{\mathbf{J}}_i - \tilde{\mathbf{u}}\, \tilde{c}_i. \tag{1.7}$$

The relative fluxes then obey the condition

$$\sum_i m_i \tilde{\mathbf{j}}_i = 0. \tag{1.8}$$

Explicit expressions for the fluxes are obtained from phenomenological laws [27]. It is an experimental finding that the fluxes are proportional to local, thermodynamic driving forces. Driving forces on molecules of type i are the gradients in the chemical potentials $\tilde{\mu}_k$. Also, a gradient of potential energy per molecule, denoted by $\tilde{\psi}_k$, may be present. The phenomenological law for the fluxes of the solute molecules reads

$$\tilde{\mathbf{j}}_i = -\sum_k L_{ik} \nabla \left(\tilde{\mu}_k + \tilde{\psi}_k \right), \tag{1.9}$$

where the L_{ik} are called phenomenological coefficients. The cross-coefficients L_{ik} with $i \neq k$ obey the Onsager symmetry relation $L_{ik} = L_{ki}$ while the diagonal coefficients obey $L_{ii} \geq 0$ and $L_{ii}L_{kk} \geq L_{ik}^2$ [83]. Since the potentials are independent, Eq. (1.8) imposes a further condition on the coefficients, namely that for all i

$$\sum_k L_{ik} m_k = 0. \tag{1.10}$$

This condition allows to eliminate the phenomenological coefficients of the solvent, carrying an index s. We obtain

$$\tilde{\mathbf{j}}_i = -\sum_{k \neq \mathrm{s}} L_{ik} \nabla \left[\tilde{\mu}_k + \tilde{\psi}_k - \frac{m_k}{m_\mathrm{s}} \left(\tilde{\mu}_\mathrm{s} + \tilde{\psi}_\mathrm{s} \right) \right]. \tag{1.11}$$

Eq. (1.11) is well established for viscous solutions and is consistent with an approach coming from microscopic statistical mechanics [13]. In the following we will focus on the particularly simple case of very dilute, multicomponent solutions.

Dilute solutions

Dilute, aqueous solutions can be seen for our purposes as incompressible. Therefore, the fluid constituents take up almost all the free volume

$$\sum_i v_i \tilde{c}_i \simeq 1. \tag{1.12}$$

The solvent has a much larger volume fraction than the diluted solutes. We assume

$$v_\mathrm{s} \tilde{c}_\mathrm{s} \simeq \sum_i v_i \tilde{c}_i \simeq 1. \tag{1.13}$$

The local chemical potential of the fluid constituent of type i is then given by

$$\tilde{\mu}_i = kT \log\left(\tilde{c}_i v_i\right) - kT \log(\sum_i v_i \tilde{c}_i) + v_i \tilde{p}_\mathrm{H} + \epsilon_i, \tag{1.14}$$

where $\tilde{p}_\mathrm{H}$ is the hydrostatic pressure and an internal, chemical energy of the molecules is denoted by ϵ_i. The expression for the chemical potentials , Eq. 1.14, is in accord with a derivation from classical expressions for a local free energy [59, 107]. On insertion of the chemical potentials into Eq. (1.11), it becomes clear that the pressure $\tilde{p}_\mathrm{H}$ affects relative solute fluxes if the molecular masses m_i or volumes v_i of the solution constituents are different. This very basic result seems to have been neglected throughout the literature on diffusiophoresis on the hydrodynamic level. Pressure-driven fluxes complicate the governing equations considerably. In order to avoid this issue, we will in the following always assume that all fluid constituents are similar to the solvent as

$$v_{i \neq \mathrm{s}} \simeq v_\mathrm{s}, \tag{1.15}$$

$$m_{i \neq \mathrm{s}} \simeq m_\mathrm{s}. \tag{1.16}$$

Now, particle fluxes and mass fluxes are equivalent. We will also assume throughout this thesis that the size of the molecules is much smaller than any other lengthscale in the system. In order to calculate the fluxes from Eq. (1.11), we take a closer look at the coefficients L_{ik}. They can be interpreted as generalized friction coefficients, relating thermodynamic forces to fluxes. For diluted solutes, the diagonal coefficients L_{ii} are proportional to the product of a solute volume fraction and the solvent volume fraction. The solvent volume fraction is close to unity and we can therefore set $L_{ii} = \tilde{c}_i D_i/kT$ with a diffusion coefficient D_i. The cross-coefficients L_{ki} are proportional to the product of two solute volume fractions. We therefore have $L_{ik} = L_{ki} \approx 0$ for $k \neq i$ to lowest order in solute volume fractions. Upon employing these results along with Eq. (1.13) we finally obtain

$$\tilde{\mathbf{j}}_i = -D_i \left(\nabla \tilde{c}_i + \frac{\tilde{c}_i}{kT} \nabla \tilde{\psi}_i \right). \tag{1.17}$$

The solute conservation Equation (1.3), for a steady state in absence of chemical reactions in the volume, becomes

$$0 = \nabla \cdot \left(-D_i \nabla \tilde{c}_i - D_i \frac{\tilde{c}_i}{kT} \nabla \tilde{\psi}_i + \tilde{\mathbf{u}}\, \tilde{c}_i \right). \tag{1.18}$$

Convective transport vs. diffusive transport

The convection term $\nabla \cdot (\tilde{\mathbf{u}}\, \tilde{c}_i)$ in Eq. (1.18) is nonlinear since it contains a product of the field variables $\tilde{\mathbf{u}}$ and $\tilde{c}_i$. However, on short lengthscales, diffusive transport often dominates over convective transport. The relative magnitude of the two modes of transport can be quantified by nondimensionalization of the transport equation. Assuming only one diffusion constant D, we multiply Eq. (1.18) with R^2/D. Then we nondimensionalize the space variables with R and $\tilde{\mathbf{u}}$ with a typical fluid speed scale $\mathcal{U}$. The convection term obtains a prefactor, called Peclét number. It reads

$$\mathrm{Pe} \equiv \frac{\mathcal{U} R}{D}. \tag{1.19}$$

Typical values for colloidal particles moved by a phoretic effect are $\mathcal{U} \sim 10\,\mu\mathrm{m/s}$, $D \sim 10^{-9}\,\mathrm{m^2/s}$ and $R \sim 1\,\mu\mathrm{m}$ leading to $\mathrm{Pe} \sim 10^{-2}$. This value suggests that convection can be neglected. However, a problem occurs for distances larger than $\sim R/\mathrm{Pe}$. Due to different orders of radial derivatives, the convection terms dominate the diffusion terms for large $\tilde{r}$ in Eq. (1.18). An analytical technique due to Acrivos and Taylor [3] provides remedy. The expansion scheme for $\mathrm{Pe} \ll 1$ guarantees that the inner solution, near the particle, is still dominated by diffusion. Outer solutions, which are affected by convection, are matched asymptotically with the inner solutions. A lengthy calculation shows that the Pe^0 solution of such a matching scheme is for autonomous, phoretic swimmers just

the solution of Eq. (1.18) without the convection term. Usually, the range L of the solute-swimmer interaction is much shorter than the distance $\sim R/\mathrm{Pe}$, at which the outer solution becomes important. The interaction that drives the swimmer then only takes place in the diffusion-dominated region. A modification of the concentration profile by convection far away from the swimmer becomes irrelevant. Accordingly, we will avoid the asymptotic matching throughout this thesis by assuming that $L\,\mathrm{Pe} \ll R$.

Diffusion in a freely rotating frame of reference

The frame of reference introduced in Sec. 1.4.1 is fixed at the center of the swimmer and aligned with its swimming direction. A freely moving swimmer undergoes rotational diffusion, resulting in a modification of the diffusion equation in this frame of reference. The solute fluxes from Eq. (1.17) read in the co-moving frame

$$\tilde{\mathbf{j}}_i = -D\left(\nabla\tilde{c}_i + \frac{\tilde{c}_i}{kT}\nabla\tilde{\psi}_i\right) - \hat{\mathbf{e}}_\theta\tilde{r}\,D_{\mathrm{rot}}\,\partial_\theta\tilde{c}_i, \tag{1.20}$$

where $D_{\mathrm{rot}} = kT/\left(8\pi\eta R^3\right)$ is the rotational diffusion coefficient of the swimmer. Due to the assumed azimuthal symmetry, only the angular derivative in θ occurs. When nondimensionalizing the flux, we multiply Eq. (1.20) with R/D. The relative magnitude of the rotational correction is then found to be

$$R^2 D_{\mathrm{rot}}/D. \tag{1.21}$$

We employ the Einstein relation to calculate the diffusion coefficient of solute molecules with radius a as $D = kT/\left(6\pi\eta a\right)$. This yields $R^2 D_{\mathrm{rot}}/D = 3a/(4R)$. While the solute radii a are in the Å range, the size of the swimmer is restricted by fabrication techniques to $R \gtrsim 100\,\mathrm{nm}$. Accordingly, since $a \ll R$, the relative contribution of the particle rotation to the concentration profile is negligible near the swimmer. However, for large distance from the particle, the rotation of the frame leads to a perfectly homogeneous concentration distribution. Depending on the values of Pe and $R^2 D_{\mathrm{rot}}/D$ one finds intermediate regimes where convection is the dominant transport mechanism. This point has not yet found appreciation in the literature. Nevertheless, we avoid the multiple-scale problem in this thesis by focusing on the diffusion-dominated region.

1.4.3 Momentum conservation in the fluid

Navier-Stokes equation

A further conservation law, naturally entailed by a mass flow on a mesoscopic scale, is the Navier-Stokes equation

$$\tilde{\rho}\,\partial_t\tilde{\mathbf{u}} + \tilde{\rho}\,\tilde{\mathbf{u}}\cdot\nabla\tilde{\mathbf{u}} - \nabla\cdot\tilde{\sigma} = -\sum_i \tilde{c}_i\nabla\tilde{\psi}_i, \tag{1.22}$$

where we write the vector gradient with ∇ operating on a vector. The stress tensor $\tilde{\sigma}(\tilde{r},\theta)$ is a measure for the flux of momentum through the fluid and depends on the nature of the fluid. The right hand side of Eq. (1.22) is called the body force. We think of $-\tilde{c}_i\nabla\tilde{\psi}_i$ as the average force acting on a small fluid parcel due to the local forces on the point-like molecules of type i. In the following we will focus on the steady state where the time derivative vanishes.

Microhydrodynamics of a dilute solution

The common incompressibility condition, applicable for single component fluids, reads

$$\nabla\cdot\tilde{\mathbf{u}}=0. \tag{1.23}$$

The equation is in general not valid for multicomponent fluids that are incompressible. However, it can be used for dilute solutions with an incompressible solvent in steady state since Eq. (1.6) yields then

$$0=\partial_t\tilde{\rho}=-\nabla\cdot(\sum_i m_i\tilde{c}_i\tilde{\mathbf{u}})\approx-\tilde{c}_{\mathrm{s}}m_{\mathrm{s}}\,\nabla\cdot\tilde{\mathbf{u}}. \tag{1.24}$$

The typical solvent employed for the realization of phoretic swimmers is water. Water is a Newtonian fluid, i.e., the stress tensor depends linearly on the rate of deformation tensor. The stress tensor reads [95]

$$\tilde{\sigma}\equiv\eta\left(\nabla\tilde{\mathbf{u}}+(\nabla\tilde{\mathbf{u}})^T\right)-\tilde{p}\,\mathbf{I}=2\eta\tilde{\mathbf{E}}-\tilde{p}\,\mathbf{I}. \tag{1.25}$$

The pressure accounting for the incompressibility of the fluid is denoted by $\tilde{p}$. For incompressible fluids, the pressure can be thought of as a Lagrange multiplier that enforces the condition Eq. (1.23). The quantity $\tilde{\mathbf{E}}$ is called the strain rate tensor. We assume that the viscosity η is spatially constant. Corrections of the local viscosity due to concentration variations are proportional to the volume fractions of the solutes and therefore negligible.

The second term on the left hand side of Eq. (1.22) is nonlinear in $\tilde{\mathbf{u}}$. Its magnitude can be assessed through the Reynolds number Re, which appears in the Navier-Stokes equation when it is nondimensionalized. It reads

$$\mathrm{Re}\equiv\frac{\rho\mathcal{U}\,\mathrm{R}}{\eta}. \tag{1.26}$$

Employing $\mathcal{U}\sim10\,\mu$m/s, $\rho\simeq10^3\,\mathrm{kg/m^3}$, $\eta\simeq10^{-3}\,\mathrm{Pa\,s}$ and $R\sim1\,\mu$m we have $\mathrm{Re}\sim10^{-5}$. Therefore, it is a very good approximation to neglect the inertia of the fluid. This leads to the Stokes equation for a dilute solution in steady state

$$\nabla\cdot\tilde{\sigma}=\eta\nabla^2\tilde{\mathbf{u}}-\nabla\,\tilde{p}=\sum_i\tilde{c}_i\nabla\tilde{\psi}_i. \tag{1.27}$$

The Stokes equation is linear in the fluid velocity and pressure. Since we are treating the fluid in the overdamped limit, we will also neglect the inertia of the swimmer.

From an experimental point of view, it is important to determine the timescales on which the steady state velocity of the swimmer can be measured. Hydrodynamic fluctuations require temporal averages which are longer than a timescale of $\tau_h \equiv \rho R^2/\eta \sim 10^{-6}\,\mathrm{s}$. If the particle can rotate freely, its swimming velocity can only be measured by temporal averages which are shorter than the timescale of Brownian rotation τ_h. We find $\tau_{\mathrm{rot}} = 1/D_{\mathrm{rot}} = 8\pi\eta R^3/kT \sim 6\,\mathrm{s}$. Therefore, there exists a clearly defined range of timescales, $\tau_{\mathrm{h}} \ll \tau \ll \tau_{\mathrm{rot}}$, over which the velocity is quasi-stationary in the laboratory frame.

1.4.4 Swimming speed and force balance

In the co-moving frame, the particle speed $\tilde{U}$ enters the stationary solution of the Stokes equation through the boundary conditions as

$$\begin{aligned} \tilde{\mathbf{u}}(\infty,\theta) &= -\tilde{U}\hat{\mathbf{e}}_z, \\ \tilde{\mathbf{u}}(R,\theta) &= 0. \end{aligned} \tag{1.28}$$

The speed $\tilde{U}$ is determined from the balance of forces on the swimmer. The force which the swimmer exerts via the potential $\tilde{\psi}$ on the fluid must also act on itself, resulting in a "reactio" force $\tilde{\mathbf{F}}_{\mathrm{reactio}}$. This force, hydrodynamic forces on the surface of the particle $\tilde{\mathbf{F}}_{\mathrm{surf}}$ and an external force $\tilde{\mathbf{F}}_{\mathrm{m}} = F_{\mathrm{m}}\,\hat{\mathbf{e}}_z$ balance each other as

$$0 = \tilde{\mathbf{F}}_{\mathrm{m}} + \tilde{\mathbf{F}}_{\mathrm{reactio}} + \tilde{\mathbf{F}}_{\mathrm{surf}} = \tilde{F}_{\mathrm{m}}\hat{\mathbf{e}}_z + \int \sum_i \tilde{c}_i \nabla\tilde{\psi}_i \mathrm{d}\tilde{V} + \int \tilde{\sigma}\hat{\mathbf{e}}_r \mathrm{d}\tilde{A}_{\tilde{r}=R}. \tag{1.29}$$

$\tilde{A}_{\tilde{r}=R}$ is the swimmer's surface. Since the swimmer is spherical, we identify the normal vector on its surface with the unit radial vector $\hat{\mathbf{e}}_r$. A volume element of the fluid in the system is denoted by $\mathrm{d}\tilde{V}$. The Stokes equation (1.27) can be written in integral form as

$$\int \sum_i \tilde{c}_i \nabla\tilde{\psi}\,\mathrm{d}\tilde{V} = -\int \tilde{\sigma}\,\hat{\mathbf{e}}_r \mathrm{d}\tilde{A}_{\tilde{r}=R} + \int \tilde{\sigma}\,\hat{\mathbf{e}}_r \mathrm{d}\tilde{A}_{\tilde{r}=\infty}. \tag{1.30}$$

Here $\tilde{A}_{\tilde{r}=\infty}$ is some arbitrary surface, which we choose such that it completely encloses the volume where body forces are present. Inserting (1.30) into (1.29) we have

$$0 = \tilde{\mathbf{F}}_{\mathrm{m}} + \int \tilde{\sigma}\,\hat{\mathbf{e}}_r \mathrm{d}\tilde{A}_{\tilde{r}=\infty}, \tag{1.31}$$

which expresses a balance of external forces on whole the system. Eq. (1.31) permits to calculate the force on the swimmer only from the hydrodynamic farfield. This "insensitiveness" of the force balance to details of the nearfield will be exploited in various ways later. If no body forces are present, the force balance on a dragged particle reads

$$0 = \tilde{\mathbf{F}}_{\mathrm{m}} - \mathbf{T}\,\tilde{\mathbf{U}}. \tag{1.32}$$

The resistance tensor of translation is given by $\mathbf{T} = 6\pi\eta R\,\mathbf{I}$ for a spherical particle. Given an expression for the body force, a simple formula for the speed $\tilde{U}$ can be derived from the reciprocal theorem for the Stokes equation [121]. The integral form of this theorem reads

$$\int \tilde{\mathbf{u}}'\,\tilde{\sigma}\,\mathbf{n}\mathrm{d}\tilde{A} + \int \tilde{\mathbf{u}}'\,\nabla\cdot\tilde{\sigma}\mathrm{d}\tilde{V} = \int \tilde{\mathbf{u}}\,\tilde{\sigma}'\mathbf{n}\,\mathrm{d}\tilde{A} + \int \tilde{\mathbf{u}}\,\nabla\cdot\tilde{\sigma}'\mathrm{d}\tilde{V}, \tag{1.33}$$

where we have two (non related) fluid velocities $\tilde{\mathbf{u}}'$ and $\tilde{\mathbf{u}}$, both satisfying a Stokes equation. The surface normal, pointing into the fluid, is denoted by $\mathbf{n}$. We choose the auxiliary field $\tilde{\mathbf{u}}'$ to be a velocity tensor that is the solution to the force free Stokes equation $\nabla\cdot\tilde{\sigma}' = 0$. The boundary conditions for $\tilde{\mathbf{u}}'$ are

$$\begin{aligned}\tilde{\mathbf{u}}'|_{r=R} &= \mathbf{I},\\ \tilde{\mathbf{u}}'|_{r\to\infty} &= 0.\end{aligned} \tag{1.34}$$

For a spherical particle, the solution for $\tilde{\mathbf{u}}'$ reads in Cartesian coordinates [53]

$$\tilde{\mathbf{u}}' = \frac{3R}{4\tilde{r}}\left(\delta_{ij} + \frac{\tilde{r}_i\tilde{r}_j}{\tilde{r}^2}\right) + \frac{3R^3}{4\tilde{r}^3}\left(\frac{\delta_{ij}}{3} - \frac{\tilde{r}_i\tilde{r}_j}{\tilde{r}^2}\right). \tag{1.35}$$

The other fluid velocity, $\tilde{\mathbf{u}}$, is chosen such that it satisfies the Stokes equation with body forces, Eq. (1.27) with the boundary conditions in Eq. (1.28). Eq. (1.33) becomes

$$\begin{aligned}\tilde{\mathbf{F}}_{\mathrm{surf}} = \int \mathbf{I}\tilde{\sigma}\,\mathbf{n}\mathrm{d}A_{\tilde{r}=R} &= -\int \tilde{\mathbf{u}}'\nabla\cdot\tilde{\sigma}\mathrm{d}\tilde{V} + \int \tilde{\mathbf{u}}\tilde{\sigma}'\,\mathbf{n}\mathrm{d}\tilde{A}_{\tilde{r}=R}\\ &= -\int \tilde{\mathbf{u}}'\sum_i \tilde{c}_i\nabla\tilde{\psi}_i\,\mathrm{d}\tilde{V} - 6\pi\eta R\tilde{\mathbf{U}}.\end{aligned} \tag{1.36}$$

The force balance Eq. (1.29) reads

$$\tilde{\mathbf{F}}_{\mathrm{m}} = -\tilde{\mathbf{F}}_{\mathrm{surf}} - \tilde{\mathbf{F}}_{\mathrm{reactio}} = 6\pi\eta R\tilde{\mathbf{U}} + \int [\tilde{\mathbf{u}}' - \mathbf{I}]\sum_i \tilde{c}_i\nabla\tilde{\psi}_i\,\mathrm{d}\tilde{V}, \tag{1.37}$$

which provides a simple relation between the swimming speed $\tilde{\mathbf{U}}$ and the externally applied force. For a spherical particle, swimming in $\hat{\mathbf{e}}_z$ direction, we have

$$\begin{aligned}\tilde{U} = \frac{\tilde{F}_{\mathrm{m}}}{6\pi\eta R} - \frac{1}{6\pi\eta R}\int [(\frac{3R}{2\tilde{r}} - \frac{R^3}{2\tilde{r}^3} - 1)\cos\theta \sum_i \tilde{c}_i\partial_r\tilde{\psi}_i\\ -(\frac{3R}{4\tilde{r}} + \frac{R^3}{4\tilde{r}^3} - 1)\sin\theta \sum_i \tilde{c}_i\frac{\partial_\theta\tilde{\psi}_i}{R}]\mathrm{d}\tilde{V}.\end{aligned} \tag{1.38}$$

We will refer to Eq. (1.38) as Teubner's formula [121]. It should be noted that Teubner's formula is only useful in the strictly linear regime where the body forces are independent of the fluid velocity $\tilde{\mathbf{u}}$. If convection modifies the concentration fields $\tilde{c}_i$, a calculation of $\tilde{U}$ is not possible since the velocity appears in the integral on the right hand side of Eq. (1.38). Therefore, the equation can only be used rigorously in perturbative approaches, where convection plays no role. Weak potentials with $\tilde{\psi}/kT \ll 1$ or, alternatively, very short ranged potentials $L/R \ll 1$, permit this approach.

1.5 Boundary layer theory for phoretic swimming

We will in the following always assume that there is one dominating lengthscale of the solute-swimmer potentials $\tilde{\psi}_i$ denoted by L. Very often L is in the nanometer range with R being a micrometer or so. The separation of those two lengthscales can be employed to construct approximate analytical solutions. The theory we will discuss in this section is a nonrigorous but pedagogical approach, popularized by Anderson [6]. Systematic calculations for the same problem are detailed in later chapters.

1.5.1 The inner region

L is also the lengthscale over which the fluid speed changes strongly near the particle. Inside this boundary layer, we employ a dimensionless, stretched variable for the distance to the surface

$$y \equiv (\tilde{r} - R)/L. \tag{1.39}$$

The magnitude of the radial derivative near the surface of the swimmer can be estimated as $\partial_y \sim 1/L$ while the lateral derivative is $1/R\,\partial_\theta \sim 1/R \ll 1/L$. The short ranged nature of $\tilde{\psi}$ therefore allows to neglect the derivatives parallel to the surface near the particle. Also, we assume that the fluid velocity normal to the surface is at least one order of L/R smaller than the velocity parallel to the particle surface. The Stokes equation (1.27) can then be approximated as

$$\eta \partial_y^2 \tilde{u}_\theta \approx \frac{1}{R}\partial_\theta \tilde{p} + \frac{1}{R}\sum_i \tilde{c}_i\, \partial_\theta \tilde{\psi}_i, \tag{1.40}$$

$$-\partial_y \tilde{p} \approx \sum_i \tilde{c}_i\, \partial_y \tilde{\psi}_i, \tag{1.41}$$

where $\tilde{u}_\theta$ is the speed in $\hat{\mathbf{e}}_\theta$ direction. The equation (1.41) is equivalent to an equilibrium condition normal to the surface. The flux of solutes $\tilde{\mathbf{j}}$ is given by Eq. (1.17). In order to prevent a divergence of the radial flux for $y \to 0$ it must vanish in $O(1)$. This condition yields for the concentration in the boundary layer

$$\tilde{c}_i(\theta, y) \approx \tilde{c}_i(\theta, \infty)\, e^{-\frac{\tilde{\psi}_i(\theta,y) - \tilde{\psi}_i(\theta,\infty)}{kT}} = \tilde{c}_i^{\infty}(\theta)\, e^{-\frac{\tilde{\Psi}_i(y)}{kT}}, \tag{1.42}$$

where we have introduced the new variable $\tilde{\Psi}$ and assumed that the lateral variations of $\tilde{\Psi}$ are negligible. $\tilde{c}_i^{\infty}(\theta)$ is the concentration at the outer perimeter of the boundary layer. Integration of (1.41) yields immediately

$$\tilde{p}(\theta, y) \approx \tilde{p}(\infty) + \sum_i kT\tilde{c}_i^{\infty}(\theta)[e^{-\frac{\tilde{\Psi}_i(y)}{kT}} - 1]. \tag{1.43}$$

On inserting this pressure into Eq. (1.40) and using the no-slip boundary condition Eq. (1.28) the velocity inside the boundary layer is obtained as

$$\begin{aligned}\tilde{\mathbf{u}}_\theta(\theta,y) \approx &-\frac{kT\,L^2}{\eta\,R}\sum_i \int_0^y \int_{y'}^\infty \left[e^{-\frac{\tilde{\Psi}_i(y')}{kT}}-1\right] dy'dy\,\partial_\theta \tilde{c}_i^\infty(\theta)\,\hat{\mathbf{e}}_\theta \\ &-\frac{L^2}{\eta\,R}\sum_i \int_0^y \int_{y'}^\infty \tilde{c}_i^\infty(\theta) e^{-\frac{\tilde{\Psi}_i(y')}{kT}}\,dy'dy\,\partial_\theta \tilde{\psi}_i(\theta,\infty)\,\hat{\mathbf{e}}_\theta.\end{aligned} \tag{1.44}$$

The so-called slip velocity is the limit of the inner solution far away from the surface $\tilde{u}_{\mathrm{S}}(\theta) \equiv \tilde{u}_x(\theta,y)|_{y\to\infty}$. After partial integration one can write this quantity as

$$\tilde{\mathbf{u}}_{\mathrm{S}}(\theta) = -\frac{kT\,L^2}{\eta\,R}\sum_i K_{1,(i)}\partial_\theta \tilde{c}_i^\infty(\theta)\hat{\mathbf{e}}_\theta - \frac{L^2}{\eta\,R}\sum_i \int_0^\infty \int_{y'}^\infty e^{-\frac{\tilde{\Psi}_i(y')}{kT}}\,dy'dy\,\tilde{c}_i^\infty(\theta)\partial_\theta\tilde{\psi}_i(\theta,\infty)\,\hat{\mathbf{e}}_\theta, \tag{1.45}$$

with

$$K_{m,(i)} \equiv \int_0^\infty y^m\,(e^{\frac{-\tilde{\Psi}_i(y)}{kT}}-1)\,\mathrm{d}y. \tag{1.46}$$

The $K_{m,(i)}$ can be interpreted as the unnormalized moments of the excess surface concentrations [7]. We only write the index i if more than one potential is present. Note that the second term in Eq. (1.45) can diverge. A well defined slip velocity only results if the body force vanishes in the bulk. The slip velocity $\tilde{\mathbf{u}}_{\mathrm{S}}$ is calculated in order to employ it as inner boundary condition for an outer hydrodynamic flow. In the next section we describe an explicit solution for the outer flow that also yields the swimming speed.

1.5.2 The outer region and Lamb's general solution

Outside the boundary layer the body forces are negligible. The hydrodynamic flow is driven by the boundary condition between the inner and outer region. The flow field in the outer region around a spherical particle is given by Lamb's solution [53]. The radial variable in the outer region is $\tilde{r}$. The lateral divergence of the slip velocity $-\tilde{r}\nabla_{||}\cdot\tilde{\mathbf{u}}_{\mathrm{S}} = -\partial_\theta\tilde{u}_{\mathrm{S}}\hat{\mathbf{e}}_\theta$ relates the inner and outer flow. The Legendre transform of the divergence is

$$\tilde{\Xi}_n \equiv \frac{2n+1}{2}\int_0^\pi \left[-\tilde{r}\nabla_{||}\cdot\tilde{\mathbf{u}}_{\mathrm{S}}(\theta)\right] P_n(\cos\theta)\sin\theta\,\mathrm{d}\theta, \tag{1.47}$$

where $P_n(\cos\theta)$ are Legendre polynomials. Lamb's solution makes use of two harmonic functions, p_n and ς_n, that we express in terms of their Legendre expansions for an infinite system as

$$p_{-2} = \frac{\eta\,R}{2\tilde{r}^2}\left(3\tilde{U}-\tilde{\Xi}_1\right) P_1(\cos\theta) \qquad n=1 \tag{1.48}$$

$$p_{-(n+1)} = -\frac{\eta(2n-1)}{(n+1)R}\left(\frac{R}{\tilde{r}}\right)^{n+1}\tilde{\Xi}_n P_n(\cos\theta) \qquad n>1 \tag{1.49}$$

$$\varsigma_{-2} = \frac{R^3}{4\tilde{r}^2}\left(\tilde{U} - \tilde{\Xi}_1\right) P_1(\cos\theta) \qquad n = 1 \tag{1.50}$$

$$\varsigma_{-(n+1)} = -\frac{R}{2(n+1)}\left(\frac{R}{\tilde{r}}\right)^{n+1} \tilde{\Xi}_n P_n(\cos\theta) \qquad n > 1 \tag{1.51}$$

The solution for the hydrodynamic flow in laboratory frame is given by

$$\tilde{\mathbf{u}} = \sum_{n=1}^{\infty}\left[\nabla\varsigma_{-(n+1)} - \frac{n-2}{\eta\, 2n(2n-1)}\tilde{r}^2\nabla p_{-(n+1)} + \frac{n+1}{\eta\, n(2n-1)}\tilde{r}p_{-(n+1)}\right], \tag{1.52}$$

which can be evaluated in principle for any given tangential slip velocity $\tilde{\mathbf{u}}_{\mathrm{S}}$. The speed $\tilde{U}$ must be calculated from a balance of hydrodynamic force, body force and external force $\tilde{\mathbf{F}}_{\mathrm{m}}$. According to Eq. (1.31), it suffices to calculate the hydrodynamic force on a surface very far away of the swimmer to obtain the force balance. The Stokeslet, which decays $\sim 1/r$, is the only contribution of the fluid flow that is non-vanishing here. Lamb's solution yields

$$4\pi\nabla\left(\tilde{r}^3 p_{-2}\right)|_{\tilde{r}=R} = 2\pi\eta R\left(3\tilde{U} - \tilde{\Xi}_1\right)\hat{\mathbf{e}}_z = \tilde{\mathbf{F}}_{\mathrm{m}}, \tag{1.53}$$

where we have assumed that $\tilde{F}_{\mathrm{m}}\hat{\mathbf{e}}_z$ is parallel to $\tilde{\mathbf{U}}$. Particle speed is given by

$$\tilde{U} = \frac{\tilde{F}_{\mathrm{m}}}{6\pi\eta R} + \frac{\tilde{\Xi}_1}{3}, \tag{1.54}$$

which only depends on the dipole moment of the concentration. Contributions to the slip velocity with $p_{n<-2}$ and $\varsigma_{n<-2}$ do not influence the swimming speed. If the external forces vanish, the swimming speed becomes independent of the radius R of the swimmer. It can be shown from Eq. (1.38) that the swimming speed is for similar average concentration gradients even independent of the shape of the particle when $L \ll R$. As a concrete example, we consider the case where the tangential component of the slip velocity is $\sim \sin\theta$ and then $\tilde{\Xi}_{n>1} = 0$. The potential is to be radially symmetric $\tilde{\psi} = \tilde{\psi}(r)$. We have for $\tilde{\Xi}_1$ explicitly

$$\tilde{\Xi}_1 = \frac{3}{2}\int_0^\pi \tilde{u}_{\mathrm{S}}\sin^2\theta\,\mathrm{d}\theta = -\frac{3\,L^2 kT}{2\eta}\sum_i K_{1,(i)}\int_0^\pi \frac{\partial_\theta \tilde{c}_i^{\infty}(\theta)}{R}\sin^2\theta\,\mathrm{d}\theta \tag{1.55}$$

where partial integration was used. Note that $\tilde{\Xi}_1$ is three times the average of the surface velocity projected on the direction of movement. Usage of $\tilde{\Xi}_{n>1} = 0$ in Eq. (1.52) leads to simple expressions for the outer fluid velocity

$$\begin{aligned}
\tilde{u}_r &= \left(\frac{R}{\tilde{r}}\left[\frac{3\tilde{U}}{2} - \frac{\tilde{\Xi}_1}{2}\right] + \frac{R^3}{\tilde{r}^3}\left[-\frac{\tilde{U}}{2} + \frac{\tilde{\Xi}_1}{2}\right]\right)\cos\theta, \\
\tilde{u}_\theta &= \left(\frac{R}{\tilde{r}}\left[-\frac{3\tilde{U}}{4} + \frac{\tilde{\Xi}_1}{4}\right] + \frac{R^3}{\tilde{r}^3}\left[-\frac{\tilde{U}}{4} + \frac{\tilde{\Xi}_1}{4}\right]\right)\sin\theta.
\end{aligned} \tag{1.56}$$

1.5.3 Diffusiophoresis and hydrodynamic surface slip

It has been suggested that the hydrodynamic no-slip boundary condition could lose its validity on hydrophobic surfaces. Ajdari and Bocquet [4] found that a finite fluid slip modifies the speed of phoretic swimming. The no-slip boundary condition is replaced with the Navier boundary condition on the swimmer

$$\Lambda \tilde{u}|_{y=0} = \eta \partial_y \tilde{u}|_{y=0} \tag{1.57}$$

where a slip-length $b \equiv \eta/\Lambda$ can be defined. The length b is the distance at which the velocity would become zero if it decayed linearly into the surface. The slip velocity at the outer periphery of the boundary layer can be calculated in analogy to the no-slip case. For simplicity, we focus here on a single, nonionic solute with concentration $\tilde{c}_1$ and a radially symmetric potential $\tilde{\psi}(y)$. The slip velocity becomes

$$\tilde{\mathbf{u}}_{\mathrm{S}}(x) \approx \frac{-kT}{\eta} \sum_i \left(L^2 K_{1,(i)} + L\, b\, K_{0,(i)} \right) \frac{\partial_\theta \tilde{c}_i^{\infty}(x)}{R} \hat{\mathbf{e}}_\theta. \tag{1.58}$$

When $b\, K_{0,(i)} > 0$, the new second term in Eq. (1.58) increases the swimming speed.

1.6 A little beyond the classical models of phoresis

The emphasize of this thesis is on the classical, coarse grained theories where the solutes are dilute, point-like molecules. However, it is instructive to consider a model that describes the system on a statistical level. We would also like to treat the solute molecules on the same footing as the swimmer, namely as particles with a non-vanishing size. To do this, we employ a formalism for colloidal suspensions, discussed e.g. in [32]. We show that the classical equations describing diffusiophoresis follow as a special limit and calculate corrections for finite solute sizes.

As before, we neglect inertia. A joint probability density for the position of N particles is denoted by $\tilde{\mathcal{P}}(\tilde{\mathbf{r}}_1 \dots \tilde{\mathbf{r}}_N)$. The coordinate of the swimmer is $\tilde{\mathbf{r}}_1$. The particles of number n and m interact through an additive potential $\tilde{\psi}_{nm}$. Upon defining

$$\tilde{\Upsilon}(\tilde{\mathbf{r}}_1 \dots \tilde{\mathbf{r}}_N) \equiv \sum_{n<m} \tilde{\psi}_{nm}(\tilde{\mathbf{r}}_n, \tilde{\mathbf{r}}_m) + kT \log[\tilde{\mathcal{P}}(\tilde{\mathbf{r}}_1 \dots \tilde{\mathbf{r}}_N)], \tag{1.59}$$

the probability density function can, in principle, be calculated from the stationary Smoluchowski equation which reads

$$0 = \sum_{m,n=1}^{N} \nabla_{\tilde{r}_n} \cdot \left[\mathbf{D}_{mn}\, \tilde{\mathcal{P}} \nabla_{\tilde{r}_n} \tilde{\Upsilon} \right], \tag{1.60}$$

where $\mathbf{D}_{mn}$ is the symmetric diffusion matrix which contains hydrodynamic interactions. The mean velocity of the swimmer at position $\mathbf{r}_1$, interacting with $N-1$ solute particles

at positions $\mathbf{r}_n$, is calculated as

$$\langle \tilde{\mathbf{U}}_1 \rangle = -\frac{1}{kT} \langle \sum_{n=1}^{N} \mathbf{D}_{1\,n} \nabla_{r_n} \tilde{\Upsilon} \rangle. \tag{1.61}$$

We now assume very dilute solutions, where the solutes do not interact with each other. Therefore, we only need consider the steady-state two-particle probability distribution function $\tilde{\mathcal{P}}_2$. $\tilde{\mathcal{P}}_2(\mathbf{r}_2, \mathbf{r}_1) \equiv P_{12}(\tilde{\mathbf{r}})/\tilde{V}$ is the probability to find the swimmer at position $\tilde{\mathbf{r}}_1$ somewhere in the volume $\tilde{V}$ and a further particle at a distance $\tilde{\mathbf{r}} = \tilde{\mathbf{r}}_2 - \tilde{\mathbf{r}}_1$. The swimmer has radius R and the solute has radius a. It is required that the solutes are much smaller than the lengthscale of the potential $a \ll L$. For the two-particle probability density function Eq. (1.60) simplifies to

$$0 = \nabla \cdot \left[(\mathbf{D}_{11} + \mathbf{D}_{22} - 2\,\mathbf{D}_{12}) \left(\nabla \tilde{\mathcal{P}}_{12}(\tilde{\mathbf{r}}) + \frac{1}{kT} \tilde{\mathcal{P}}_{12}(\tilde{\mathbf{r}}) \nabla \tilde{\psi}(\tilde{r}) \right) \right]. \tag{1.62}$$

where $\nabla = \nabla_{\tilde{r}}$. The tensor $\mathbf{D}_{mn}$ containing the hydrodynamic interaction between the swimmer and the solute molecule is given in [32] up to $O((R/\tilde{r})^4)$ as

$$\mathbf{D}_{11}^{kl} = \delta_{kl}\, kT/\left(6\pi\eta\, R\right), \tag{1.63}$$

$$\mathbf{D}_{22}^{kl} = \delta_{kl}\, kT/\left(6\pi\eta\, a\right), \tag{1.64}$$

$$\mathbf{D}_{12}^{kl} = \frac{kT}{6\pi\eta} \left[\frac{3}{4\tilde{r}} (\delta_{kl} + \frac{x_k\, x_l}{\tilde{r}^2}) + \frac{1}{4\tilde{r}^3} \left[a^2 + R^2 \right] (\delta_{kl} - 3\frac{x_k\, x_l}{\tilde{r}^2}) \right]. \tag{1.65}$$

The average speed is calculated with the two-particle approximation and Eq. (1.61) as

$$\begin{aligned} \langle \mathbf{U}_1 \rangle \approx & -\frac{N}{kT} \langle (\mathbf{D}_{11} - \mathbf{D}_{12})\, \nabla_{r_1} \tilde{\Upsilon}_2 \rangle \\ = & -\frac{N}{kT} \int \mathrm{d}\tilde{V}_2 \int \mathrm{d}\tilde{V}_1 \tilde{\mathcal{P}}_2(\mathbf{r}_1, \mathbf{r}_2)\, (\mathbf{D}_{11} - \mathbf{D}_{12})\, \nabla_{r_1} \tilde{\Upsilon}_2(\mathbf{r}_2, \mathbf{r}_1) \\ = & -\frac{1}{6\pi\eta\, R} \int N \tilde{\mathcal{P}}_{12}(\mathbf{r}) \left[\left(\frac{3R}{2\tilde{r}} - \frac{R^3 + R\, a^2}{2\tilde{r}^3} - 1 \right) \partial_r \tilde{\psi}\, \cos(\theta) \right. \\ & \left. - \left(\frac{3R}{4\tilde{r}} + \frac{R^3 + R\, a^2}{4\tilde{r}^3} - 1 \right) \frac{\partial_\theta \tilde{\psi}}{r}\, \sin(\theta) \right] \mathrm{d}\tilde{V}, \end{aligned} \tag{1.66}$$

where the swimming velocity is aligned with $\hat{\mathbf{e}}_z$ and incompressibility of the solvent was used. We can identify $N\,\tilde{\mathcal{P}}_{12}$ with the concentration $\tilde{c}$ from the preceding sections. Upon taking the limit $a/R \to 0$ we find that Eq. (1.62) agrees with the classical diffusion equation and Eq. (1.66) agrees with Teubner's formula for the speed (1.38). Thus, the classical theory of diffusiophoresis is confirmed here.

When $R \gg L \gg a$, the boundary layer theory from Sec. 1.5.1 can be employed to calculate corrections up to $O(a/R)$. A radially symmetric potential is assumed that interacts with one type of solute. Remarkably, we find that the formula for the slip velocity (1.45) is not directly modified by the corrections. The swimming speed can be calculated from Eq. (1.54) up to $O(a/R)$. A finite size of the solute molecules merely

influences the concentration gradient outside of the boundary layer that appears in $\tilde{\Xi}_1$. The concentration at the outer periphery of the boundary layer $\tilde{c}^{\infty}(\theta)$ results to lowest order in L/R from Eq. (1.62) as

$$\tilde{c}^{\infty}(\theta) \approx \sum_{k=1}^{\infty} \iota_{-k} \left(1 - \frac{3a}{4(k+1)R}\right) P_k(\cos(\theta)) + \iota_1 \cos(\theta) + \iota_0 + \tilde{c}(\infty). \tag{1.67}$$

The coefficients ι_{-k} of the expansion in Legendre polynomials depend on the boundary conditions of the considered system. The new concentration $\tilde{c}^{\infty}(\theta)$ can be used in Eq. (1.55) to calculate the swimming speed from Eq. (1.54) up to $O(a/R)$. We find for self-diffusiophoresis of a free particle a correction factor for $\tilde{U}$ of $(1-3a/(8R))$. The speed of passive diffusiophoresis in an externally applied concentration gradient is reduced by a factor of $(1 - a/(8R))$. We conclude that diffusiophoretic motion is slowed down by the effect of finite solute size when $a \ll L \ll R$ holds.

Chapter 2

Self-electrophoretic motion

In this chapter, nonlinear, self-electrophoretic swimming through electrocatalytic decomposition of H_2O_2 is investigated. In our model, the solution surrounding the swimmer also contains a low concentration of salt. A combined numerical and analytical approach is chosen to obtain a deeper understanding of this, experimentally well studied, kind of motion. The reader is referred back to Sec. 1.2 for a phenomenological introduction to the self-electrophoretic mechanism.

2.1 Redox reactions at the metal swimmer

The electrochemical reactions leading to the decomposition of H_2O_2 at the swimmer's surface are complicated and not well understood. Fig. 2.1 illustrates schematically how the coupled reduction and oxidation of H_2O_2 cause an electric current through the swimmer and a corresponding flux of protons around the swimmer. Experiments with comparatively large (mm-sized) electrodes suggest that the decomposition of H_2O_2 at metal surfaces in acidic medium happens via a formation of oxides at the surfaces [15]. We illustrate the processes with simplified prototypical reaction pathways. These schemes merely present one possible way to justify the mathematical model we use later on.

During the electrokinetic reduction of H_2O_2, H^+ ions in the vicinity of the metal surface combine with electrons from the metal substrate S. The following reaction has been used previously for a simulation of the reduction on platinum electrodes [80]

$$\begin{aligned} S + H_2O_2 + H^+ + e^- &\rightarrow S(OH) + H_2O, \\ S(OH) + H^+ + e^- &\rightarrow S + H_2O. \end{aligned} \tag{2.1}$$

Additional processes that possibly slow down the reduction are neglected here. Applying the steady-state condition, we find that the concentration of $S(OH)$ is independent of $[H^+]$. This implies that the effective rate equation for H^+ consumption is first order in

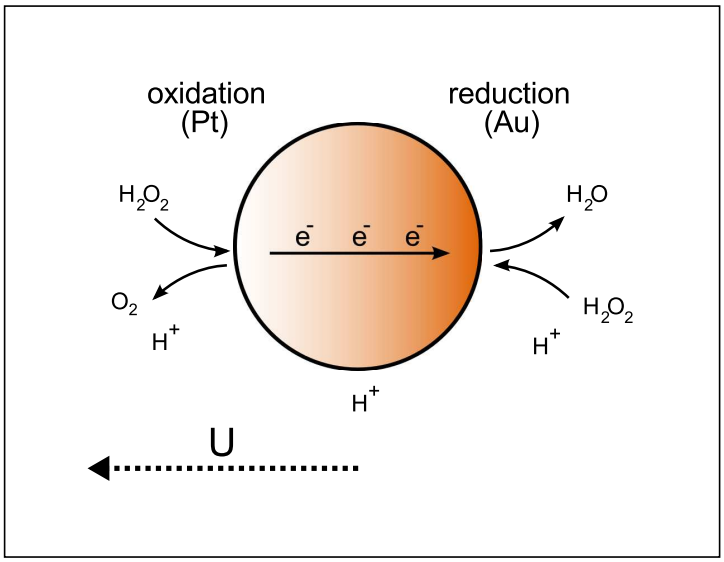

Figure 2.1: Sketch of the electrokinetic process taking place at the bimetallic swimmer in an H_2O_2 solution. Note that the swimmer is found to move with the oxidizing end forwards.

$[H^+]$ and $[H_2O_2]$. A second order reaction rate cannot be excluded, but we deem the suggested presence of a multi-step decomposition sufficient to allow the simpler modeling of the reduction as a first order process.

The oxidation of H_2O_2 at metal electrodes has been studied in great detail by Hall et al. [50, 51]. It is also found to depend on surface oxide films. After diffusive encounter with the oxide, H_2O_2 reduces the surface film as

$$S(OH)_2 + H_2O_2 \rightleftarrows S(OH)_2 \cdot H_2O_2 \rightarrow S + 2H_2O + O_2. \tag{2.2}$$

Hydrogen ions are released when the surface is oxidized again

$$S + 2H_2O \rightarrow S(OH)_2 + 2H^+ + 2e^-. \tag{2.3}$$

Neglecting side processes, one can again assume that the reaction is first order in $[H_2O_2]$. Wang et al. [130] have suggested an alternative oxidation process with a transfer of four electrons. This is neglected here for simplicity. The presence of multi-step reactions suggests that inhibitory mechanisms could lead to a Michaelis-Menten-like kinetics [115]. If the saturation of swimming speed seen in Fig. 1.2 is due to nonlinear reaction kinetics, nonlinearity should only set in for $c_{H_2O_2} \gtrsim 5\,\%$ wt/v. Here, we do not model nonlinear reactions but focus on low concentrations of educts and products.

2.2 Model of a conducting swimmer in an ionic solution

The concentrations of monovalent salt anions and cations are denoted by $\tilde{c}_{\mathrm{i},-}$ and $\tilde{c}_{\mathrm{i},+}$, respectively. The hydroxide (OH^-) and proton (H^+) concentrations, resulting from the spontaneous dissociation of water and from a dissociation of H_2O_2, are denoted by $\tilde{c}_{\mathrm{H}-}$ and $\tilde{c}_{\mathrm{H}+}$. All types of ions are assumed to have the same diffusion constant D. Concentrations of cations and anions are written summarily with

$$\begin{aligned} \tilde{c}_+ &\equiv \tilde{c}_{\mathrm{H},+} + \tilde{c}_{\mathrm{i},+}, \\ \tilde{c}_- &\equiv \tilde{c}_{\mathrm{H},-} + \tilde{c}_{\mathrm{i},-}. \end{aligned} \tag{2.4}$$

The ions couple to an electric field $\tilde{\phi}$. In the bulk, far away from the swimmer, we have charge neutrality and the concentrations of ions are equal $\tilde{c}_-(\infty) = \tilde{c}_+(\infty)$.

We nondimensionalize length with the swimmer radius R and the concentrations of ions $\tilde{c}_{\{\mathrm{H,i}\},\pm}$ with the bulk concentration of salt ions

$$\mathcal{C}_\mathrm{i} \equiv \tilde{c}_{\mathrm{i},+}(\infty) = \tilde{c}_{\mathrm{i},-}(\infty). \tag{2.5}$$

Energies are normalized with the thermal energy scale kT. The charge per ion is denoted by Ze where we set $Z = 1$ throughout this thesis. Accordingly, the electric potential $\tilde{\phi}$ is made nondimensional with the thermal voltage $kT/Ze \simeq 25\,\mathrm{mV}$. Diffusive fluxes are nondimensionalized with $D\mathcal{C}_\mathrm{i}/R$. The velocity scale of the flow $\tilde{\mathbf{u}}$ and the swimming speed $\tilde{U}$ is given by a typical speed $\mathcal{U}$. The associated Peclét number is defined in Eq. (1.19).

2.2.1 Poisson-Boltzmann and diffusion equations

The fluxes of cations and anions are given in dimensionless form by

$$\mathbf{J}_{\{\mathrm{H,i}\},+} = -\nabla c_{\{\mathrm{H,i}\},+} - c_{\{\mathrm{H,i}\},+}\nabla\phi + \mathrm{Pe}\,\mathbf{u}\,c_{\{\mathrm{H,i}\},+}, \tag{2.6}$$

$$\mathbf{J}_{\{\mathrm{H,i}\},-} = -\nabla c_{\{\mathrm{H,i}\},-} + c_{\{\mathrm{H,i}\},-}\nabla\phi + \mathrm{Pe}\,\mathbf{u}\,c_{\{\mathrm{H,i}\},-}. \tag{2.7}$$

Diffusion equations guarantee the conservation of substance in the fluid. They determine the concentration field and read

$$\nabla \cdot \mathbf{J}_{\{\mathrm{H,i}\},+} = 0, \tag{2.8}$$

$$\nabla \cdot \mathbf{J}_{\{\mathrm{H,i}\},-} = 0. \tag{2.9}$$

A connection between the ion density and the electric field is given by the Poisson-Boltzmann equation. It reads in dimensionless form

$$\nabla^2\phi = -\frac{1}{2\,\lambda^2}(c_+ - c_-). \tag{2.10}$$

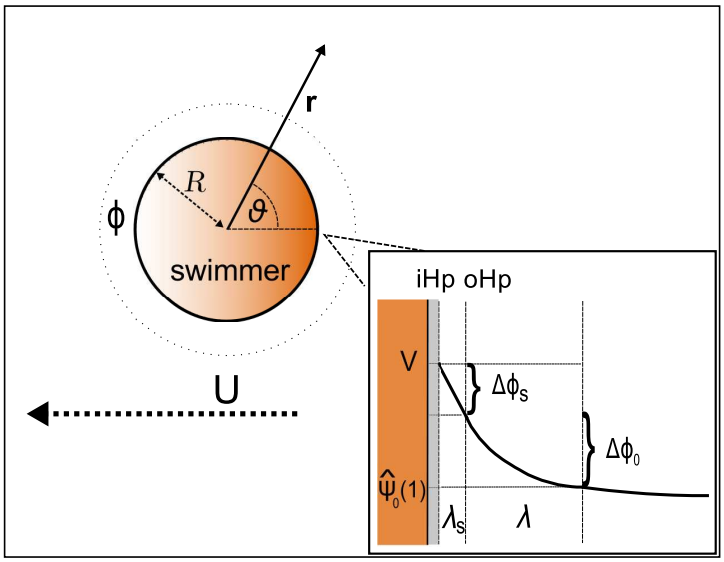

Figure 2.2: Schematic representation of the model for a self-electrophoretic swimmer with radius $\mathcal{R}$ moving with swimming speed U. The electric potential outside the swimmer is denoted by ϕ. The inset shows an enlarged version of our double layer model. The swimmer surface is covered by an immobile, compact layer of salt ions, termed Stern layer. The inner Helmholtz plane (iHp) and outer Helmholtz plane (oHp) delimit the modeled region of the Stern layer with thickness λ_s. The voltage drop across the diffuse layer is $\Delta\phi_s$. Bordering to the outer Helmholtz plane we have the diffuse layer, where dilute solutes form a charge cloud around the swimmer. The diffuse layer has a thickness λ. The voltage drop across the diffuse layer is $\Delta\phi_0$.

The lengthscale of the potential ϕ in Eq. (2.10) is given by the dimensionless Debye length λ, which we define as

$$\lambda \equiv \sqrt{\frac{\varepsilon\, kT}{8\pi\,(Ze)^2\,\mathcal{C}_\mathrm{i}}}\,\frac{1}{R} \tag{2.11}$$

with ε being the permittivity of the solution.

2.2.2 Stern layer and boundary conditions

In the bulk, far away from the swimmer, the electric potential takes on an uniform value, which is set to zero

$$\phi(r \to \infty, \theta) = 0. \tag{2.12}$$

The presence of salt in the solution suggests some form of adsorption of ions onto the metal surface. The inset of Fig. 2.2 illustrates the employed model of a Stern (compact) layer of immobile ions covering the metal surface [28]. All the charge in the Stern layer is assumed to be concentrated in one plane, called inner Helmholtz plane (iHp). This plane

almost coincides with the metal surface. We do not consider the details of the structure beyond the inner Helmholtz plane. The boundary between the Stern layer and the diffuse layer is termed outer Helmholtz plane (oHp). The voltage difference between inner and outer Helmholtz plane is called Stern layer voltage drop $\Delta\phi_s(\theta)$. The electric potential V at the inner Helmholtz plane is determined by $\Delta\phi_s(\theta)$ and the change of the potential between outer Helmholtz plane and infinity $\phi(1,\theta)$ as

$$V = \Delta\phi_s(\theta) + \phi(1,\theta). \tag{2.13}$$

Since an electric current is flowing through the swimmer, the potential V cannot be strictly constant inside the metal. However, the electric conductivity of the metal swimmer is much higher than the conductivity of the surrounding solution. Therefore, the variation of V is negligible. The potential drop $\Delta\phi_s(\theta)$ across the Stern layer needs to be determined. Since the Stern layer outside the inner Helmholtz plane is charge free, Gauss's law can be employed to arrive at

$$\Delta\phi_s(\theta) = -\lambda_s \frac{\partial\phi(r,\theta)}{\partial r}|_{r=1}, \tag{2.14}$$

where the parameter λ_s is the dimensionless thickness of the Stern layer between inner and outer Helmholtz plane.

The electrocatalytic process leading to a decomposition of H_2O_2 is supposed to take place at the inner Helmholtz plane. It leads to an absorption and emission of H^+ ions with a rate $\alpha(\theta)$, nondimensionalized with the flux $\mathcal{C}_\mathrm{i}\, D/R$. Boundary conditions, determining the concentrations of ions, result as

$$\hat{\mathbf{e}}_r \mathbf{j}_{\mathrm{H},+}(1,\theta) = \alpha(\theta), \tag{2.15}$$

$$\hat{\mathbf{e}}_r \mathbf{j}_{\mathrm{i},\pm}(1,\theta) = \hat{\mathbf{e}}_r \mathbf{j}_{\mathrm{H},-}(1,\theta) = 0, \tag{2.16}$$

$$c_{\mathrm{i},\pm}(r\to\infty,\theta) = 1, \tag{2.17}$$

$$c_{\mathrm{H},\pm}(r\to\infty,\theta) = \delta. \tag{2.18}$$

The constant δ is the relative concentration of H^+ ions in the bulk. It is defined by

$$\delta \equiv \tilde{c}_{\mathrm{H},+}(\infty)/\mathcal{C}_\mathrm{i}. \tag{2.19}$$

In order to keep the charge of the swimmer constant the exchange of cations at its surface must satisfy

$$\int \hat{\mathbf{e}}_r \mathbf{j}_{\mathrm{H},+}(1,\theta)\, \mathrm{d}A_{r=1} = 0. \tag{2.20}$$

The redox reactions at the swimmer's surface cause proton fluxes and involve a charge transfer. Therefore, the electric potential influences the reaction rate. This dependence is modeled with Butler-Volmer kinetics [81, 19, 16]. One assumes that the reaction takes place at the inner Helmholtz plane, which almost coincides with the metal surface of the

swimmer (see Fig. 2.2). Since the Stern layer is only described in an effective way, the energetic cost of passing from the outer to the inner Helmholtz plane must be incorporated explicitly into the reaction rates. This is commonly done with a so-called Frumkin correction where the rates depend exponentially on $\Delta\phi_s(\theta)$. Rates $\sim e^{\pm\frac{\Delta\phi_s(\theta)}{2}}$ are chosen here, where the transfer coefficient, modifying $\Delta\phi_s$ in the exponents, is set to 1/2. Further effects of the compact salt layer, that could, e.g., reduce the catalytic activity by covering the active sites, are neglected. Evidently, ϕ also modifies the reaction rate by influencing the concentration of protons right outside the Stern layer $c_{\mathrm{H},+}(1,\theta)$. This dependence is however implicit and it does not appear in the rate equation.
We assume that the same types of reactions happen on both sides of the swimmer. However, the two different metal properties lead to different rate constants on opposite sides of the particle. The following rate of proton exchange at the swimmer's surface is assumed:

$$\alpha(\theta) = -\left(\kappa_1 + k_1\cos\theta\right) e^{-\frac{\Delta\phi_s(\theta)}{2}} c_{\mathrm{H},+}(1,\theta) c_{H_2O_2} + \left(\kappa_2 - k_2\cos\theta\right) e^{\frac{\Delta\phi_s(\theta)}{2}} c_{H_2O_2}, \qquad (2.21)$$

with $\kappa_1 \geq k_1$ and $\kappa_2 \geq k_2$. The first term in Eq. (2.21) models the catalytic reduction of H_2O_2 while the second term models the provision of H^+ ions through an oxidation. The reaction rate constants vary from $\kappa_1 + k_1, \kappa_2 - k_2$ on one side of the swimmer to $\kappa_1 - k_1, \kappa_2 + k_2$ on the other side. The smooth variation between the two values is a simplifying assumption. It is further assumed that a diffusive supply of H_2O_2 is not the bottleneck of the reaction mechanism and that the encounter of H_2O_2 with the surface can be incorporated in the effective rate constants. The linear dependence of $\alpha(\theta)$ on the bulk concentration of H_2O_2 rescales all rate constants in the same way. $c_{H_2O_2}$ is expressed in (dimensionless) fractions of 1 % wt/v.

For a single metal, an electric potential can be defined with respect to infinity at which the electric current vanishes. Such potentials are given for the surface properties at $\vartheta = 0$ and $\vartheta = \pi$ by $V^{\mathrm{mix}}_{\vartheta=0} \equiv \ln[\delta(\kappa_1 + k_1)/(\kappa_2 - k_2)]$ and $V^{\mathrm{mix}}_{\vartheta=\pi} \equiv \ln[\delta(\kappa_1 - k_1)/(\kappa_2 + k_2)]$ respectively. These are not equilibrium electrode potentials since both the forward and the reverse reaction rely on the continuous dissociation of H_2O_2. The difference of the potentials can be compared to measurements of mixed potentials as

$$\tilde{V}^{\mathrm{mix}}_{\vartheta=0} - \tilde{V}^{\mathrm{mix}}_{\vartheta=\pi} = \frac{kT}{Ze} \ln\left[\frac{(\kappa_1 + k_1)(\kappa_2 + k_2)}{(\kappa_2 - k_2)(\kappa_1 - k_1)}\right]. \qquad (2.22)$$

Wang et al. [130] found mixed potentials of $15 - 150\,\mathrm{mV}$ for their microswimmers.

2.2.3 Hydrodynamic equations

The mass flow velocity $\mathbf{u}$ is determined by the Stokes equation (1.27) with an electrostatic body force

$$\nabla\cdot\sigma = \nabla^2\mathbf{u} - \nabla p = g\left(c_+ - c_-\right)\nabla\phi \qquad (2.23)$$

where the nondimensional constant

$$g \equiv \frac{R\mathcal{C}_{\mathrm{i}}kT}{\eta\mathcal{U}} \tag{2.24}$$

was defined. The boundary conditions on the fluid flow are

$$\mathbf{u}(r \to \infty, \theta) = -U\hat{\mathbf{e}}_z, \tag{2.25}$$

$$\mathbf{u}(0, \theta) = 0. \tag{2.26}$$

For a body force $g\,(c_+ - c_-)\,\nabla\phi$ that is independent of the fluid velocity $\mathbf{u}$ one can employ Teubner's formula, Eq. (1.38), to calculate the speed.

2.3 Theory for thin diffuse layers

In this section, a systematic expansion for small dimensionless Debye length, $\lambda \ll 1$, is presented. The theory is in line with the classical approach outlined, e.g, by Hunter [55] but applies to active swimming and is not limited to a linear response regime.

2.3.1 Nonlinear theory

The strategy applied in the following is to solve the nonlinear field equations both in an outer region, far away from the surface, and inside the diffuse layer. The inner and outer solutions are then matched to each other, such that an uniformly valid solution can be constructed. New variables for the concentrations are defined as

$$\begin{aligned} m^{\{\mathrm{H,i}\}} &\equiv c_{\{\mathrm{H,i}\},+} - c_{\{\mathrm{H,i}\},-} \\ &= m_0^{\{\mathrm{H,i}\}} + \lambda\, m_1^{\{\mathrm{H,i}\}} + \ldots, \\ M^{\{\mathrm{H,i}\}} &\equiv c_{\{\mathrm{H,i}\},+} + c_{\{\mathrm{H,i}\},-} \\ &= M_0^{\{\mathrm{H,i}\}} + \lambda\, M_1^{\{\mathrm{H,i}\}} + \ldots, \\ \phi &= \phi_0 + \lambda\,\phi_1 + \ldots\,. \end{aligned} \tag{2.27}$$

Outer variables carry a hat ($\hat{}$), variables for the fields inside the diffuse layer do not carry a hat. The potential ϕ_0 is written as sum of an inner and outer solution

$$\phi_0 = \psi_0 + \hat{\psi}_0. \tag{2.28}$$

The equations determining the outer variables $\hat{M}_0^{\{\mathrm{H,i}\}}$, $\hat{m}_0^{\{\mathrm{H,i}\}}$ and $\hat{\psi}_0$ are written in terms of r and θ. The Poisson-Boltzmann equation (2.10) in the outer region reads with $\hat{m} \equiv \hat{m}^{\mathrm{H}} + \hat{m}^{\mathrm{i}}$

$$\nabla^2\left(\hat{\psi}_0 + \lambda\hat{\psi}_1 \ldots\right) = -\frac{1}{2\lambda^2}\left(\hat{m}_0 + \lambda\hat{m}_1 + \lambda^2\hat{m}_2 \ldots\right), \tag{2.29}$$

which is singular for $\lambda \to 0$ and therefore we require $\hat{m}_0 = \hat{m}_1 = 0$. This provides the condition of charge neutrality outside the diffuse layer. The number of lowest order outer variables is hence reduced by one

$$\hat{m}_0^{\mathrm{H}} = -\hat{m}_0^{\mathrm{i}}. \tag{2.30}$$

Note that the condition of charge neutrality does not require that the charges of the different ions balance individually. The relation $\hat{m}^{\mathrm{H}} = \hat{m}^{\mathrm{i}} = 0$ only holds in the bulk, infinitely far away from the particle. Concerning the singular behavior of Eq. (2.29), it is clear that a charge of (vanishing) magnitude $\sim \lambda^2 \sim 1/\mathcal{C}_{\mathrm{i}}$ results in a non-vanishing lowest order electric field in the outer region. Therefore, the electric potential cannot be neglected in the diffusion equations (2.8,2.9) outside the diffuse layer. To lowest order Eqns. (2.8, 2.9) read in the outer region

$$\nabla \cdot \left(\nabla \hat{m}_0^{\mathrm{H}} + \hat{M}_0^{\mathrm{H}} \nabla \hat{\psi}_0 \right) = 0, \tag{2.31}$$

$$\nabla \cdot \left(-\nabla \hat{m}_0^{\mathrm{H}} + \hat{M}_0^{\mathrm{i}} \nabla \hat{\psi}_0 \right) = 0, \tag{2.32}$$

$$\nabla \cdot \left(\nabla \hat{M}_0^{\mathrm{H}} + \hat{m}_0^{\mathrm{H}} \nabla \hat{\psi}_0 \right) = 0, \tag{2.33}$$

$$\nabla \cdot \left(\nabla \hat{M}_0^{\mathrm{i}} - \hat{m}_0^{\mathrm{H}} \nabla \hat{\psi}_0 \right) = 0. \tag{2.34}$$

The convection terms do not appear in lowest order because the fluid velocity scales as λ^2 (see below). The boundary conditions for $r \to \infty$ are given by the bulk concentration of ions as

$$\hat{M}_0^{\mathrm{H}}(r \to \infty, \theta) = 2\,\delta, \tag{2.35}$$

$$\hat{M}_0^{\mathrm{i}}(r \to \infty, \theta) = 2, \tag{2.36}$$

$$\hat{m}_0^{\mathrm{H}}(r \to \infty, \theta) = 0, \tag{2.37}$$

$$\hat{\psi}_0(r \to \infty, \theta) = 0. \tag{2.38}$$

Near the surface, a stretched radial coordinate $y \equiv (r-1)/\lambda$ is employed like in Sec. 1.5.1. The diffusion equations in the inner region are expanded up to $O(\lambda^0)$ and read

$$0 = -\,\partial_y \left(\partial_y m_0^{\{\mathrm{H,i}\}} + M_0^{\{\mathrm{H,i}\}} \partial_y \psi_0 \right), \tag{2.39}$$

$$0 = -\,\partial_y \left(\partial_y M_0^{\{\mathrm{H,i}\}} + m_0^{\{\mathrm{H,i}\}} \partial_y \psi_0 \right). \tag{2.40}$$

The lowest order ion flux is $O(1)$. However, the fluxes pertaining to concentrations of $O(\lambda^0)$ vanish since the radial derivative introduces a factor of $1/\lambda$

$$-\left(\partial_y m_0^{\{\mathrm{H,i}\}} + M_0^{\{\mathrm{H,i}\}} \partial_y \psi_0 \right)_{y=0} = 0, \tag{2.41}$$

$$-\left(\partial_y M_0^{\{\mathrm{H,i}\}} + m_0^{\{\mathrm{H,i}\}} \partial_y \psi_0 \right)_{y=0} = 0. \tag{2.42}$$

The leading order result for the variables $m_0^{\{\mathrm{H,i}\}}(y,\theta)$, $M_0^{\{\mathrm{H,i}\}}(y,\theta)$ in the diffuse layer are then given by

$$m_0^{\{\mathrm{H,i}\}}(y,\theta) = a^{\{\mathrm{H,i}\}}(\theta)\, e^{-\psi_0(y,\theta)} - b^{\{\mathrm{H,i}\}}(\theta)\, e^{\psi_0(y,\theta)}, \tag{2.43}$$

$$M_0^{\{\mathrm{H,i}\}}(y,\theta) = a^{\{\mathrm{H,i}\}}(\theta)\, e^{-\psi_0(y,\theta)} + b^{\{\mathrm{H,i}\}}(\theta)\, e^{\psi_0(y,\theta)}, \tag{2.44}$$

with yet unknown constants. Matching between the diffuse layer and the outer region as $\lim_{y\to\infty}\{m_0^{\{\mathrm{H,i}\}}, M_0^{\{\mathrm{H,i}\}}\} = \lim_{r\to 1}\{\hat{m}_0^{\{\mathrm{H,i}\}}, \hat{M}_0^{\{\mathrm{H,i}\}}\}$ yields

$$a^{\{\mathrm{H,i}\}}(\theta) - b^{\{\mathrm{H,i}\}}(\theta) = \hat{m}_0^{\{\mathrm{H,i}\}}(1,\theta), \tag{2.45}$$

$$a^{\{\mathrm{H,i}\}}(\theta) + b^{\{\mathrm{H,i}\}}(\theta) = \hat{M}_0^{\{\mathrm{H,i}\}}(1,\theta). \tag{2.46}$$

The number of constants $a^{\{\mathrm{H,i}\}}$, $b^{\{\mathrm{H,i}\}}$ in the solutions is larger than the number of equations. One needs to consider the matching of the $O(\lambda)$ solutions in order to obtain the full lowest order solution. The result of this further matching process are conservation equations for the radial solute fluxes, which are not derived here for brevity

$$\Big(-\partial_r \hat{M}_0^{\mathrm{H}}(r,\theta) - \hat{m}_0^{\mathrm{H}}(r,\theta)\partial_r\hat{\psi}_0(r,\theta)\Big)_{r=1} = \alpha_0(\theta), \tag{2.47}$$

$$\Big(-\partial_r \hat{M}_0^{\mathrm{i}}(r,\theta) + \hat{m}_0^{\mathrm{H}}(r,\theta)\partial_r\hat{\psi}_0(r,\theta)\Big)_{r=1} = 0, \tag{2.48}$$

$$\Big(-\partial_r \hat{m}_0^{\mathrm{H}}(r,\theta) - \hat{M}_0^{\mathrm{H}}(r,\theta)\partial_r\hat{\psi}_0(r,\theta)\Big)_{r=1} = \alpha_0(\theta), \tag{2.49}$$

$$\Big(\partial_r \hat{m}_0^{\mathrm{H}}(r,\theta) - \hat{M}_0^{\mathrm{i}}(r,\theta)\partial_r\hat{\psi}_0(r,\theta)\Big)_{r=1} = 0. \tag{2.50}$$

$\alpha_0(\theta)$ is the lowest order reaction rate at the surface, see Eq. (2.21). In the inner region, the Poisson-Boltzmann equation is non-singular. It reads up to $O(\lambda^0)$

$$\partial_y^2\psi_0(y,\theta) = -\frac{m_0}{2} = B(\theta)\sinh\psi_0(y,\theta). \tag{2.51}$$

This equation, determining the nonequilibrium concentration near the surface, has the same form as the corresponding equilibrium equation. The result for the potential in the diffuse layer is

$$\phi_0(y,\theta) = \psi_0(y,\theta) + \hat{\psi}_0(1,\theta) = 2\ln\left[\frac{1+\gamma(\theta)e^{-\sqrt{B(\theta)}y}}{1-\gamma(\theta)e^{-\sqrt{B(\theta)}y}}\right] + \hat{\psi}_0(1,\theta), \tag{2.52}$$

with

$$B(\theta) = \Big(\hat{M}_0^{\mathrm{H}}(1,\theta) + \hat{M}_0^{\mathrm{i}}(1,\theta)\Big)/2. \tag{2.53}$$

We also employed a yet undefined function $\gamma(\theta)$. The value of the potential at the outer periphery of the diffuse layer $\hat{\psi}_0(1,\theta)$ is determined through the solution of Eqns. (2.31-2.34). Given $\hat{\psi}_0(1,\theta)$, the overall change in potential over the diffuse layer $\Delta\phi_0(\theta)$ is according to Eq. (2.13)

$$\Delta\phi_0(\theta) \equiv \psi_0(0,\theta) = V_0 - \Delta\phi_s(\theta) - \hat{\psi}_0(1,\theta). \tag{2.54}$$

The voltage drop over the Stern layer is calculated through Eq. (2.14), which is in terms of inner variables

$$\Delta\phi_s(\theta) = -\frac{\lambda_s}{\lambda}\frac{\partial\psi_0(y,\theta)}{\partial y}|_{y=0} = \frac{\lambda_s}{\lambda}\sqrt{B(\theta)}\frac{\gamma(\theta)}{1-\gamma(\theta)^2}. \tag{2.55}$$

Insertion of Eq. (2.55) into Eq. (2.54) yields a transcendental equation for $\gamma(\theta)$ as

$$V_0 = \frac{\lambda_s}{\lambda}\sqrt{B(\theta)}\frac{\gamma(\theta)}{1-\gamma(\theta)^2} + 2\ln\left[\frac{1+\gamma(\theta)}{1-\gamma(\theta)}\right] + \hat{\psi}_0(1,\theta), \tag{2.56}$$

which now allows the full determination of the potential in the diffuse layer. The voltage drop across the Stern layer $\Delta\phi_s(\theta)$ is calculated through Eq. (2.14). $\Delta\phi_0(\theta)$ can be interpreted as an angle-dependent zeta potential. In order to calculate the lowest order swimming speed in $\hat{\mathbf{e}}_z$-direction Teubner's formula (1.38) is expanded for $\lambda \ll 1$. The lowest order result is

$$U_0 = g\lambda^2\int_0^\infty\int_0^\pi \frac{m_0(y,\theta)}{2}\left[y^2\partial_y\phi_0(y,\theta)\cos\theta - y\partial_\theta\phi_0(y,\theta)\sin\theta\right]\sin\theta\,\mathrm{d}\theta\mathrm{d}y. \tag{2.57}$$

On inserting Eqns. (2.43, 2.44, 2.52) including the matched constants and using partial integration we find

$$\begin{aligned} U \approx U_0 = \; & g\lambda^2\int_0^\pi [\Delta\phi_0(\theta)\,\frac{\partial\hat{\psi}_0(1,\theta)}{\partial\theta}\,\sin^2(\theta) - \\ & 4\ln\left(\cosh\left(\frac{\Delta\phi_0(\theta)}{4}\right)\right)\frac{\partial\ln\left(B(\theta)\right)}{\partial\theta}\,\sin^2(\theta)\,]\mathrm{d}\theta. \end{aligned} \tag{2.58}$$

We will omit the index at U_0 in the following since we do not deal with higher orders in λ. An explicit calculation of the swimming speed requires the knowledge of the outer fields at $r = 1$. Therefore, the pertaining differential Eqns. (2.31-2.34) need to be solved with the boundary conditions (2.35-2.38, 2.47-2.50). Moreover, the potential V_0 of the swimmer depends through the charge conservation equation (2.20) on α and must be determined simultaneously with the concentration fields. The whole task can only be done numerically. To this end, we implement an efficient pseudospectral method [20, 24], where the discretized system of differential equations is solved with the Newton-Raphson method. In radial direction, we use a Chebychev grid with 30 nodes. The grid in angular direction, for $\theta = 0\ldots\pi$, is uniformly spaced with 40 nodes.

Remarkably, Eq. (2.58) has the same form as the celebrated formula by Dukhin and Derjaguin [34, 6], which was derived for the linear response regime. The only difference is that the potential drop across the diffuse layer cannot be approximated by the equilibrium zeta potential and is now θ-dependent. The dependence of U on $\Delta\phi_0$ allows to separate electrophoretic and chemiphoretic (diffusiophoretic) contributions in the lowest order swimming speed [96]. The first term in the integrand of Eq. (2.58) changes

sign with $\Delta\phi_0$, similar to electrophoresis, where the particle swimming is also reversed with the sign of the zeta potential. Therefore, the first term can be interpreted as the electrophoretic part. The second term does not change sign with the potential $\Delta\phi_0$ since $-4\ln(\cosh(\Delta\phi_0/4)) = 2\ln(1-\gamma^2)$ is negative semi-definite. Its dependence on a gradient in overall concentration suggests an interpretation of the second term as chemiphoretic contribution.

2.3.2 Analytical approximation

We assume now that the chemical properties of the two metals of which the swimmer consists are quite similar. This case can be modeled by setting $\kappa_1,\ \kappa_2 \gg k_1,\ k_2$. If k_1 and k_2 are neglected, no net cation flux can take place since a radially symmetric flux violates the charge conservation. Although being a nonequilibrium steady state, the concentrations of ions follow an equilibrium distribution throughout the whole system. Solutions for the outer field variables of order $(k_1^0,\ k_2^0)$ are easily determined from Eqns. (2.31-2.34) with $\hat{\psi}_{0,0} = 0$ to be $\hat{M}^{\mathrm{H}}_{0,0} = 2\delta$, $\hat{M}^{\mathrm{i}}_{0,0} = 2$, $\hat{m}^{\mathrm{H}}_{0,0} = \hat{m}^{\mathrm{i}}_{0,0} = 0$. The second indices 0 designate the solution of order $(k_1^0,\ k_2^0)$. The inner fields of order k_1^0, k_2^0 obey the differential equations

$$0 = -\left(\partial_y m^{\mathrm{H,i}}_{0,0} + M^{\mathrm{H,i}}_{0,0}\partial_y\phi_{0,0}\right), \tag{2.59}$$

$$0 = -\left(\partial_y M^{\mathrm{H,i}}_{0,0} + m^{\mathrm{H,i}}_{0,0}\partial_y\phi_{0,0}\right), \tag{2.60}$$

and the solutions are given by Eqns. (2.43, 2.44) with $a^{\mathrm{H}}_{0,0} = b^{\mathrm{H}}_{0,0} = \delta$, and $a^{\mathrm{i}}_{0,0} = b^{\mathrm{i}}_{0,0} = 1$. The indices again denote the λ^0 and k_1^0, k_2^0 order. The potential $\phi_{0,0}$ is

$$\phi_{0,0}(y) = 2\ln\left[\frac{1+\gamma_0 e^{-\sqrt{B_0}y}}{1-\gamma_0 e^{-\sqrt{B_0}y}}\right], \tag{2.61}$$

with $B_0 = \delta+1$ and $\gamma_0 = \tanh(\phi_{0,0}(0)/4)$. The chemical reaction rate, Eq. (2.21), becomes

$$0 = -\kappa_1 e^{-\frac{\Delta\phi_{s,0}}{2}}\delta\, e^{-\phi_{0,0}(0)}c_{H_2O_2} + \kappa_2 e^{\frac{\Delta\phi_{s,0}}{2}}c_{H_2O_2}, \tag{2.62}$$

It follows that the swimmer's potential in steady state

$$V_{0,0} \equiv \Delta\phi_{s,0} + \phi_{0,0}(0) = \ln(\kappa_1\delta/\kappa_2) \tag{2.63}$$

does not depend explicitly on the H_2O_2 concentration to lowest order. Nevertheless, $V_{0,0}$ is not the equilibrium potential. For the outer variables of first order in $k_1,\ k_2$ we demand $\hat{m}^{\mathrm{i}}_{0,1} = -\hat{m}^{\mathrm{H}}_{0,1}$. The field equations read then

$$\nabla^2\hat{\psi}_{0,1} = \nabla^2 M^{\mathrm{H}}_{0,1} = \nabla^2 M^{\mathrm{i}}_{0,1} = 0, \tag{2.64}$$

$$\nabla^2 m^{\mathrm{H}}_{0,1} + (1+\delta)\nabla^2\hat{\psi}_{0,1} = 0. \tag{2.65}$$

The corresponding boundary conditions are

$$\begin{aligned} -\partial_r \hat{M}^{\mathrm{H}}_{0,1}|_{r=1} &= \alpha_{0,1}, \\ -\partial_r \hat{M}^{\mathrm{i}}_{0,1}|_{r=1} &= 0, \\ -\left(\partial_r \hat{m}^{\mathrm{H}}_{0,1} - 2\delta\partial_r\hat{\psi}_{0,0}\right)|_{r=1} &= \alpha_{0,1}, \\ \left(\partial_r \hat{m}^{\mathrm{H}}_{0,1} - 2\partial_r\hat{\psi}_{0,0}\right)|_{r=1} &= 0, \\ \hat{M}^{\mathrm{H}}_{0,1}|_{r=\infty} = \hat{M}^{\mathrm{i}}_{0,1}|_{r=\infty} = \hat{m}^{\mathrm{H}}_{0,1}|_{r=\infty} &= 0, \\ \hat{\psi}|_{r=\infty} &= 0. \end{aligned} \tag{2.66}$$

Taken together, these equations yield

$$\hat{M}^{\mathrm{i}}_{0,1} = 0, \tag{2.67}$$

$$\hat{M}^{\mathrm{H}}_{0,1} = \sum_{n=0}^{\infty} A_n\, P_n(\cos\theta)\, r^{-n-1}, \tag{2.68}$$

$$\hat{m}^{\mathrm{H}}_{0,1} = \hat{M}^{\mathrm{H}}_{0,1}/(\delta+1), \tag{2.69}$$

$$\hat{\psi}_{0,1} = \hat{M}^{\mathrm{H}}_{0,1}/(2\delta+2), \tag{2.70}$$

where the coefficients of the expansion in Legendre polynomials $P_n(\cos\theta)$ are calculated from

$$-\partial_r \hat{M}^{\mathrm{H}}_{0,1}|_{r=1} = \sum_{n=0}^{\infty} (n+1)\, A_n P_n(\cos\theta) = \alpha_{0,1}. \tag{2.71}$$

For the corresponding inner variables of first order in k_1, k_2 the differential equations

$$0 = -\left(\partial_y m_{0,1} + M_{0,1}\partial_y\psi_{0,0} + M_{0,0}\partial_y\phi_{0,1}\right), \tag{2.72}$$

$$0 = -\left(\partial_y M_{0,1} + m_{0,1}\partial_y\psi_{0,0} + m_{0,0}\partial_y\phi_{0,1}\right), \tag{2.73}$$

result in

$$m^{\mathrm{H,i}}_{0,1} = a^{\mathrm{H,i}}_{0,1} e^{-\phi_{0,0}} - b^{\mathrm{H,i}}_{0,1} e^{\phi_{0,0}} - \phi_{0,1} M^{\mathrm{H,i}}_{0,0}, \tag{2.74}$$

$$M^{\mathrm{H,i}}_{0,1} = a^{\mathrm{H,i}}_{0,1} e^{-\phi_{0,0}} + b^{\mathrm{H,i}}_{0,1} e^{\phi_{0,0}} - \phi_{0,1} m^{\mathrm{H,i}}_{0,0}. \tag{2.75}$$

Matching now as $\lim_{y\to\infty} M^{\mathrm{H,i}}_{0,1} = \hat{M}^{\mathrm{H,i}}_{0,1}|_{r=1}$, $\lim_{y\to\infty} m^{\mathrm{H}}_{0,1} = \hat{m}^{\mathrm{H}}_{0,1}|_{r=1}$, $\lim_{y\to\infty}\psi_{0,1} = \hat{\psi}_{0,1}|_{r=1}$ we find $b^{\mathrm{i}}_{0,1} = -a^{\mathrm{i}}_{0,1} = 0$, $b^{\mathrm{H}}_{0,1} = 0$ and

$$a^{\mathrm{H}}_{0,1} = \sum_{n=0}^{\infty} A_n P_n(\cos\theta). \tag{2.76}$$

Up to first order in k_1, k_2, the H^+ concentration just outside the Stern layer follows as

$$c_{\mathrm{H}+} \approx \delta e^{-\phi_{0,0}} + \frac{M^{\mathrm{H}}_{0,1} + m^{\mathrm{H}}_{0,1}}{2} = \delta e^{-\phi_{0,0}} + \left(a^{\mathrm{H}}_{0,1} - \delta\phi_{0,1}\right) e^{-\phi_{0,0}}. \tag{2.77}$$

Now the reaction rate α_0 can be calculated in first order. The concentration from Eq. (2.77) is inserted in Eq. (2.21) with (2.62). The boundary condition for the potential Eq. (2.63) in order k_1^0, k_2^0 is also employed along with the corresponding first order Stern layer boundary condition

$$V_{0,1} = \psi_{0,1}(0,\theta) + \Delta\phi_{s,1}(\theta), \tag{2.78}$$

to yield

$$\alpha_{0,1}(\theta) = e^{\frac{\Delta\phi_{s,0}}{2}} \left(-\frac{a^{\mathrm{H}}_{0,1}\kappa_2}{\delta} + \kappa_2 V_{0,1} - \cos\theta \left(k_2 + k_1 \frac{\kappa_2}{\kappa_1} \right) \right). \tag{2.79}$$

This expression along with Eqns. (2.71, 2.76) allows to determine $a^{\mathrm{H}}_{0,1}$. Since the swimmer can not emit a net flux of cations, we demand that the radially symmetric part of $\alpha_{0,1}$ vanishes. Therefore we find with Eqns. (2.71, 2.76), $A_0 = 0$, $V_{0,1} = 0$, and

$$a^{\mathrm{H}}_{0,1} = -\delta \frac{k_2 + k_1 \frac{\kappa_2}{\kappa_1}}{2\delta\, e^{-\frac{\Delta\phi_{s,0}}{2}} + \kappa_2} \cos\theta. \tag{2.80}$$

In order to calculate the swimming speed with Eq. (2.57) we first consider the body force in the diffuse layer

$$m_0 \nabla\phi_0 \approx (m^{\mathrm{H}}_{0,1} + m^{\mathrm{i}}_{0,1})\, \hat{\mathbf{e}}_r\, \partial_r \phi_{0,0} + (1+\delta)(e^{-\phi_{0,0}} - e^{\phi_{0,0}}) \nabla\phi_{0,1}. \tag{2.81}$$

On inserting the expressions for $m_{0,1}$, we find

$$m_0 \nabla\phi_0 \approx a^{\mathrm{H}}_{0,1} e^{-\phi_{0,0}}\, \hat{\mathbf{e}}_r\, \partial_r \phi_{0,0} + (1+\delta) \nabla \left((e^{-\phi_{0,0}} - e^{\phi_{0,0}}) \phi_{0,1} \right). \tag{2.82}$$

Since the second term in the body force is a gradient, it only modifies the hydrodynamic pressure and does not cause motion of the swimmer in the incompressible limit. Therefore, the first order potential $\phi_{0,1}$ is irrelevant for the swimming speed. Inserting Eq. (2.82) with Eq. (2.80) into Eq. (2.57), the swimming speed up to first order becomes

$$U \approx g\lambda^2 \frac{8}{3} \frac{\ln(1+\gamma_0)}{1+\delta} \frac{\delta \left(k_2 + k_1 \frac{\kappa_2}{\kappa_1} \right) c_{H_2O_2}}{2\delta\, e^{-\frac{\Delta\phi_{s,0}}{2}} + \kappa_2 c_{H_2O_2}}. \tag{2.83}$$

For a weak potential outside the compact layer, $\phi_{0,0} \lesssim 1$, the dependence of the swimming speed on the particle potential can be estimated with $\ln(1+\gamma_0) \simeq (V_0 - \Delta\phi_{s,0})/4$. A slightly more general version of Eq. (2.83) for arbitrary distribution of solute emission reads

$$U \approx -g\lambda^2 \frac{2\ln(1+\gamma_0)}{1+\delta} \int_{-1}^{1} \alpha_{0,1}(\theta) \cos\theta \, \mathrm{d}\cos\theta \tag{2.84}$$

where the integral is a measure of the dipole moment of the first order H^+ emission/absorption rate $\alpha_{0,1}$. Expressions similar to Eq. (2.84) have been derived with other techniques for the linear response regime [134], but not for the steady-state system considered here.

2.4 Numerical values for the model constants

The thermal energy scale is $kT = 4.11 \times 10^{-21}$J. The solution viscosity is fixed at $\eta = 9 \times 10^{-4}$ Pa s. The permittivity of the solution around the swimmer is $\varepsilon = 80\,\varepsilon_{\text{vacuum}}$. Typically, the experimental swimmers have lengths in the 300 nm - 5 μm range. Accordingly, the radius of our swimmer is set to

$$R \equiv 1\,\mu\text{m}. \tag{2.85}$$

A velocity scale can be defined independently of the concentration scale as

$$\mathcal{U}g\lambda^2 = \frac{(kT)^2\,\varepsilon}{8\pi\eta\,(Ze)^2 R} \simeq 20.6\,\mu\text{m/s}. \tag{2.86}$$

In this chapter, the primary purpose of the salt in the solution is the explicit justification of the thin diffuse layer model. Where not mentioned otherwise, the bulk concentration of salt ions is in the following set to

$$\mathcal{C}_\text{i} = 5 \times 10^{-5}\ \text{mol/L}. \tag{2.87}$$

For a monovalent salt, e.g., $NaNO_3$ as used by Paxton et al. [89], the diffuse layer is according to Eq. (2.11) about 12 nm thick. Since this is much less than $R = 1\,\mu$m, the theory for $\lambda \ll 1$ is expected to work well. The absolute thickness of the Stern layer is assumed to be in the order of a molecular diameter [129], which might be about $0.3\,nm$.

We consider a $[10^{-4} \ldots 5]$ % solution of H_2O_2 in water. Percent of H_2O_2 concentration are given in wt/v. 1 % wt/v corresponds to 10 g H_2O_2 per liter solvent, molar mass of H_2O_2: 34.02 g/mol. The pH value decreases here almost linearly with an increase of H_2O_2 concentration [1]. It lies roughly between 7 and 5. This sets the concentration of bulk protons and hydroxide ions to $\tilde{c}_{\text{H},\pm}(\infty) \simeq [10^{-7} \ldots 10^{-5}]$ mol/L. The relative concentration of H^+ ions in the bulk is then in the range $\delta = \tilde{c}_\text{H}(\infty)/\mathcal{C}_\text{i} \simeq [10^{-3} \ldots 10^{-1}]$.

For the diffusion constant $D = 7 \times 10^{-9}\text{m}^2/\text{s}$ is chosen. The ion fluxes at the surface are then nondimensionalized with

$$\mathcal{C}_\text{i} D/R = 3.5 \times 10^{-4}\,\text{mol}/(\text{m}^2\,\text{s}). \tag{2.88}$$

A measured [89] evolution rate of O_2 for a 3.7 % solution of H_2O_2 is $8.7 \times 10^{-6}\text{mol}/(\text{m}^2\,\text{s})$. Within the reaction model, Eq. (2.21), this rate roughly determines the magnitude of the second term, responsible for the oxidation of H_2O_2. For $c_{H_2O_2} = 1$ (1 %) we estimate that $\kappa_2\, c_{H_2O_2}$ is on the order of 10^{-2}. The constants κ_1, k_1, k_2 are chosen such that reasonable values for the swimming speed and the proton fluxes are obtained.

2.5 Results

In this section, dimensional results are plotted in order to facilitate a (future) comparison with experimental data. The dimensional speed is calculated as $\tilde{U} = \mathcal{U}\, U = 20.6\,\mu\mathrm{m/s} \times \mathrm{U}/(\mathrm{g}\lambda^2)$. Results for the analytical approximation of U (Eq. (2.83)) are also shown where applicable.

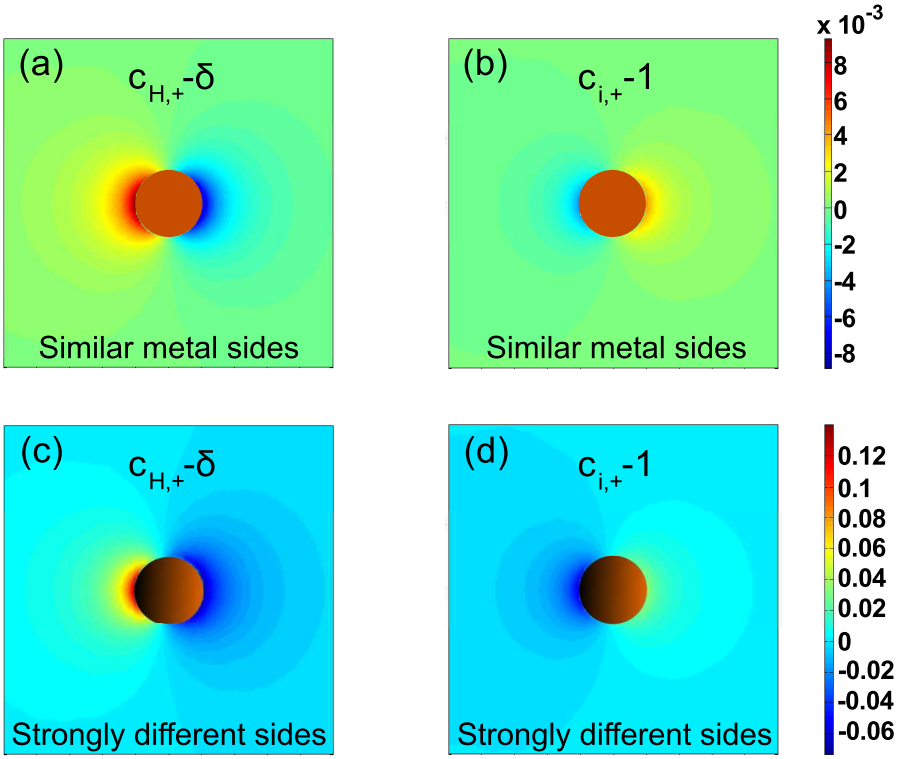

Figure 2.3: Concentrations of H^+ ions and positive salt ions. Figs. a,b and c,d each have have the same color coding. $c_{H_2O_2} = 1$ (1 %), $\kappa_1 = 0.0185$, $\kappa_2 = 0.185$, $\delta = 0.1$, and $\lambda_s = 0$. Figs. a,b: Reactivity varies only slightly across the swimmer $k_1 = 0.1\,\kappa_1$, $k_2 = 0.1\,\kappa_2$; resulting in $V_0 = -4.61$ and $U = -0.0398$. Figs. c,d: Reactivity varies strongly across the swimmer $k_1 = \kappa_1$, $k_2 = \kappa_2$; resulting in $V_0 = -5.03$ and $U = -0.485$.

2.5.1 Reaction induced concentration distortion

Fig. 2.3 shows exemplary concentration fields of positive ions around the swimmer. While the concentrations of H^+ in Figs. 2.3 a,c are directly determined through the surface reactions, the inhomogeneous distribution of positive salt ions seen in Figs. 2.3 b,d is an indirect effect. The positive salt ions accumulate oppositely to the H^+ ions. They

present a non-negligible contribution to the local charge balance. In Figs. 2.3 a,b we have $(k_1,\ k_2) \ll (\kappa_1,\ \kappa_2)$, i.e, the decomposition of H_2O_2 happens fairly homogeneously around the swimmer. In this case the concentration profile is antisymmetric and follows the distribution of surface reactivity. In Figs. 2.3 c,d we have set $k_1 = \kappa_1$ and $k_2 = \kappa_2$, i.e., the reaction happens mainly in an asymmetric way, where oxidation and reduction take place on different sides of the swimmer. Also, the concentration of H^+ ions in the bulk is not assumed to be excessive. Therefore the reaction is, to some extent, a diffusion limited process. Then, the concentration variation around the swimmer feeds back on the overall reaction rate, Eq. (2.21). Consequently, the antisymmetric distribution of the cations seen in Figs. 2.3 a,b is lost.

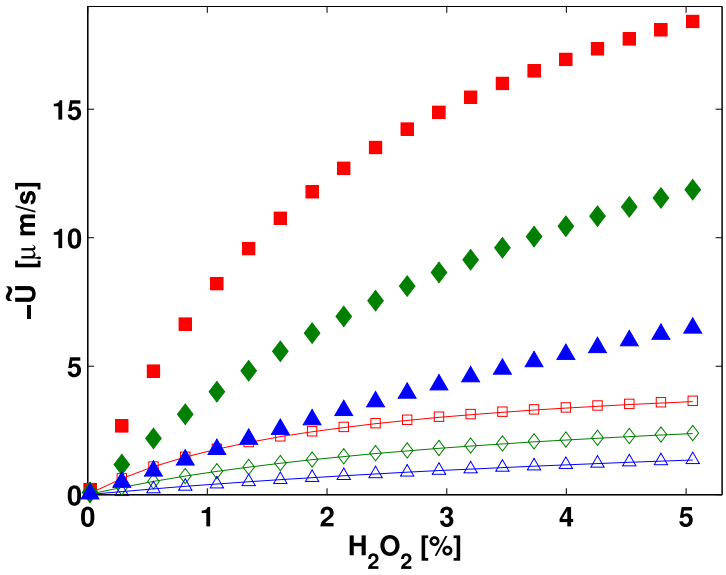

Figure 2.4: Swimming speed $\tilde{U}$ vs. H_2O_2 concentration at fixed pH value. $\kappa_1 = 0.005$, $\delta = 0.1$, $\lambda_s = 0$. Symbols are numerical results. Full lines are approximative speeds from Eq. (2.83). (■): $\kappa_2 = 0.1$, $k_2 = \kappa_2$, $k_1 = \kappa_1$. (□): $\kappa_2 = 0.1$, $k_2 = 0.25\,\kappa_2$, $k_1 = 0.25\,\kappa_1$. (♦): $\kappa_2 = 0.05$, $k_2 = \kappa_2$, $k_1 = \kappa_1$. (◊): $\kappa_2 = 0.05$, $k_2 = 0.25\,\kappa_2$, $k_1 = 0.25\,\kappa_1$. (▲): $\kappa_2 = 0.025$, $k_2 = \kappa_2$, $k_1 = \kappa_1$. (△): $\kappa_2 = 0.025$, $k_2 = 0.25\,\kappa_2$, $k_1 = 0.25\,\kappa_1$.

2.5.2 Swimming and H_2O_2 concentration, fixed pH

Fig. 2.4 demonstrates the dependence of the swimming speed $\tilde{U}$ on the concentration of H_2O_2 with a fixed pH value. A fixed pH value means that the availability of H^+ in the bulk, determined by δ, does not change with H_2O_2 concentration. Eq. (2.83) approximates the numerically calculated swimming speed well for $k_1 < \kappa_1$ and $k_2 < \kappa_2$. However, the

condition $k_2 < \kappa_1$ for the validity of the analytical approximation seems here unnecessary.

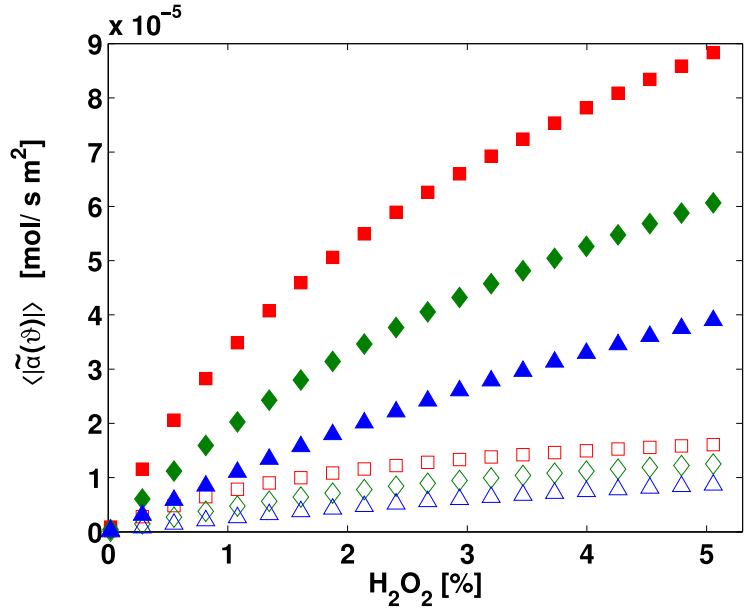

Figure 2.5: Average ion current $\langle|\alpha(\theta)|\rangle$ vs. H_2O_2 concentration at fixed pH value. Symbols are the same as in Fig. 2.4.

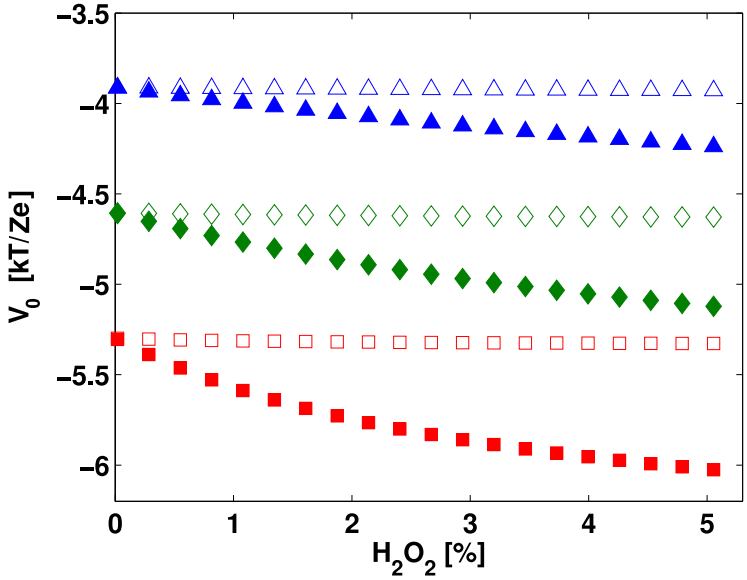

Figure 2.6: Electric potential of the swimmer V_0 vs. H_2O_2 concentration at fixed pH value. Symbols are the same as in Fig. 2.4.

The curves in Fig. 2.4 have a concave shape, which is not attributed to a saturation of the catalytic surface in our model. Rather, it results from a limitation of the reaction rate through the diffusion around the swimmer. Quantitative understanding of this effect

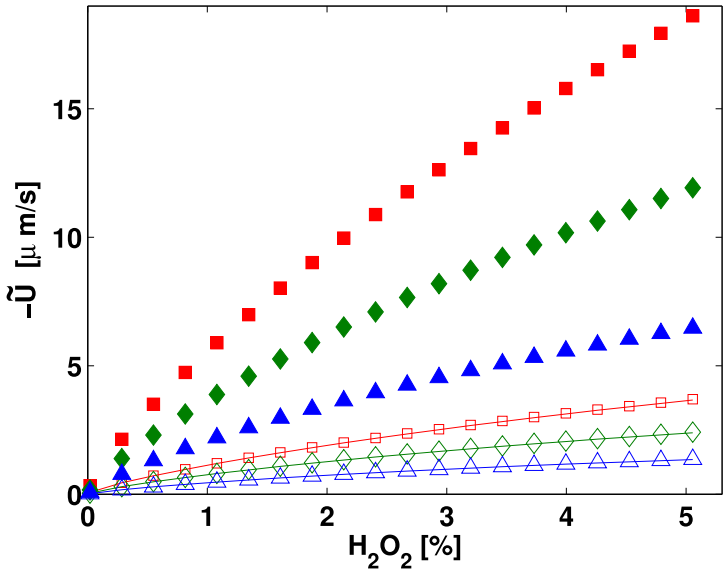

Figure 2.7: Dependence of swimming speed $\tilde{U}$ on H_2O_2 concentration where the pH value varies with $c_{H_2O_2}$. We use $\delta = 0.002 + 0.02\, c_{H_2O_2}$. Symbols are the same as in Fig. 2.4.

can be gained from the approximative equation (2.83). Here the swimming speed levels of since the rate of ion flux through the swimmer saturates for $\kappa_2 c_{H_2O_2} \gtrsim 2\delta\, e^{-\frac{\Delta\phi_{s,0}}{2}}$. This estimate is seen to hold also for the results from the nonlinear numerics. A negative Stern-layer voltage-drop $\Delta\phi_s$ shifts the saturation of the speed to higher values of $c_{H_2O_2}$, while also reducing the speed (see Sec. 2.5.5). Figs. 2.5,2.6 show how the average reaction rate $\langle|\alpha(\theta)|\rangle$ and the electric potential on the swimmer's surface V_0 change with the increase of H_2O_2. Note that $\langle|\alpha(\theta)|\rangle$ cannot be identified with the measurable oxygen evolution rate. $\langle|\alpha(\theta)|\rangle$ vanishes for equal redox potentials on both sides of the swimmer, i.e., if $k_1 = k_2 = 0$, while the oxygen evolution rate in this limit is, within the present model, an unknown constant. The measured values for the mixed potential from [130] are in accord with estimates from our model constants. From Eq. 2.22 we calculate approximate mixed potential differences of $15 - 150\,\mathrm{mV}$ if we fix the constants $k_1/\kappa_1 = k_2/\kappa_2$ roughly between 0.1 and 0.9.

2.5.3 Swimming and H_2O_2 concentration, variable pH

Since the concentration of H_2O_2 also influences the pH value we plot in Fig. 2.7 the speed vs. $c_{H_2O_2}$ with H_2O_2-dependent δ. The pH value decreases almost linearly with an increase of H_2O_2 concentration [1]. Therefore we set $\delta = \delta_0 + \delta_1\, c_{H_2O_2}$ where the dissociated water molecules at a pH value of 7 contribute $\delta_0 = (10^{-7}\mathrm{mol/L})/\mathcal{C}_\mathrm{i}$. The slope of the function is roughly estimated as $\delta_1 = 0.02$. As seen from Eq. (2.83), the speed does

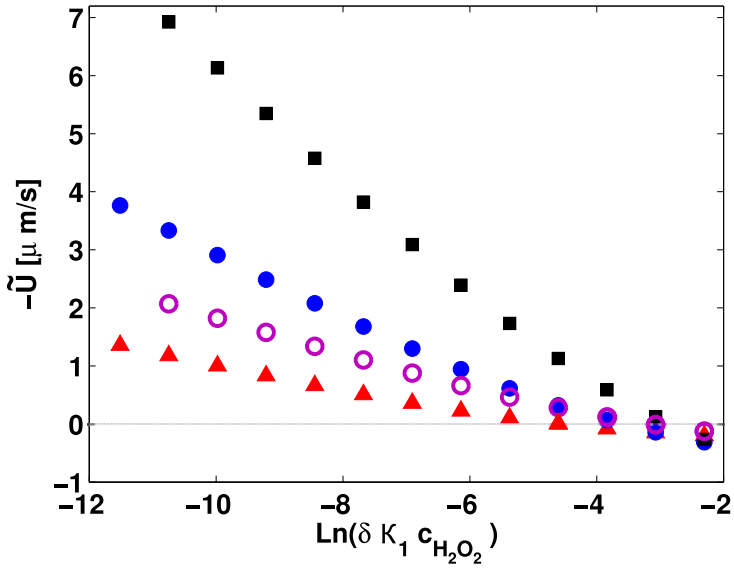

Figure 2.8: Dependence of swimming speed $\tilde{U}$ on the rate constant of H_2O_2 reduction κ_1 at $c_{H_2O_2} = 1$ (1 %) with $k_2 = \kappa_2$, $k_1 = \kappa_1$, and $\lambda_s = 0$. (■): $\delta = 0.1$, $\kappa_2 = 0.05$. (●): $\delta = 0.1$, $\kappa_2 = 0.025$. (○): $\delta = 0.01$, $\kappa_2 = 0.025$. (▲): $\delta = 0.1$, $\kappa_2 = 0.01$.

not saturate in this case until $\delta \gtrsim 1$. The curves in Fig. 2.7 show a reduced tendency to level-off in the investigated range of H_2O_2 concentration.

2.5.4 Swimming and H_2O_2 reduction rate

In Fig. 2.8 we investigate the role of the rate constants of H_2O_2 reduction, κ_1 and k_1, for the swimming speed. The quotient of κ_1 and k_1 is held constant. Eq. (2.83) therefore suggests that the swimming speed is only influenced through its dependence on the particle potential V_0 via the function γ. The approximation for the swimmer's potential, Eq. (2.63), in turn suggests that V_0 depends logarithmically on $\kappa_1\delta/\kappa_2$. The numerical data qualitatively supports a scaling of $\tilde{U}$ with this logarithm. The magnitude of the swimming speed is seen to decrease with an increase of κ_1. The negative sign of $\tilde{U}$ is in accordance with the experimental finding that the swimming occurs in direction of the H_2O_2-oxidizing end [130]. However, the swimming direction is reversed for $\kappa_1\delta > \kappa_2$, which results from the sign change of V_0.

2.5.5 Effect of the Stern layer

The Stern layer modifies the swimming speed for $V_0 < 0$ by reducing the reaction rate and the potential change in the diffuse layer, appearing in Eq. (2.58). Fig. 2.9 demonstrates

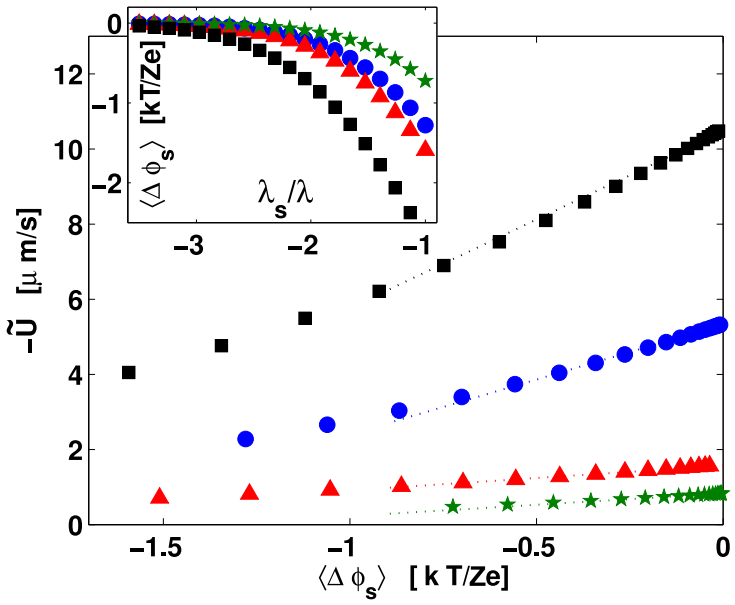

Figure 2.9: Dependence of swimming speed $\tilde{U}$ on the average Stern layer voltage drop $\langle\Delta\phi_s(\theta)\rangle$. Inset: dependence of $\langle\Delta\phi_s(\theta)\rangle$ on relative Stern layer thickness λ_s/λ. $c_{H_2O_2} = 1$ (1 %) with $k_2 = \kappa_2$, $k_1 = \kappa_1$. (■): $\delta = 0.1$, $\kappa_1 = 0.001$, $\kappa_2 = 0.1$. (•): $\delta = 0.1$, $\kappa_1 = 0.001$, $\kappa_2 = 0.05$. (★): $\delta = 0.1$, $\kappa_1 = 0.001$, $\kappa_2 = 0.01$. (▲): $\delta = 0.01$, $\kappa_1 = 10^{-4}$; $\kappa_2 = 0.01$. (Dotted lines): slopes predicted by an expansion of Eq. (2.83) for small $\Delta\phi_s$.

that $\tilde{U}$ decreases for our rate constants almost linearly with the average Stern layer voltage drop $\langle\Delta\phi_s(\theta)\rangle$. The approximation from Eq. (2.83) does not yield satisfactory absolute values for $\tilde{U}$ in Fig. 2.9 since we have here $k_1 = \kappa_1$ and $k_2 = \kappa_2$. However, Eq. (2.83) can be expanded for small $\Delta\phi_s$. It then predicts the slopes of the decrease of $\tilde{U}$ with $\Delta\phi_s$ fairly well. The inset of Fig. 2.9 demonstrates that $\Delta\phi_s$ depends nonlinearly on on the thickness of the layer λ_s/λ. This nonlinear relationship occurs since the Stern layer voltage drop is determined through a transcendental equation (see appendix, Eq. (2.56)).

The swimming speed scales within the thin diffuse layer model, Eq. (2.58), as the inverse of the overall bulk ion concentration $1/(\mathcal{C}_\mathrm{i} + \mathcal{C}_\mathrm{i}\delta)$. Experimental data qualitatively supports this scaling, but also indicates that the decrease of speed with salt concentration may be somewhat stronger [89]. One reason may be the Stern layer, which influences the reaction rate. In our simple model, the connection between the Stern layer and the reaction is given through the appearance of $\Delta\phi_s$ in the Butler-Volmer equation (2.21). For simplicity, we keep here the absolute thickness of the Stern layer constant. The variations of the bulk salt concentration still affects the Stern layer voltage drop $\Delta\phi_s$ since $\lambda_s/\lambda \sim \sqrt{\mathcal{C}_\mathrm{i}}$. Fig. 2.10 demonstrates that this suffices to cause a reduction of the swimming speed compared with the standard scaling. A precise measurement of the effect

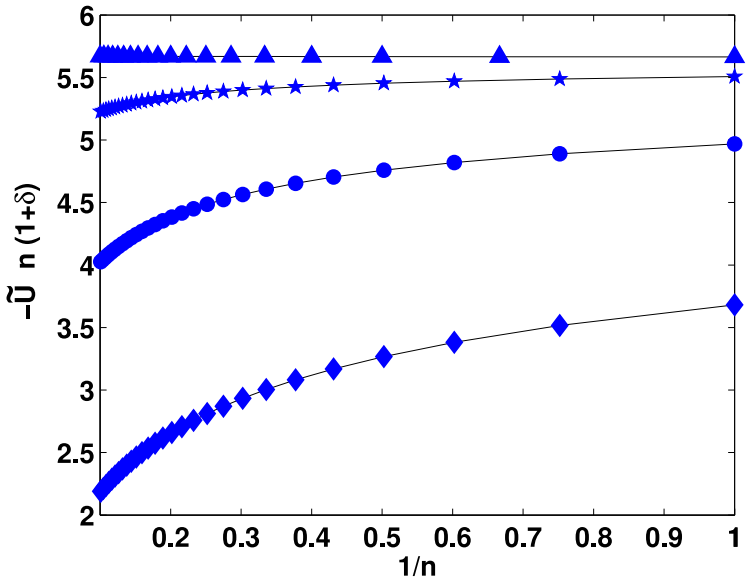

Figure 2.10: Deviation of $\tilde{U}$ from the standard thin diffuse layer scaling with the inverse ion concentration $\sim 1/(\mathcal{C}_\mathrm{i}+\mathcal{C}_\mathrm{i}\delta)$. Bulk salt concentrations are varied $\mathcal{C}_\mathrm{i} = n\times(5\times10^{-5}$ mol/L) with $n = 1\ldots10$. Speed is multiplied with $n(1+\delta)$ to remove the standard scaling. $c_{H_2O_2} = 3.7$ (3.7 %), $\kappa_1 = k_1 = 0.005$, $\kappa_2 = k_2 = 0.025/n$, $\delta = 0.1/n$. (▲): $\lambda_s/\lambda = 0$. (★): $\lambda_s/\lambda = 0.005\sqrt{n}$. (●): $\lambda_s/\lambda = 0.025\sqrt{n}$. (♦): $\lambda_s/\lambda = 0.1\sqrt{n}$.

of salt ions, along with a more refined model of the ion adsorption is called for to improve the quantitative understanding here.

2.6 Discussion

In this chapter we introduce a new model for self-electrophoresis to improve on many shortcomings of previous models and render predictions applicable to the experimental situation. In Sec. 2.2 we explain how the model is set up. We consider two types of ions to capture the effect of salt or pollutants in the solution. The extra salt fluxes couple to reaction-driven proton fluxes. A Stern layer models adsorption of salt ions to the swimmer's surface. The nonlinear conservation equations are complemented by a Butler-Volmer kinetics for the chemical reaction. In Sec. 2.3.1 we introduce the thin diffuse layer approximation. Although this approximation hardly alleviates the numerical solution of the diffusion equations, it renders the hydrodynamics relatively simple and serves to avoid a quite demandingly high density of grid nodes near the swimmer. The numerical results in Sec. 2.5 are in full qualitative agreement with an analytical approximation for the swimming speed given in Eq. (2.83).

The first order Butler-Volmer reaction kinetics leads to a linear increase of swimming speed at low H_2O_2 concentrations. Diffusion limitation of the reaction rate causes a saturation of the swimming speed at high H_2O_2 concentrations (Fig. 2.4). However, high concentrations of available protons in the bulk can widely suppress the leveling off of the speed. A decrease of the pH value with an increase of the H_2O_2 concentration has similar effects since this provides more H^+ ions for the catalytic reduction (Fig. 2.7). This data is in qualitative agreement with the experiment. (Fig. 1.2)

The swimmer's potential V plays an important role for the swimming speed since it is directly related to the potential drop across the diffuse layer (the zeta potential). In our model, we found V to be in most cases much lower than $-40\,\mathrm{mV}$, which is about the zeta potential of a metal particle without the presence of H_2O_2. This value was used previously as a rough estimate [91]. Such a high potential V can only be found within our model if the overall oxidation and reduction rates are similar (see Eq. (2.63)). Experimental determination of the potential of the swimmer is possible, e.g., through a measurement of the electrophoretic motion of actively moving particles.

A Stern layer reduces the swimming speed by modifying the potential drop across the diffuse layer and by lowering the reaction rate. For simplicity, we keep the absolute width of the Stern layer constant. Still, it causes a decrease of speed with increased salt concentration that is stronger than the inverse of the bulk ion concentration (Fig. 2.9). This finding in agreement with qualitative experimental results [89].

It should be emphasized that the thin diffuse layer model may describe the swimming well, even in absence of electrolytes in the solution. Spontaneous dissociation of H_2O_2 in the bulk can be an important factor here. A reasonable pH value of 6 translates, e.g., to a double layer thickness, Eq. (2.11), of about 90 nm. This number is an order of magnitude smaller than R. It justifies the approximative use of the thin diffuse layer model for H_2O_2 concentrations, say, above the 2 % range. A contamination of the water with atmospheric carbon dioxide has also been found to be important for electrophoresis in a salt-free environment [23]. The somewhat unknown details of the reaction mechanism at the surface of the swimmer could further contribute to making the thin diffuse layer model valid. It is for example possible that the reactions at the swimmer's surface lead, beyond this model, to an accumulation of other types of ions and radicals.

In spite of the successful qualitative explanation of the experimental data, a few simplifying assumptions prohibit the direct fit of the model constants. First, we consider a spherical swimmer with a reactivity varying like a cosine across the surface. This geometry is chosen for its numerical robustness since no sharp edges and sudden changes are present. However, the experimentally studied swimmers are short, bimetallic rods where the reactivity varies quite suddenly across the boundary from one metal to the other. The

second strong assumption is that all solutes have similar diffusivities.
Our approach to not model salt adsorption to the swimmer explicitly could also be somewhat refined. We hope to justify our theory somewhat by the low (sub millimolar) concentrations of salt. The influence of ion adsorption on electrophoretic mobility is a long standing problem. A number of different models have been suggested to quantitatively account for different kinds of salt ions [55, 74]. The common statement that the capacitance of the compact layer is roughly independent of salt concentration is somewhat justified for nonreactive, metallic interfaces [48] but remains an assumption for the system investigated here. Is well known that charged double layers can exhibit lateral ion transport if they are highly charged [17]. When contributions of the order $\lambda\, e^{-\Delta\phi_0/2}$ are non-negligible, corrections to the λ^0 theory must incorporate electro-osmosis and electromigration in the diffuse layer. These surface conduction phenomena were neglected in order to focus on the important features of the model.

In conclusion of this chapter on self-electrophoresis, it can be said that the presented work is the first closed model that captures all the important experimental trends [108]. The model quantitatively supports an explanation of the motion of bimetallic particles through a self-electrophoretic effect.

Chapter 3

Self-diffusiophoretic motion

This chapter is devoted to a simple model of self-diffusiophoresis in a three-component solution. The fluid contains two types of solutes, designated by a and b, and a solvent (s). The dilute concentrations of the solutes are denoted by $\tilde{c}_{\mathrm{a}}$ and $\tilde{c}_{\mathrm{b}}$. All fluid constituents have the same diffusion constant D. In contrast to the charged solutes examined in Chap. 2, the solutes do not interact with each other in this model. Only the solute of b-type interacts via a fixed, radially symmetric, potential $\tilde{\psi}$ with the swimmer. The potential is assumed to decay over a characteristic lengthscale L. The interaction could represent, e.g., a van der Waals force when the solutes have different polarizabilities. In order to make sure that the total force on the fluid is, even for a linear concentration gradient ($\tilde{c}_{\mathrm{b}} \sim \tilde{r}\cos\theta$), convergent we assume in the following

$$\tilde{\psi}\left(\tilde{r} \to \infty\right) < O\left(\tilde{r}^{-3}\right). \tag{3.1}$$

The spherical swimmer, placed in an infinitely large container, is depicted in Fig. 3.1. As before, the radius of the swimmer is denoted by R. A chemical transformation $a \leftrightarrow b$ takes place at the swimmer's surface with rate $\tilde{\alpha}_{\{\mathrm{a,b}\}}\varpi(\theta)$. The θ-dependence of the solute flux at the surface is contained in the dimensionless function $\varpi(\theta)$. We will always assume that the emission of solutes happens in a spatially asymmetric way. $\tilde{\alpha}_{\{\mathrm{a,b}\}}$ has the dimensions of solute flux and quantifies the magnitude of the reaction rate.

3.1 The model equations

Convective transport renders the diffusion equation (1.18) nonlinear since the fluid velocity and the concentration fields are both unknown. In order to make the system more amenable to analytical calculations the nondimensionalized equations are linearized in this section around equilibrium. The natural length- and energy scales are the radius of the swimmer, R, and the thermal energy kT. Accordingly, we rescale as $r \equiv \tilde{r}/R$ and

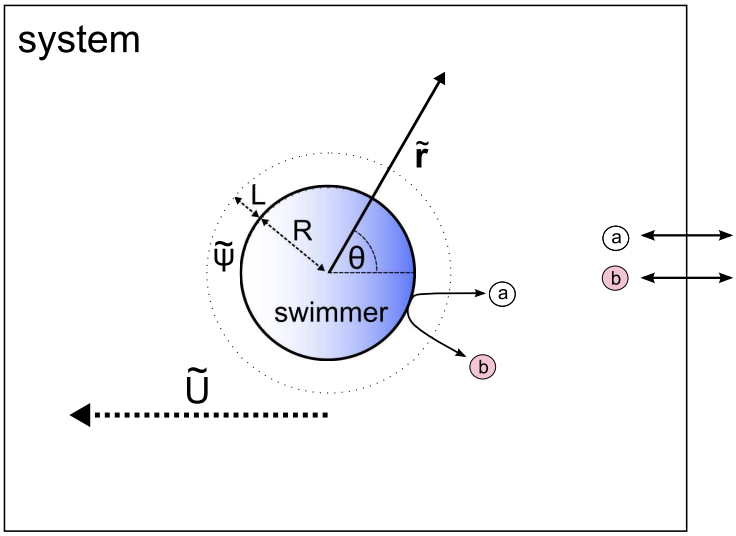

Figure 3.1: Schematic representation of the model for an active swimmer. Molecules of type a and b are dissolved in the fluid surrounding the swimmer with radius R. The molecules are transformed into each other through chemical surface reactions and the overall concentrations are maintained constant. An interaction between the swimmer and the type b molecules occurs through the potential $\tilde{\psi}$, whose lengthscale is given by L. An inhomogeneous distribution of solutes causes the swimmer to move with the speed $\tilde{U}$.

$\psi \equiv \tilde{\psi}/kT$. The intrinsic lengthscale L of the potential $\tilde{\psi}$ is nondimensionalized as

$$\lambda \equiv L/R. \tag{3.2}$$

The swimming is driven by an asymmetric concentration perturbation of the equilibrium distribution of b-type solutes $\tilde{c}_{\mathrm{b}}^{\mathrm{eq}}(\tilde{r})$. Owing to the radial symmetry of $\tilde{\psi}$, only the dipole moment of the concentration perturbation

$$\frac{3}{2}\int_{-1}^{1} \frac{R\,\tilde{\alpha}_{\mathrm{b}}}{D}\,\varpi(\theta)\,\cos\theta\,\mathrm{d}(\cos\theta) \tag{3.3}$$

contributes here. We can accordingly define the concentration scale $\mathcal{C}$, which is relevant for the particle motion, as

$$\mathcal{C} \equiv R\,\tilde{\alpha}_{\mathrm{b}}/D. \tag{3.4}$$

In the following we will always assume that the concentration perturbation $\mathcal{C}$ is much smaller than the equilibrium concentration scale. We can then define a new dimensionless parameter as

$$\xi \equiv \mathcal{C}/\tilde{c}_{\mathrm{b}}^{\mathrm{eq}}(\infty). \tag{3.5}$$

We employ $\mathcal{C}$ for the nondimensionalization of concentrations. The equilibrium perturbations of the concentration fields are

$$c_{\rm a} \equiv \frac{\tilde{c}_{\rm a} - \tilde{c}_{\rm a}^{\rm eq}(\infty)}{\mathcal{C}}, \tag{3.6}$$

$$c_{\rm b} \equiv \frac{\tilde{c}_{\rm b} - \tilde{c}_{\rm b}^{\rm eq}(\infty)e^{-\psi}}{\mathcal{C}}. \tag{3.7}$$

A typical diffusiophoretic speed magnitude [6] is given for $\lambda \lesssim 1$ by

$$\mathcal{U} \equiv \frac{kT\,L^2}{\eta}\frac{\mathcal{C}}{R}. \tag{3.8}$$

The associated Peclét number is defined in Eq. (1.19). Sample calculations, employing measured particle speeds [89, 54], show that Pe is typically smaller than 10^{-2}. The Peclét number thus constitutes, besides ξ, a second small expansion parameter.

3.1.1 Diffusion equations

The solute fluxes $\tilde{\mathbf{j}}$ are nondimensionalized by $D\mathcal{C}/R$ and obey the boundary conditions

$$\hat{\mathbf{e}}_r \mathbf{j}_{\{\rm a,b\}}(1,\theta) = \frac{R\,\tilde{\alpha}_{\{\rm a,b\}}\,\varpi(\theta)}{D\mathcal{C}} \equiv \alpha_{\{\rm a,b\}}\varpi(\theta). \tag{3.9}$$

Employing the nondimensional hydrodynamic velocity field $\mathbf{u} \equiv \tilde{\mathbf{u}}/\mathcal{U}$, the equations for solute conservation (1.18) become

$$\nabla^2 c_{\rm b} + \nabla\cdot(c_{\rm b}\nabla\psi) - \frac{\rm Pe}{\xi}\mathbf{u}\nabla e^{-\psi} = {\rm Pe}\,\mathbf{u}\nabla c_{\rm b}, \tag{3.10}$$

$$\nabla^2 c_{\rm a} = {\rm Pe}\,\mathbf{u}\nabla c_{\rm a},\,. \tag{3.11}$$

The form of Eqns. (3.10, 3.11) suggests a perturbation scheme in Pe to cope with the nonlinearities. However, difficulties arise if ξ is of the same magnitude as Pe. Then only the right hand sides of Eqns. (3.10, 3.11) are small. Furthermore, because $\xi \sim \mathcal{C}$ and also Pe $\sim \mathcal{C}$, it is in the spirit of a linear response theory in $\mathcal{C}$ to set

$${\rm Pe}\,\mathbf{u}\nabla c_{\rm a} \simeq {\rm Pe}\,\mathbf{u}\nabla c_{\rm b} \simeq 0. \tag{3.12}$$

3.1.2 Hydrodynamic equations

The Stokes equation (1.27) is given in dimensionless form by

$$\nabla^2\mathbf{u} - \nabla p - \frac{1}{\lambda^2}c_{\rm b}\nabla\psi = 0, \tag{3.13}$$

where $p \equiv \tilde{p}R/(\mathcal{U}\eta)$. The fluid boundary conditions are, as before,

$$\begin{aligned}\mathbf{u}(\infty,\theta) &= -U\hat{\mathbf{e}}_z,\\ \mathbf{u}(1,\theta) &= 0.\end{aligned} \tag{3.14}$$

The force balance is given by Eq. (1.29). For concrete numerical and analytical calculations, the Stokes equation (3.13) is rewritten with the stream function formalism [53]. Due to the linearization approach, the mobility of the swimmer, relating U to $\alpha_{\{\mathrm{a,b}\}}$, can be calculated straightforwardly with a procedure described by O'Brien and White [82]. In brief, one determines the force balance for the case $\alpha_{\{\mathrm{a,b}\}} = 0$, $U \neq 0$ and also for $\alpha_{\{\mathrm{a,b}\}} \neq 0$, $U = 0$. The combination of the results yields the response of the particle speed to a non-vanishing reaction rate.

3.2 Swimming speed - reaction limited case

We assume here that the diffusion of the a and b-type molecules is so fast that the concentration profiles are entirely determined by reactivity of the swimmer's surface. The emission rate of the solute of type b is fixed as $\varpi(\theta) = (1 + \cos\theta)$ and $\tilde{\alpha}_{\mathrm{b}} = \kappa = \text{const}$. Then

$$\hat{\mathbf{e}}_r \tilde{\mathbf{j}}_{\mathrm{b}}(\theta) = \kappa\,(1 + \cos\theta) \tag{3.15}$$

and $\mathcal{C} = \kappa R/D$. This boundary condition for the surface interacting solute does not contain c_{a}. The species a is thus irrelevant for the particle swimming in this section. The concentration field c_{b} is determined by the differential Eq. (3.10) with Eq. (3.12). In spite of its linearity, there seems to be no analytical solution of this equation available for arbitrary ψ. The nature of the potential ψ, comprising a variety of possible physical interactions, is important for the diffusiophoretic speed. The reaction limited model studied in this section offers the possibility to investigate the role of the potential in a relatively simple setting.

3.2.1 Analytical approximation

The speed of active swimmers is calculated in this section analogous to work by Anderson and Prieve [8] for passive swimmers. We resort to a technique of matched asymptotic expansions for $\lambda \ll 1$. The diffusion equation (3.10, 3.12) becomes in spherical coordinates

$$\begin{aligned} &\partial_r^2 c_{\mathrm{b}}(r,\theta) + \left(\psi'(r) + \frac{2}{r}\right)\partial_r c_{\mathrm{b}}(r,\theta) \\ &+ \left(\psi''(r) + \frac{2}{r}\psi'(r)\right) c_{\mathrm{b}}(r,\theta) + \frac{1}{r^2\sin\theta}\partial_\theta\left(\sin\theta\,\partial_\theta c_{\mathrm{b}}(r,\theta)\right) \\ &- \frac{\mathrm{Pe}}{\xi}\hat{\mathbf{e}}_r\mathbf{u}\,\partial_r\, e^{-\psi(r)} = 0. \end{aligned} \tag{3.16}$$

Due to the radial symmetry of $\psi(r)$, only the dipole moment of the concentration field can move the particle. In absence of a coupling between different spherical harmonics it is therefore sufficient to consider the field contributions which are $\sim \cos\theta$. We split the

concentration field of the b-type solute into an inner field $C_{\mathrm{b}}(y)\cos\theta$ and an outer field $\hat{C}_{\mathrm{b}}(r)\cos\theta$. $C_{\mathrm{b}}(y)$ is written in terms of the inner variable $y=(r-1)/\lambda$. The outer field lies in the region with $r \gg \lambda+1$ where the effect of the surface potential ψ is negligible. Eq. (3.16) thus becomes here in the outer region

$$\partial_r^2 \hat{C}_{\mathrm{b}}(r) + \frac{2}{r}\partial_r \hat{C}_{\mathrm{b}}(r) - \frac{2}{r^2}\hat{C}_{\mathrm{b}}(r) = 0. \tag{3.17}$$

For active diffusiophoresis, the concentration perturbation must vanish far away of the swimmer. Therefore, the solution of Eq. (3.17) is given by $\hat{C}_{\mathrm{b}}(r) = A/r^2$, where the coefficient A is yet undetermined. The smallness of λ suggests an expansion of the inner and outer fields as

$$C_{\mathrm{b}} = C_{\mathrm{b}\,0}(y) + C_{\mathrm{b}\,1}(y)\lambda + C_{\mathrm{b}\,2}(y)\lambda^2 + O(\lambda^3), \tag{3.18}$$

$$\begin{aligned}\hat{C}_{\mathrm{b}} &= \frac{1}{r^2}\left(A_0 + A_1\lambda + A_2\lambda^2 + \ldots\right) = A_0 + \\ &(A_1 - 2A_0 y)\,\lambda + \left(A_2 - 2A_1 y + 3A_0 y^2\right)\lambda^2 + O(\lambda^3).\end{aligned} \tag{3.19}$$

In the inner region we substitute r by $\lambda y + 1$ in Eq. (3.16) and expand for small λ. The resulting equations for the two lowest coefficients $C_{\mathrm{b}\,0}$ and $C_{\mathrm{b}\,1}$ are

$$\partial_y\left(\partial_y C_{\mathrm{b}\,0}(y) + C_{\mathrm{b}\,0}(y)\partial_y\psi\right) = 0, \tag{3.20}$$

$$\partial_y\left(\partial_y C_{\mathrm{b}\,1}(y) + C_{\mathrm{b}\,1}(y)\partial_y\psi\right) + 2\left(\partial_y C_{\mathrm{b}\,0}(y) + C_{\mathrm{b}\,0}(y)\partial_y\psi\right) = 0. \tag{3.21}$$

The boundary condition Eqns. (3.9, 3.15) yield for the coefficients of $C_{\mathrm{b}}(y)$

$$\frac{-\lambda}{\lambda}\left(\partial_y C_{\mathrm{b}\,1}(y) + C_{\mathrm{b}\,1}(y)\partial_y\psi\right)|_{y=0} = \frac{\kappa R}{D\mathcal{C}} = 1; \tag{3.22}$$

$$\frac{-\lambda^n}{\lambda}\left(\partial_y C_{\mathrm{b}\,n}(y) + C_{\mathrm{b}\,n}(y)\partial_y\psi\right)|_{y=0} = 0 \qquad \text{when} \qquad n \neq 1. \tag{3.23}$$

Employing the above equations, the concentration is

$$C_{\mathrm{b}} = e^{-\psi}a_0 + \lambda\, e^{-\psi}\left[a_1 - \int_0^y \left(e^{\psi(y')} - 1\right)\mathrm{d}y' - y\right] + O\left(\lambda^2\right). \tag{3.24}$$

The $O(\lambda)$ term diverges for $y \to \infty$. In order to make this divergence explicit, we have removed it from the integral in Eq. (3.24) by subtracting 1. The unknown constants in the inner and outer solution are determined by matching them asymptotically [125] through $\hat{C}_{\mathrm{b}\,n}(y \to 0) = C_{\mathrm{b}\,n}(y \to \infty)$. The resulting conditions, which must be valid for all y, are

$$A_0 = a_0, \tag{3.25}$$

$$A_1 - 2A_0 y = a_1 - \int_0^\infty \left(e^{\psi(y')} - 1\right)\mathrm{d}y' - y. \tag{3.26}$$

This yields the lowest order coefficients $a_0 = A_0 = 1/2$ and the innermost concentration field is thus given by $C_\mathrm{b} \approx \exp(-\psi)/2$.

In order to calculate the fluid flow near the surface of the swimmer, we employ the Stokes equation (3.13) and assume that the body force vanishes in the outer region. Applying the curl to Eq. (3.13) and defining a stream function $S(r)$ via $\mathbf{u} = \nabla \times (\sin\theta S(r)/r\,\hat{\mathbf{e}}_\varphi)$ the Stokes equation becomes

$$\partial_r^4 S(r) - \frac{4\,\partial_r^2 S(r)}{r^2} + \frac{8\,\partial_r S(r)}{r^3} - \frac{8S(r)}{r^4} = -\frac{C_\mathrm{b}(r)}{\lambda^2}\,\partial_r \psi(r). \tag{3.27}$$

In the outer region, where the body force vanishes, we have the stream function $\hat{S} = X/r + Y\,r + Z\,r^2$. The constants X,Y and Z are expressed as a power series of λ. The fluid velocity in the outer region thus is

$$\frac{\hat{\mathbf{e}}_\theta \hat{\mathbf{u}}}{\sin\theta} = \frac{-\partial_r \hat{S}(r)}{r} = -2Z_0 - Y_0 + X_0 + O(\lambda), \tag{3.28}$$

$$\frac{\hat{\mathbf{e}}_r \hat{\mathbf{u}}}{\cos\theta} = \frac{2\hat{S}(r)}{r^2} = 2Z_0 + 2Y_0 + 2X_0 + O(\lambda). \tag{3.29}$$

In the inner region, we expand Eq. (3.27) for small λ and insert $C_\mathrm{b}(y)$ for the concentration field. The leading order differential equation for the stream function near the surface of the swimmer $S(y)$ reads

$$\frac{1}{\lambda}\partial_y^4 S(y) = -\frac{e^{-\psi}}{2}\partial_y \psi(y). \tag{3.30}$$

This yields

$$\begin{aligned} S(y) =& k_0 + l_0\,y + m_0\,y^2 + n_0\,y^3 - \frac{\lambda}{2}h(y) \\ & \lambda\left(k_1 + l_1\,y + m_1\,y^2 + n_1\,y^3\right) + O\left(\lambda^2\right); \end{aligned} \tag{3.31}$$

$$h(y) \equiv \int_0^y \int_0^{y'} \int_{y''}^\infty \left(e^{-\psi(y''')} - 1\right) \mathrm{d}y'''\mathrm{d}y''\mathrm{d}y'. \tag{3.32}$$

The fluid flow in the inner region becomes

$$\begin{aligned} &\frac{\hat{\mathbf{e}}_\theta \mathbf{u}(y)}{\sin\theta} \approx -\frac{1}{\lambda}\left(l_0 + 2m_0\,y + 3n_0\,y^2\right) + \frac{1}{2}\partial_y h(y) + \\ &\left(-l_1 + l_0 y - 2m_1 y + 2m_0 y^2 - 3n_1 y^2 + 3n_0 y^3\right) + O(\lambda), \end{aligned} \tag{3.33}$$

$$\frac{\hat{\mathbf{e}}_r \mathbf{u}(y)}{\cos\theta} \approx 2\left(k_0 + l_0\,y + m_0\,y^2 + n_0\,y^3\right) + O(\lambda). \tag{3.34}$$

Due to the no slip boundary conditions on the surface of the swimmer we have $k_0 = l_0 = l_1 = 0$. The far field boundary condition on the outer velocity field $\mathbf{u}|_{r\to\infty} = -U\hat{\mathbf{e}}_z$ yields $Z = -U/2$. Matching the lowest order velocities through $\mathbf{u}(y)_n\,(y \to \infty) = \hat{\mathbf{u}}_n\,(y \to 0)$,

as done for the concentrations above, we find

$$0 = -\frac{1}{\lambda}\left(2m_0\, y + 3n_0\, y^2\right), \tag{3.35}$$

$$-2Z_0 - Y_0 + X_0 = \frac{K_1}{2} - 2m_1 y + 2m_0 y^2 - 3n_1 y^2 + 3n_0 y^3, \tag{3.36}$$

$$2Z_0 + 2Y_0 + 2X_0 = 2m_0\, y^2 + 2n_0\, y^3, \tag{3.37}$$

where we have used $\partial_y h(y)|_{y\to\infty} = K_1$ with $K_\mathrm{n} = \int_0^\infty y^\mathrm{n}\left(e^{-\psi(y)} - 1\right)\mathrm{d}y$ (see Eq. (1.46)).

From Eq. (3.35) we deduce that $m_0 = n_0 = 0$. On imposing the physical constraint that $\partial_y h(y)$ remains finite for $y \to \infty$ we conclude that $m_1 = n_1 = 0$ in order to avoid divergence of the right hand side of Eq. (3.36). Finally, Eqns. (3.36, 3.37) yield together the two last constants $X_0 = (K_1 - U_0)/4$ and $Y_0 = (3U_0 - K_1)/4$. This fully determines the lowest order velocity fields. To further relate the speed of the swimmer U_0 to the balance of forces, one only needs to consider the Stokeslet $\hat{\mathbf{u}} \sim 1/r$, whose long range nature reflects the presence of external forces. For a free swimmer the Stokeslet vanishes and we therefore have $Y_0 = 0$. This condition determines the lowest order swimming speed

$$U_0 = \frac{\tilde{U}_0}{\mathcal{U}} = \lambda^2 \frac{\kappa\, kT}{\mathcal{U}\eta\, D}\frac{R^2}{3}\int_0^\infty y\,\left(e^{-\psi(y)} - 1\right)\mathrm{d}y = \frac{1}{3}\frac{\kappa\, kT\, L^2}{\mathcal{U}\, D\eta}K_1 = \frac{K_1}{3}. \tag{3.38}$$

We extend the scheme presented above to a correction of $O(\lambda^3)$. The calculation is rather straightforward but the details are lengthy and therefore omitted here. The result, written as a first order Padé approximant of the swimming speed reads

$$\tilde{U} \approx \tilde{U}_0 / \left[1 + \lambda\left(K_0 + \frac{7\, K_2}{2\, K_1} + \frac{\mathrm{Pe}}{\xi}\frac{G}{2} + \frac{N}{K_1}\right)\right], \tag{3.39}$$

where the following definitions are employed

$$G \equiv \int_0^\infty \int_0^y y'\,\left(e^{-\psi(y')} - 1\right)\mathrm{d}y'\left(e^{-\psi(y)} - 1\right)\mathrm{d}y, \tag{3.40}$$

$$\begin{aligned} N \equiv & -2\int_0^\infty \int_0^y y'\,\left(e^{-\psi(y')} - 1\right)\mathrm{d}y'\left(e^{\psi(y)} - 1\right)\mathrm{d}y \\ & + \int_0^\infty y^2\left(e^{-\psi(y)} - 1\right)\left(e^{\psi(y)} - 1\right)\mathrm{d}y. \end{aligned} \tag{3.41}$$

Note that the chemical reaction must occur at a finite distance from the physical hard-core boundary of the swimmer. Therefore, the potential $\psi(r = 1)$ cannot diverge in active diffusiophoresis and all the constants defined above remain finite.

3.2.2 Numerical results

In order to go beyond the $\lambda \ll 1$ limit, we solve Eqns. (3.10-3.13, 3.12) numerically for the boundary conditions given in Eqns. (3.14, 3.15). Results are displayed in Figs. 3.2, 3.3, 3.4

where the swimming speed is plotted as $\lambda^2 U = L^2\tilde{U}/(R^2\mathcal{U})$ in order to demonstrate the physical dependence of the speed on the interaction length L. As it is the case for other phoretic effects[109, 97], convection causes a nonmonotoneous relation between particle speed and λ (Fig. 3.2). An increasing magnitude of the surface potential $\psi(1)$ reduces the range of validity of the lowest order approximation U_0 to smaller values of λ (Fig. 3.3). The Padé approximant of U, Eq. (3.39), then describes the case of strong surface interactions much more satisfyingly [9]. Therefore, the Padé approximant presents a significant improvement over the lowest order estimate U_0, in spite of being useful only for $\lambda < 1$.

Fig. 3.4 shows the swimming speed for a truncated van der Waals-like interaction where the potential decays $\sim 1/r^6$ only far away of the swimmer. The result demonstrates that multiple lengthscales of the interaction potential may modify the simple scaling of $\tilde{U}_0 \sim L^2$. Furthermore, the similarity of the results for $\mathrm{Pe}/\xi = 0$ and $\mathrm{Pe}/\xi = 5$ qualifies the simple notion that convection of solutes reduces the speed of the particle. Since, for Fig. 3.4, we have $\psi(r) \ll 1$ when $\lambda > 1$, the influence of the Peclét number is suppressed almost completely. This dependence of the effect of convection on the strength of the surface interaction also appears through the constant G in the Padé approximant given in Eqns. (3.39, 3.40).

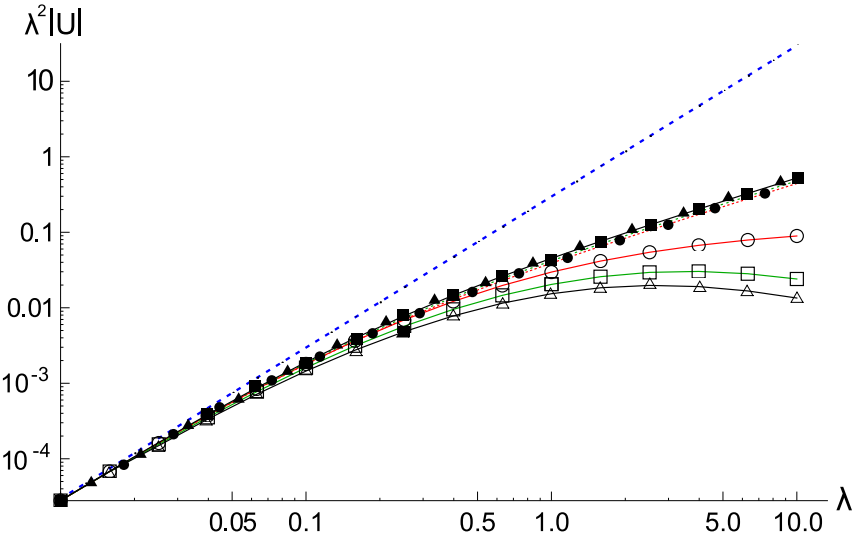

Figure 3.2: Swimming speed vs. interaction lengthscale λ for an exponential repulsion: $\psi(r) = \exp\left[-(r-1)/\lambda\right]$. (Dashed line) Swimming speed in lowest order approximation $\lambda^2|U_0|$ for $\lambda \ll 1$ from Eq. (3.38). (○) Numerical solution for $\mathrm{Pe}/\xi = 0$. (●) Padé approximant, Eq. (3.39), for $\mathrm{Pe}/\xi = 0$. (□) Numerical solution for $\mathrm{Pe}/\xi = 5$. (■) Padé approximant for $\mathrm{Pe}/\xi = 5$. (△) Numerical solution for $\mathrm{Pe}/\xi = 10$. (▲) Padé approximant for $\mathrm{Pe}/\xi = 10$.

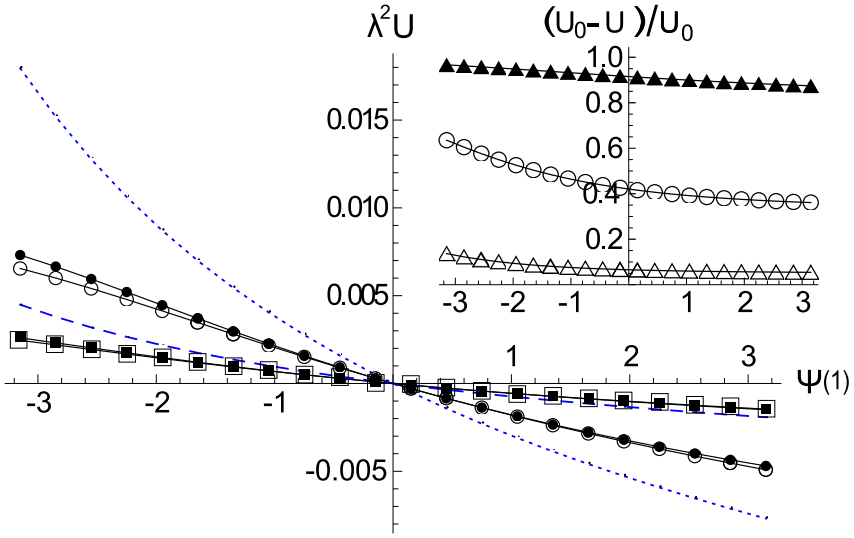

Figure 3.3: Swimming speed vs. interaction potential magnitude $\psi(1)$ for $\psi(r) = \psi(1)\exp\left[-(r-1)/\lambda\right]$ with $\mathrm{Pe}/\xi = 0$. (□) Numerical solution for $\lambda = 0.05$. (■) Padé approximant, Eq. (3.39), for $\lambda = 0.05$. (Dashed line) $\lambda^2|U_0|$ from Eq. (3.38) for $\lambda = 0.05$. (○) Numerical solution for $\lambda = 0.1$. (●) Padé approximant for $\lambda = 0.1$. (Dotted line) $\lambda^2|U_0|$ for $\lambda = 0.1$. Inset: Relative deviation of the lowest order approximation $(U_0 - U)/U_0$ vs. $\psi(1)$ with $\mathrm{Pe}/\xi = 0$. (▲) $\lambda = 1$. (○) $\lambda = 0.1$. (△) $\lambda = 0.01$.

3.2.3 Comparison with passive diffusiophoresis

It is of interest to compare the swimming speed given in Eqns. (3.38, 3.39) with the analogous formulae for passive diffusiophoresis in an externally imposed concentration gradient. The results are those given by Anderson et al. [7]. See also Sec. 1.5 and Sec. 6.1.4. Here the boundary conditions for the concentration of the solute of type b read

$$\begin{aligned} \hat{\mathbf{e}}_r \tilde{\mathbf{j}}_\mathrm{b}(1,\theta) &= 0, \\ \nabla\tilde{c}|_\infty &= \text{const.} \times \hat{\mathbf{e}}_z. \end{aligned} \tag{3.42}$$

The lowest order result for swimming speed in passive diffusiophoresis $\tilde{U}^p$ is

$$\tilde{U}_0^p = |\nabla\tilde{c}|_\infty \frac{kTL^2}{\eta} K_1. \tag{3.43}$$

The formulae (3.38) and (3.43) for active and passive swimming are, apart from a replacement of $\kappa/3D$ by $|\nabla\tilde{c}|_\infty$, the same. These different prefactors result from the dipole moments of the concentration fields around the swimmer. The concentration far away from the particle is given by $\tilde{c}_\mathrm{b} \approx R\kappa/D\,[1/r + \cos\theta/(2r^2)]$ in our case and $\tilde{c}_\mathrm{b} \approx R|\nabla\tilde{c}|_\infty\,[r + 1/(2r^2)]\cos\theta$ for an externally imposed concentration gradient. At $r = 1$, the self generated dipole is therefore only $\sim \kappa RD/2$ while the imposed concentra-

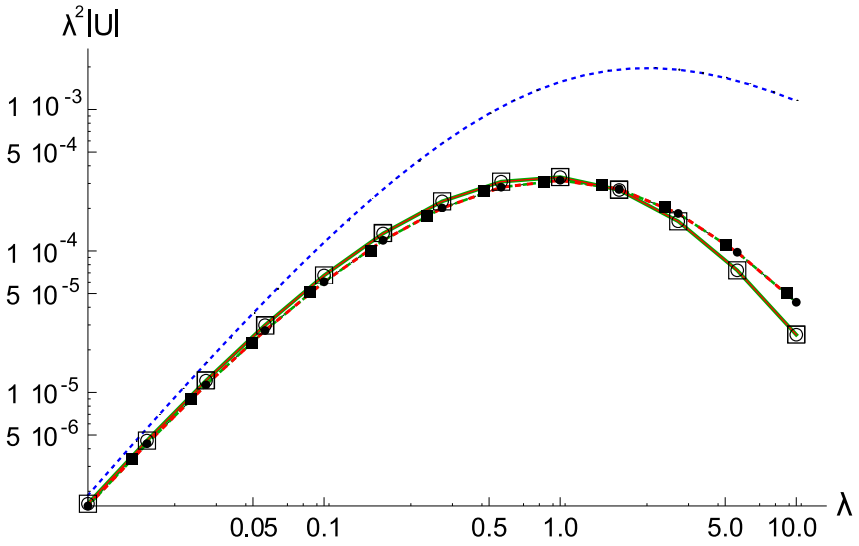

Figure 3.4: Swimming speed vs. λ for a van der Waals -like attraction: $\psi(r) = -A\lambda^3/(r-1+\lambda)^3/(r-1+\lambda+2)^3$ with $A = 1$. λ is here interpreted as solute radius divided by the swimmer radius and the potential is truncated at a distance λ away from the surface. (Dashed line) $\lambda^2|U_0|$ from Eq. (3.38). (∘) Numerical solution for $\mathrm{Pe}/\xi = 0$. (•) Padé approximant, Eq. (3.39), for $\mathrm{Pe}/\xi = 0$. (□) Numerical solution for $\mathrm{Pe}/\xi = 5$. (■) Padé approximant for $\mathrm{Pe}/\xi = 5$.

tion dipole is $\sim 3\,R|\nabla\tilde{c}|_\infty/2$. This leads to the differing factor of 1/3, appearing in the swimming speeds.

The general agreement of both lowest order formulae for active and passive diffusiophoresis can be rationalized by noting that both concentrations are, in close proximity to the swimmer's surface, in radial equilibrium. Accordingly, the lowest order solute flux also vanishes for active diffusiophoresis since the diffusive exchange of solute near the active swimmer is $\sim \partial c_\mathrm{b}/\partial(\lambda y) = O(1/\lambda)$ while the emission/absorption of solute, determined by $\varpi(\theta)$, is only of $O(1)$.

For passive diffusiophoresis [9], the analogous formula to the first order swimming speed Eq. (3.39) is, in our notation,

$$\tilde{U}^p \approx \tilde{U}_0^p \Big/ \left[1 + \lambda\left(K_0 + \frac{K_2}{2\,K_1} + \frac{\mathrm{Pe}}{\xi}\frac{G}{2}\right)\right]. \tag{3.44}$$

The main difference between Eq. (3.39) and Eq. (3.44) is the appearance of the term $\lambda N/K_1$ for active diffusiophoresis. The constant N, defined in Eq. (3.41), contains an integral over $\exp(\psi(r))$. It increases the relative importance of the λ^1 correction for strong repulsive surface interactions. For monotonic potentials, N is a positive quantity. Therefore, the correction for active swimmers increases the swimming speed for purely repulsive interactions where we have $K_1 < 0$. Convective corrections $\sim \mathrm{Pe}/\xi$ are, both

for active and passive swimming, relevant if the equilibrium concentration scale $\tilde{c}_{\mathrm{b}}^{\mathrm{eq}}$ is much larger than the concentration disturbance $\mathcal{C}$. It is an interesting side note to the convective correction that the constant G is related to the hydrodynamic dissipation in the boundary layer (see Chap. 6.1) $\tilde{W}_{\mathrm{hyd}} \approx L^3\, G\, 4\pi\, \left(kT\,\mathcal{C}\right)^2 / \left(3\eta\right)$.

3.3 Swimming speed - general case

The kinetics of the chemical transformations at the swimmer's surface depend in general on the local concentrations and correlation functions of educts and products. An inhomogeneous reactivity profile on the swimmer, realized, e.g., through partial coating with a catalyst, couples to the angular solute distributions. Therefore, resulting solute flux at the swimmer might not have the same angular dependence as the reactivity profile. We term the interplay between reaction and diffusion "reaction induced concentration distortion".

For the considered case of dilute solutions one might anticipate that the fraction of unoccupied catalytic sites on the swimmer is always very small. Then the overall reaction rates depend linearly on the concentrations of the reactants. For simplicity, a reversible, first order kinetics for the reaction $a \leftrightarrow b$ is assumed. In this section we employ as boundary conditions for the concentration fields at $r = 1$

$$\hat{\mathbf{e}}_r \tilde{\mathbf{j}}_{\mathrm{b}}(1,\theta) = (1+\cos\theta)\left[\tilde{k}_{\mathrm{ab}}\tilde{c}_{\mathrm{a}}(1,\theta) - \tilde{k}_{\mathrm{ba}}\tilde{c}_{\mathrm{b}}(1,\theta)\right], \tag{3.45}$$

$$\hat{\mathbf{e}}_r \tilde{\mathbf{j}}_{\mathrm{a}}(1,\theta) = -\hat{\mathbf{e}}_r \tilde{\mathbf{j}}_{\mathrm{b}}(1,\theta), \tag{3.46}$$

where $\tilde{k}_{\mathrm{ab}}$ and $\tilde{k}_{\mathrm{ba}}$ are rate constants which we nondimensionalize with D/R. The concentration dependence of the flux at the swimmer surface is also termed a radiation boundary condition. Similar mathematical problems have occurred in the calculation of mean first passage times for the combined encounter and reaction of asymmetric molecules [128, 116].

In equilibrium, where the fluxes vanish, the radially symmetric distributions of solutes obey $\tilde{c}_{\mathrm{a}}^{\mathrm{eq}}(r) = \tilde{c}_{\mathrm{a}}^{\mathrm{eq}}(\infty)$, $\tilde{c}_{\mathrm{b}}^{\mathrm{eq}}(r) = \tilde{c}_{\mathrm{b}}^{\mathrm{eq}}(\infty)e^{-\psi(r)}$ and

$$\frac{\tilde{c}_{\mathrm{a}}^{\mathrm{eq}}\left(\infty\right)}{\tilde{c}_{\mathrm{b}}^{\mathrm{eq}}\left(\infty\right)} = \frac{\tilde{k}_{\mathrm{ba}}e^{-\psi(1)}}{\tilde{k}_{\mathrm{ab}}}. \tag{3.47}$$

A finite reaction rate at the swimmer's surface is ultimately driven by chemical potential differences far away, at the boundary of the system. Within the linear response regime we expect that $\left(\tilde{c}_{\{\mathrm{a,b}\}}(\infty)/\tilde{c}_{\{\mathrm{a,b}\}}^{\mathrm{eq}}(\infty) - 1\right) \ll 1$. Therefore, the chemical potential difference at $\tilde{r} \to \infty$ becomes

$$\begin{aligned}\Delta\mu_\infty \equiv \frac{\tilde{\mu}_{\mathrm{a}}(\infty) - \tilde{\mu}_{\mathrm{b}}(\infty)}{kT} \approx \frac{\tilde{c}_{\mathrm{a}}\left(\infty\right)}{\tilde{c}_{\mathrm{a}}^{\mathrm{eq}}(\infty)} - \frac{\tilde{c}_{\mathrm{b}}\left(\infty\right)}{\tilde{c}_{\mathrm{b}}^{\mathrm{eq}}(\infty)} = \\ \frac{1}{\tilde{k}_{\mathrm{ab}}\tilde{c}_{\mathrm{a}}^{\mathrm{eq}}}\left[\tilde{k}_{\mathrm{ab}}\,\tilde{c}_{\mathrm{a}}(\infty) - \tilde{k}_{\mathrm{ba}}e^{-\psi(1)}\,\tilde{c}_{\mathrm{b}}(\infty)\right].\end{aligned} \tag{3.48}$$

The concentration scale Eq. (3.4) can now be defined as

$$\mathcal{C} = \frac{R}{D}\,\tilde{k}_{\mathrm{ab}}\,\tilde{c}_{\mathrm{a}}^{\mathrm{eq}}(\infty)\,\Delta\mu_\infty = k_{\mathrm{ba}}\,\tilde{c}_{\mathrm{b}}^{\mathrm{eq}}(\infty)e^{-\psi(1)}\,\Delta\mu_\infty. \tag{3.49}$$

Nondimensionalization of Eq. (3.45) yields together with Eq. (3.9)

$$\hat{\mathbf{e}}_r\mathbf{j}_{\mathrm{b}}(1,\theta) = \hat{\mathbf{e}}_r\tilde{\mathbf{j}}_{\mathrm{b}}(1,\theta)\times R/(D\,\mathcal{C}) = \varpi(\theta). \tag{3.50}$$

The parameter ξ and the velocity scale $\mathcal{U}$ are accordingly given by

$$\xi = \frac{\mathcal{C}}{\tilde{c}_{\mathrm{b}}^{\mathrm{eq}}(\infty)} = \Delta\mu_\infty e^{-\psi(1)}\,k_{\mathrm{ba}}, \tag{3.51}$$

$$\mathcal{U} = \frac{kTL^2}{\eta}\frac{k_{\mathrm{ab}}\tilde{c}_a^{\mathrm{eq}}\Delta\mu_\infty}{R}. \tag{3.52}$$

The calculation of the concentration perturbations $c_{\{\mathrm{a,b}\}}$ around the swimmer proceeds by expanding latter quantities in Legendre polynomials $P_n(\cos\theta)$ as

$$\begin{aligned} c_{\mathrm{a}} =& c_{\mathrm{a}}\,(\infty) + \sum_{n=0}^{\infty} c_{\mathrm{a}}^n(r)P_n\,(\cos\theta)\,, \\ c_{\mathrm{b}} =& c_{\mathrm{b}}\,(\infty)\,e^{-\psi(r)} + \sum_{n=0}^{\infty} c_{\mathrm{b}}^n(r)P_n\,(\cos\theta)\,, \end{aligned} \tag{3.53}$$

which includes the boundary conditions at $r\to\infty$. The boundary conditions at the surface of the swimmer, Eqns. (3.45, 3.46), couple different coefficients of the expansion Eq. (3.53) and one has

$$\frac{-2}{2n+1}\left[\partial_r c_{\mathrm{b}}^n + c_{\mathrm{b}}^n\partial_r\psi\right]|_{r=1} = \int_0^\pi P_n\,(\cos\theta)\,\varpi(\theta)\sin\theta\mathrm{d}\theta, \tag{3.54}$$

$$-\left[\partial_r c_{\mathrm{b}}^n + c_{\mathrm{b}}^n\partial_r\psi\right]|_{r=1} = \left[\partial_r c_{\mathrm{a}}^n\right]|_{r=1}. \tag{3.55}$$

3.3.1 Analytical approximations

Again, a swimmer with short interaction length $\lambda \ll 1$ is considered. Calculations of the solutions to leading order in λ are done employing the methods presented in Sec. 3.2.1. Far away of the swimmer, where $\psi(r)\to 0$, Eqns. (3.10, 3.12) can be replaced by Laplace's equations and $c_{\{\mathrm{a,b}\}}^n(r) = A_{\{\mathrm{a,b}\}}^n/r^{n+1}$ holds in Eq. (3.53). For c_{a}, this expansion is valid throughout the whole system. For the b-type solute we have to leading order near the surface of the swimmer $c_{\mathrm{b}}^n(y)\approx a_{\mathrm{b}}^n e^{-\psi(y)}$. Matching these solutions and employing the boundary condition Eq. (3.55) leads to $a_{\mathrm{b}}^n = A_{\mathrm{b}}^n = -A_{\mathrm{a}}^n$. Finally, Eq. (3.54) yields a recursion equation for the constants A_{b}^n

$$\begin{aligned} \left[2\delta_{n,0} + \frac{2}{3}\delta_{n,1}\right] =& \frac{2\,(n+1+k_+)}{2n+1}A_{\mathrm{b}}^n + \frac{2n\,k_+}{(2n+1)\,(2n-1)}A_{\mathrm{b}}^{n-1} + \\ & \frac{2(n+1)k_+}{(2n+1)\,(2n+3)}A_{\mathrm{b}}^{n+1}. \end{aligned} \tag{3.56}$$

Here we defined

$$k_+ \equiv k_{\mathrm{ab}} + k_{\mathrm{ba}} e^{-\psi(1)} = k_{\mathrm{ab}} \left(1 + \frac{\tilde{c}_{\mathrm{a}}^{\mathrm{eq}}(\infty)}{\tilde{c}_{\mathrm{b}}^{\mathrm{eq}}(\infty)} \right). \tag{3.57}$$

Eq. (3.56) can be written in matrix form as $B_j = w_{jn} A_{\mathrm{b}}^n$. The off-diagonal elements of $\{w_{jn}\}$ decay like $\sim 1/n$ and we can invert a finite matrix $\{w_{jn}\}$ to determine a numerical approximation of the $\{A_{\mathrm{b}}^n\}$. In the following, plots of analytical results involving A_{b}^n, are created by employing Eq. (3.56) and $n_{\max} = 70$. Since $\psi(r)$ is radially symmetric, the swimming speed depends only on the dipole moment of the concentration field. An expansion of Eq. (1.38) for small λ yields for the lowest order the free swimming speed

$$U_0 = \frac{\tilde{U}_0}{\mathcal{U}} = \frac{K_1}{3} 2A_{\mathrm{b}}^1. \tag{3.58}$$

For small bare rates, and therefore small k_+, one can expand the inner concentration field of the b-type solute

$$\begin{aligned} c_{\mathrm{b}} =& c_{\mathrm{b}}(\infty) e^{-\psi(r)} + e^{-\psi(r)} \times \\ & \left[A_{\mathrm{b}}^0 + A_{\mathrm{b}}^1 \cos\theta + A_{\mathrm{b}}^2 P_2(\cos\theta) + A_{\mathrm{b}}^3 P_3(\cos\theta) + O(k_+^3) \right] \end{aligned} \tag{3.59}$$

with following approximations for the constants

$$A_{\mathrm{b}}^0 \approx \frac{42 + 2k_+}{42 + 51k_+}, \qquad A_{\mathrm{b}}^1 \approx \frac{135 - 26k_+}{270 + 353k_+}, \tag{3.60}$$

$$A_{\mathrm{b}}^2 \approx -\frac{2k_+}{18 + 33k_+}, \qquad A_{\mathrm{b}}^3 \approx \frac{k_+^2}{60}. \tag{3.61}$$

The magnitude of the dipole moment is determined by $A_{\mathrm{b}}^1 \approx (1/2 - 3k_+/4)$. Reaction induced concentration distortion, emerging here through the corrections in orders of k_+, reduces the dipole moment and thus slows the particle swimming down.

3.3.2 Numerical results

To complement the analytical approximations, we calculate the swimming speed numerically. Eqns. (3.45, 3.46) with fixed concentrations far away of the swimmer are employed for numerical solution of Eqns. (3.10-3.12). The boundary conditions result in an infinite system of equations where the solute concentrations far away of the swimmer $c_{\{\mathrm{a,b}\}}(\infty)$ determine the reaction speed. The system can be truncated above a certain order $n_{\max}$ of the Legendre polynomials. For $n_{\max} = 4$ the errors in the presented data is negligible. Fig. 3.5 contains an exemplary plot of how the reaction induced concentration distortion influences the swimming speed U. The chosen velocity scale $\mathcal{U}$ (Eq. 3.52) contains the linear dependence on $c_{\{\mathrm{a,b}\}}(\infty)$. With the employed first order reactions, the concentration distortion depends nonlinearly on the bare rates k_{ab} and k_{ba} but linearly on the concentration scales $c_{\{\mathrm{a,b}\}}(\infty)$. Thus, in an experiment in the linear regime, with fixed

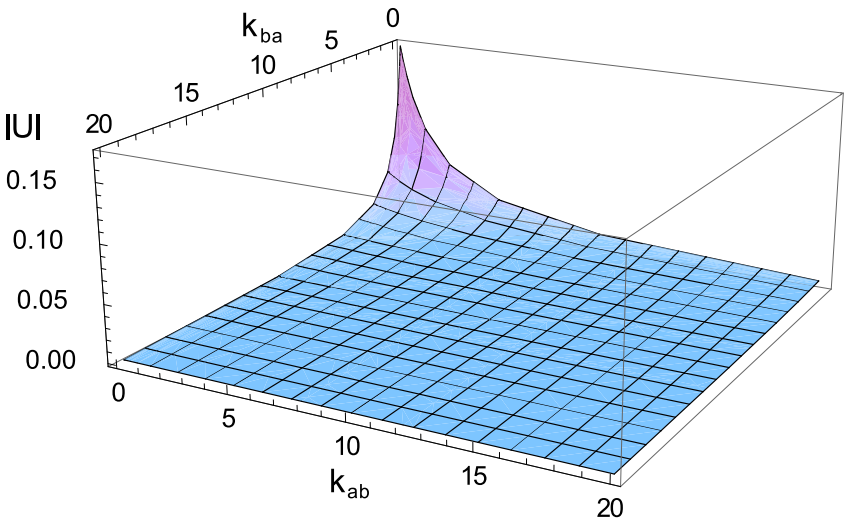

Figure 3.5: Particle speed U as a function of k_{ab} and k_{ba} for $\psi(r) = \exp\left[-(r-1)/\lambda\right]$, $\mathrm{Pe}/\xi = 1$ and $\lambda = 0.1$.

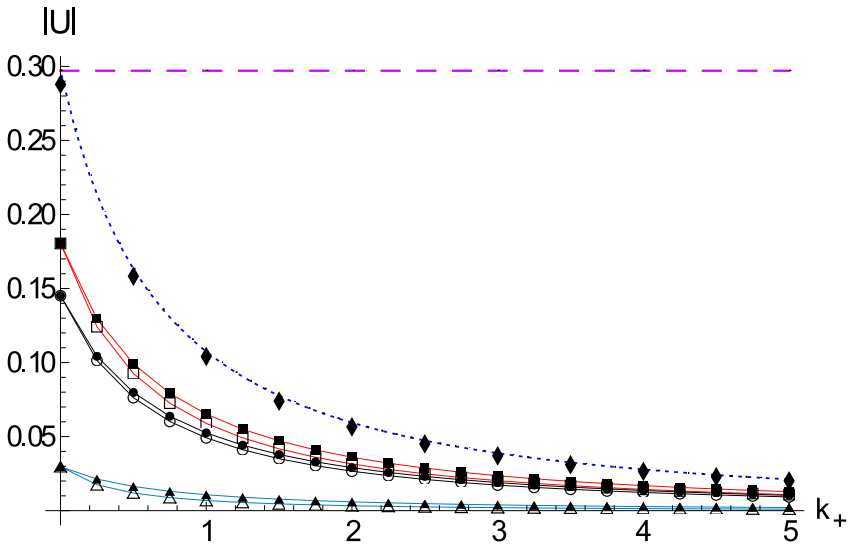

Figure 3.6: Rate constant dependence of the swimming speed U for $\psi(r) = \exp\left[-(r-1)/\lambda\right]$. See Eq. (3.57) for the definition of k_+. (Dashed line) Reaction induced concentration distortion neglected as explained in the text, leading to $U = K_1/3$ with $K_1 \simeq -0.89$. (Dotted line) Approximation U_0 (Eq. (3.58)) for $\lambda \ll 1$ which takes the concentration distortion into account. Full symbols are numerical results for $k_{\mathrm{ba}} = 0$ and open symbols are results for $k_{\mathrm{ab}} = 0$. (♦) $\lambda = 0.005$, $\mathrm{Pe}/\xi = 0$. (■,□) $\lambda = 0.1$, $\mathrm{Pe}/\xi = 0$. (●,○) $\lambda = 0.1$, $\mathrm{Pe}/\xi = 10$. (▲,△) $\lambda = 1$, $\mathrm{Pe}/\xi = 0$.

k_{ab} and k_{ba}, the reaction induced concentration distortion might be accounted for by a constant prefactor, modifying the swimming speed.

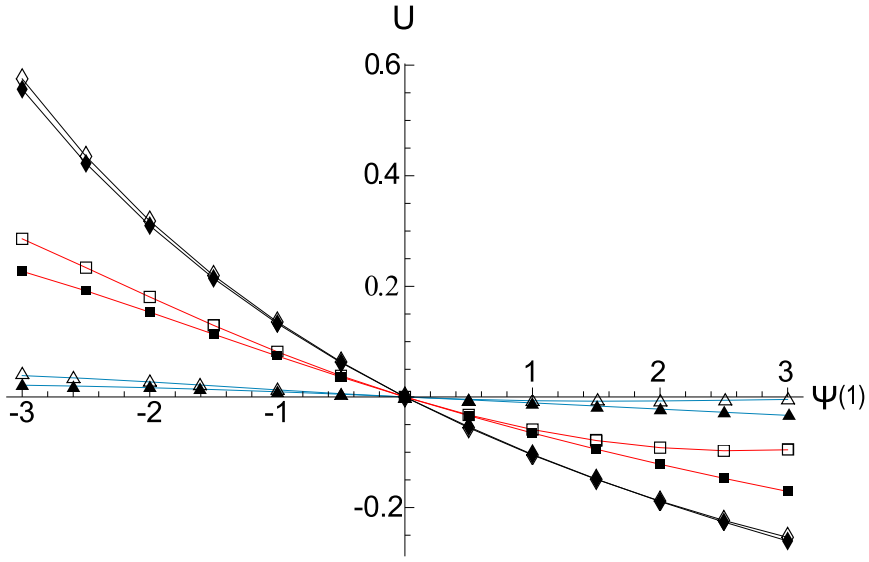

Figure 3.7: Swimming speed as a function of the potential strength $\psi(1)$. Numerical results are computed with $\psi(r) = \psi(1)\exp\left[-(r-1)/\lambda\right]$ and $\mathrm{Pe}/\xi = 0$. Full symbols indicate ($k_{\mathrm{ab}} = 1$, $k_{\mathrm{ba}}\exp(\psi(1)) = 0$). Open symbols indicate ($k_{\mathrm{ab}} = 0$, $k_{\mathrm{ba}}\exp(\psi(1)) = 1$). (♦,◊) $\lambda = 0.005$. (■,□) $\lambda = 0.1$. (▲,△) $\lambda = 1$.

In Fig. 3.6 we plot numerical results for the swimming speed as a function of k_+, defined in Eq. (3.57). Neglecting the reaction induced concentration distortion, the naive boundary condition for the concentration would be $\hat{\mathbf{e}}_r\mathbf{j}_{\mathrm{b}}|_{r=1} = (1+\cos\theta)$. The resulting swimming speed is independent of k_+. It agrees with the analytical approximation in Eq. (3.58) in the limit $k_+ \to 0$. However, Fig. 3.6 shows that neglecting reaction induced concentration distortion in this way leads to significant errors in the speed estimate for finite reaction rate constants. The analytical approximation, Eq. (3.58), is found to be useful for $\lambda \lesssim 0.01$.

Fig. 3.7 shows the dependence of swimming speed on the strength of the interaction potential $\psi(1)$. The symmetry between the effects of changing $k_{\mathrm{ab}}\exp(-\psi(1))$ and k_{ba}, apparent in the parameter k_+ in U_0 when $\lambda \ll 1$, is lost for finite λ. Increasing the strength of the interaction potential $\psi(1)$ makes this asymmetry more pronounced.

3.4 Discussion

We take in this chapter a close look at self-diffusiophoretic swimming in the linear response regime [107]. In particular, we are interested in two aspects which have not been treated so far in the literature. Namely, how swimming speed is affected by finite solute-swimmer interaction lengths and by a mass-action law for the chemical reaction. The model equations are set up in Sec. 3.1. We assume a radially symmetric solute-swimmer

interaction and include convection of solutes to a first approximation. In Sec. 3.2 we consider a reaction process where the spatial distribution of the reaction rate is independent of the concentration. This simplification allows to analyze the role of the surface interaction potential ψ with regards to the dynamics of the swimmer. The details of the interaction become important when $L/R \gtrsim 0.01$ (see Fig. 3.2). Analytical corrections to the lowest order swimming speed for $L/R \to 0$ are given in Eq. (3.39). These include various moments of the solute concentration and also the effect of solute convection. The corrections are for active diffusiophoresis qualitatively similar to those for passive diffusiophoresis [8]. However, in active diffusiophoresis, the emission of solutes can cause an increase of speed for repulsive surface interactions. This speed enhancement reflects the effect of "producing" molecules inside the region from which they are repelled. In Sec. 3.3 we consider a simple mass-action law for the reaction kinetics at the swimmers surface (see Eq. (3.45)). Here, the boundary conditions for the flux depend on the solute concentrations. This kinetics results in a modification of the concentration fields as compared to the reaction limited case. Fig. 3.6 illustrates that this reaction induced concentration distortion leads to a pronounced reduction of the swimming speed. The effect also occurs in the lowest order boundary layer approximation and a corresponding analytical result is given in Eq. 3.58.

It goes without saying that the here studied model is highly idealized. The assumption of a radially symmetric interaction potential may be inadequate for many realizations of diffusiophoretic swimmers. However, qualitative insights from the boundary layer theory may still hold. The studied linear response regime is equally criticizable, at least for the swimmers driven by H_2O_2 decomposition. Nevertheless, the linear response approximation presents a physically consistent, minimalist approach in the light of the fact that the details of the reaction process are not well understood. Moreover, we expect that the concentration dependence of a nonlinear rate equation can qualitatively reduce the swimming speed in a similar way as demonstrated here.

Chapter 4

Linear, irreversible thermodynamics

The framework for irreversible thermodynamics employed in this thesis originates from work by Kelvin, Rayleigh and Onsager [83]. It has been become very popular through work done in the Bruxelles school [45]. In Sec. 4.1 we only aim to provide a brief introduction to the formalism. A thorough discussion of linear, irreversible thermodynamics with applications can be found in the book of De Groot and Mazur [27]. A somewhat more pedagogical introduction is given in [132]. In Sec. 4.2 we suggest a model setup that allows to use the formalism for the analysis of the energetics of phoretic motion.

4.1 Thermodynamic framework

The second law of thermodynamics states that the entropy production rate in any system is either positive or zero. One reason for the generality of this statement is that the existence of an entropy function is merely postulated [98]. The definition of the entropy depends on the level of coarse-graining applied for the description of a physical system. In order to progress beyond the second law, the irreversible processes which contribute to the entropy production must be modeled. One way to do so is to assume that the variables that describe a macroscopic equilibrium can also be used to describe a mesoscopic local equilibrium. Such theories have been applied very successfully to liquid mixtures with chemical reactions and mass flow [27, 49, 68]. Their validity results from a large disparity of timescales between relaxation on a microscopic, molecular level and relaxation on the mesoscopic scale. Since the equilibrium is only local, gradients of the state variables exist. The fluxes associated to these gradients cause a local entropy production rate. The formalism involves the very same local variables that have been introduced in Chap. 1 and were used throughout the preceding parts of the thesis.

The local entropy per volume is denoted by $\tilde{s}$ and the entropy production rate per volume is denoted by $\tilde{\Theta}$. According to the second law of thermodynamics we have $\tilde{\Theta} \geq 0$.

The only way how the entropy in a control volume can be reduced is by exchanging entropy with the outside world. Entropy balance is formulated in local equilibrium thermodynamics as

$$\partial_t \tilde{s} + \nabla(\tilde{s}\,\tilde{\mathbf{u}} + \tilde{\mathbf{j}}_\Theta) = \tilde{\Theta}, \tag{4.1}$$

where $\tilde{\mathbf{j}}_\Theta$ is a flux of entropy [27]. The expression for $\tilde{\Theta}$ is model dependent. Dissipation, and therefore also the entropy production rate, is proportional to the product of thermodynamic forces and fluxes. The assumption of local equilibrium implies the use of average fluxes and forces for the calculation of the entropy production. Employing average fluxes and forces is in contrast to treating entropy itself as a fluctuating quantity [113, 114]. However, near equilibrium, the statistical average of the fluctuating entropy production rate agrees with the result from the local equilibrium theory when all correlations vanish in the long time limit. The established formula for the entropy production rate $\tilde{\Theta}$ in linear, irreversible thermodynamics is [27, 59]

$$\tilde{\Theta} = \frac{1}{T} 2\eta \tilde{\mathbf{E}} : (\nabla \tilde{\mathbf{u}}) - \frac{1}{T} \sum_i \tilde{\mathbf{j}}_i \nabla \left(\tilde{\mu}_i + \tilde{\psi}_i\right) - \frac{1}{T} \sum_{ri} \left(\tilde{\mu}_i + \tilde{\psi}_i\right) \tilde{\alpha}_{ir}, \tag{4.2}$$

where $\tilde{\alpha}_{ir}$ is the rate at which the reaction with index r changes the concentration of species i. Eq. (4.2) can be derived from a Gibbs relation for the local thermodynamic quantities [27, 132]. A little consideration of the different terms in Eq. (4.2) makes clear that entropy is produced in two distinct ways. First, heat is produced through hydrodynamic dissipation and conversion of potential energy. Second, particle fluxes change the chemical potentials and thereby cause entropy production that is not directly linked to heat. It therefore makes sense to define the heat flux $\tilde{\mathbf{j}}_\mathrm{q}$ as

$$\tilde{\mathbf{j}}_\mathrm{q} \equiv T\tilde{\mathbf{j}}_\Theta + \sum_i \tilde{\mu}_i \tilde{\mathbf{j}}_i. \tag{4.3}$$

The consistency of Eq. (4.3) with the thermodynamic formalism is shown in length, e.g., in [29, 27]. This definition allows to calculate the heat exchange rate $\delta\dot{Q}$ of a closed volume with its environment as

$$\delta\dot{Q} \equiv \int \tilde{\mathbf{j}}_\mathrm{q}\, \mathbf{n}\, \mathrm{d}\tilde{A}. \tag{4.4}$$

The normal $\mathbf{n}$ points into the volume. For thermalized boundaries that are impermeable to flux of matter we have from Eqns. (4.1, 4.3, 4.4)

$$\delta\dot{Q} = \int T\tilde{\mathbf{j}}_\Theta\, \mathbf{n}\mathrm{d}\tilde{A} = \int T\partial_t \tilde{s}\, \mathrm{d}\tilde{V} - \int T\tilde{\Theta}\, \mathrm{d}\tilde{V} \leq \int T\partial_t \tilde{s}\, \mathrm{d}\tilde{V}, \tag{4.5}$$

which is the classical form of the second law of thermodynamics.
Energy balance requires that the heat exchange rate $\delta\dot{Q}$ is balanced by the work rate $\tilde{P}$ and the rate of internal energy change $\mathrm{d}\tilde{E}/\mathrm{d}t$ as

$$\mathrm{d}\tilde{E}/\mathrm{d}t = -\tilde{P} + \delta\dot{Q}. \tag{4.6}$$

4.2 Energy balance of a system with particle exchange

We now consider a system in steady state. The equation for the entropy production rate, Eq. (4.2), contains a contribution from chemical reactions inside the system. Maintaining the steady state implies that the molecules that are modified by a chemical reaction need to be replenished from outside the system. Once a matter flow occurs across the boundaries, Eqns. (4.5, 4.6) do no longer apply and therefore $\delta\dot{Q}$ cannot be calculated. The problem is that the entropy production rate $\tilde{\Theta}$ also contains contributions that do not immediately lead to heat in the system. Diffusion of molecules constantly increases the entropy but the involved statistical motion of the molecules dissipates no energy on average. However, diffusion may still lead to an enhanced energy spending of an external agent who keeps the concentrations at the outer boundaries of the system constant.

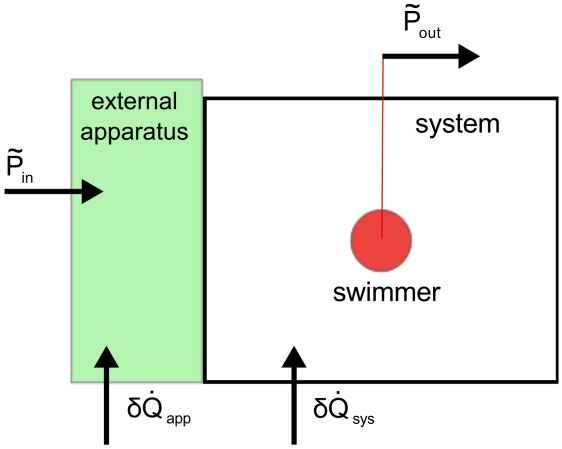

Figure 4.1: Sketch of the idealized model for energy balance.

In order to be able to calculate an estimate for the overall power and heat exchange we suggest to extend the system with an external apparatus that is connected to the system. The total of system and apparatus does not exchange matter but only work and heat with the external world. The apparatus is to maintain the values of the chemical potentials at the outer boundary of the system by replacing the molecules that were converted through the reaction. Inside the apparatus, the molecules are converted back in a reversible, ideal process consuming the power $\tilde{P}_{\text{in}}$. A power output of the system is denoted by $\tilde{P}_{\text{out}}$. We set $\tilde{P}_{\text{out}} > 0$ when the system delivers work and $\tilde{P}_{\text{in}} > 0$ if the apparatus consumes power. $\tilde{P}_{\text{in}}$ is balanced by $\tilde{P}_{\text{out}}$ plus the overall heat outflow from the system and apparatus

$$0 = -\tilde{P}_{\text{out}} + \tilde{P}_{\text{in}} + \delta\dot{Q}_{\text{sys}} + \delta\dot{Q}_{\text{app}}. \tag{4.7}$$

In steady state, Eq. (4.5) can be employed to calculate $\delta\dot{Q}_{\text{sys}} + \delta\dot{Q}_{\text{app}}$ since $\partial_t\tilde{s} = 0$. The

entropy production rate of the system $\tilde{\Theta}_{\mathrm{sys}}$ and of external apparatus $\tilde{\Theta}_{\mathrm{app}}$ yield together

$$\tilde{P}_{\mathrm{in}} = \tilde{P}_{\mathrm{out}} + \int T\tilde{\Theta}_{\mathrm{sys}}\,\mathrm{d}\tilde{V} + \int T\tilde{\Theta}_{\mathrm{app}}\,\mathrm{d}\tilde{V}_{\mathrm{app}} \tag{4.8}$$

Here $\tilde{V}_{\mathrm{app}}$ denotes the volume of the apparatus. Since the external apparatus is ideal, we set $\tilde{\Theta}_{\mathrm{app}} = 0$. However, this does not mean that the apparatus exchanges no heat with the outer world. The reversible nature of the processes in the apparatus allows to equate $\delta\dot{Q}_{\mathrm{app}}$ with the entropy flux between system and apparatus as

$$\delta\dot{Q}_{\mathrm{app}} = \int T\tilde{\mathbf{j}}_{\Theta}\,\mathbf{n}\mathrm{d}\tilde{A}_{\mathrm{app-sys}}, \tag{4.9}$$

with $\mathbf{n}$ pointing from apparatus to system. Eq. (4.9) illustrates that the entropy production in the system that does not directly lead to heat is converted to heat in the external apparatus. The formula (4.8) allows the calculation of the power input for arbitrary reaction rates and model setups. Note however, that the power input is only a lower bound for the energy consumption of an experimental setup since a real external apparatus will operate with $\tilde{\Theta}_{\mathrm{app}} > 0$.

Chapter 5

Efficiency of self-diffusiophoretic swimming

The efficiency of swimming is calculated with the model for self-diffusiophoresis that was introduced in Chap. 3. We first employ the framework for nonequilibrium thermodynamics from Chap. 4 to calculate the energy input and then provide detailed analytical and numerical results for the efficiency.

5.1 Energetic cost of self-diffusiophoresis

Energetically, the active motion considered here is very distinct from classical diffusiophoresis in externally applied concentration gradients. For the latter systems, the absolute level of concentration around the particle changes when it moves in the gradient. In our case, the absolute concentrations remain the same on average. Therefore, self-diffusiophoresis can truly be described with a steady-state model. In the model considered in Chap. 3, no external force acts on the swimmer. Particle swimming is driven by an interaction with a solute of type b via the potential ψ. Besides, we required already in Sec. 1.4.2 that the fluid constituents be very similar as

$$v_\mathrm{a} \simeq v_\mathrm{b} \simeq v_\mathrm{s}, \tag{5.1}$$

$$m_\mathrm{a} \simeq m_\mathrm{b} \simeq m_\mathrm{s}. \tag{5.2}$$

For convenience, we restate the boundary conditions for the fluxes at the swimmer's surface given in Sec. 3.3 as

$$\begin{aligned} \hat{\mathbf{e}}_r \mathbf{j}_\mathrm{b}|_{r=1} &= \varpi(\theta), \\ \hat{\mathbf{e}}_r \mathbf{j}_\mathrm{a}|_{r=1} &= -\hat{\mathbf{e}}_r \mathbf{j}_\mathrm{b}|_{r=1}, \\ \hat{\mathbf{e}}_r \mathbf{j}_\mathrm{s}|_{r=1} &= 0. \end{aligned} \tag{5.3}$$

The entropy production rate in Eq. (4.2) can be simplified for our system. The reaction rate in the volume is replaced by the surface reaction rate $\delta(r-1)\,\varpi(\theta)$ with $\delta(\ldots)$ denoting the Dirac delta function. Upon employing Eqns. (3.10-3.13), we find

$$\begin{aligned}\frac{R^2}{kT\mathcal{C}D}\times T\tilde{\Theta}_{\mathrm{sys}} = &-\mathrm{Pe}\,\mathbf{u}\,\frac{\tilde{c}_{\mathrm{b}}}{\mathcal{C}}\nabla\psi\\ &-(\mathbf{j}_{\mathrm{b}}\nabla\psi+\sum_{\{\mathrm{a,b,s}\}}\mathbf{j}_i\nabla\mu_i)\\ &+\delta(r-1)\,\varpi(\theta)\,(\mu_{\mathrm{a}}-\psi-\mu_{\mathrm{b}})\,.\end{aligned}\tag{5.4}$$

The first line on the right hand side of Eq. (5.4) is the work done by the hydrodynamic body force. Since no external force is applied to the swimmer, it can be identified with hydrodynamic dissipation. For the dilute system near equilibrium it can be rewritten as

$$-\mathbf{u}\,\frac{\tilde{c}_{\mathrm{b}}}{\mathcal{C}}\nabla\psi=-\mathbf{u}\,\left(c_{\mathrm{b}}+\frac{e^{-\psi}}{\xi}\right)\nabla\psi.\tag{5.5}$$

The term $\sim e^{-\psi}$ does not contribute to hydrodynamic dissipation since it expresses a radially symmetric force. This force cannot induce flow due to the incompressibility condition $\nabla\cdot\mathbf{u}=0$. The scaling of the hydrodynamic dissipation $\sim\mathrm{Pe}$ emphasizes an interpretation as convection of b-type solute within the potential ψ. The Peclét number also occurs implicitly in the second and third term of Eq. (5.4) since convection modifies the concentrations and therefore also the chemical potential. Hence, the common neglect of convection in dynamical problems [6] can make a proper energy balance impossible.

To calculate $\tilde{P}_{\mathrm{in}}$ as described in Sec. 4.2, we assume that the chemical potentials μ_{a},μ_{b} and μ_{s} are fixed by the external apparatus at $r\to\infty$. This, together with the assumption of diluteness, implies that the concentrations are held constant at the outer boundaries. Since no external force acts on the swimming particle, the work output of the system vanishes, i.e., $\tilde{P}_{\mathrm{out}}=0$. Inserting the entropy production rate Eq. (5.4) into the expression for the power input Eq. (4.8) and using the diffusion equation (1.18) for the solute of type b, we find

$$\begin{aligned}\frac{1}{kTD\mathcal{C}R}\int T\tilde{\Theta}_{\mathrm{sys}}\mathrm{d}\tilde{V} = &-\int[\nabla\cdot[(\mathbf{j}_{\mathrm{b}}+\mathbf{u}c_{\mathrm{b}})\,\psi]+\sum_{\{\mathrm{a,b,s}\}}\mathbf{j}_i\nabla\mu_i]\,\mathrm{d}V\\ &+\int\varpi(\theta)(\mu_{\mathrm{a}}-\psi-\mu_{\mathrm{b}})\,\mathrm{d}A_{r=1}.\end{aligned}\tag{5.6}$$

Upon using Gauss's theorem for the first term, it becomes clear that the potential ψ only occurs in surface integrals. $\psi(r)$ decays quickly for $r\to\infty$ (see Eq. (3.1)) and the corresponding surface integrals can be neglected. Using Eq. (5.3) leads to a cancellation of surface integrals at $r=1$ containing ψ. We are thus left with

$$\begin{aligned}\frac{1}{kTD\mathcal{C}R}\int T\tilde{\Theta}_{\mathrm{sys}}\mathrm{d}\tilde{V} = &-\int[\mathbf{j}_{\mathrm{b}}\nabla\mu_{\mathrm{b}}+\mathbf{j}_{\mathrm{a}}\nabla\mu_{\mathrm{a}}+\mathbf{j}_{\mathrm{s}}\nabla\mu_{\mathrm{s}}]\,\mathrm{d}V\\ &+\int\varpi(\theta)\,(\mu_{\mathrm{a}}-\mu_{\mathrm{b}})\,\mathrm{d}A_{r=1}.\end{aligned}\tag{5.7}$$

Since we consider a local equilibrium, the Gibbs-Duhem equation can be employed to relate a change of hydrodstatic pressure p_{H} to concentration changes [59] as

$$0 = \sum_i c_i \nabla \mu_i - \nabla p_{\mathrm{H}}. \tag{5.8}$$

Multiplication of Eq. (5.8) by $\mathbf{u}$ and insertion into Eq. (5.7) yields

$$\begin{aligned} \frac{1}{kTD\mathcal{C}R} \int T\tilde{\Theta}_{\mathrm{sys}} \mathrm{d}\tilde{V} =& - \int [\sum_{\{\mathrm{a,b,s}\}} (\mathbf{j}_i + \mathbf{u}c_i) \nabla \mu_i - \mathbf{u} \nabla p_{\mathrm{H}}] \, \mathrm{d}V \\ &+ \int \varpi(\theta) \left(\mu_{\mathrm{a}} - \mu_{\mathrm{b}}\right) \, \mathrm{d}A_{r=1} \\ =& - \int [\sum_{\{\mathrm{a,b,s}\}} \mathbf{J}_i \mu_i - \mathbf{u} p_{\mathrm{H}}] \, \hat{\mathbf{e}}_r \mathrm{d}A_{r=\infty} \\ &+ \int [\sum_{\{\mathrm{a,b,s}\}} \hat{\mathbf{e}}_r \mathbf{j}_i \mu_i + \varpi(\theta) \left(\mu_{\mathrm{a}} - \mu_{\mathrm{b}}\right)] \, \mathrm{d}A_{r=1}, \end{aligned} \tag{5.9}$$

where the diffusion equations and $\nabla \cdot \mathbf{u} = 0$ were used to produce the boundary integrals. Due to the boundary conditions, Eq. (5.3), the last integral in Eq. (5.9) vanishes. Since the swimmer is not subjected to external forces, the fluid flow contains no Stokeslet. With the assumptions in Eqns. (5.1, 5.2) and the incompressibility condition the boundary work of the pressure vanishes $\int \mathbf{u} p_{\mathrm{H}} \, \mathrm{d}A_{r=\infty} \to 0$ and is consequently dropped in Eq. (5.9). The power input becomes

$$\begin{aligned} \tilde{P}_{\mathrm{in}} = \int T\tilde{\Theta}_{\mathrm{sys}} \mathrm{d}\tilde{V} =& - kTD\mathcal{C}R \int \sum_{\{\mathrm{a,b,s}\}} \mathbf{J}_i \mu_i \, \hat{\mathbf{e}}_r \mathrm{d}A_{r=\infty} \\ \approx& kTD\mathcal{C}R \int \mathbf{J}_{\mathrm{b}} \Delta\mu_\infty \hat{\mathbf{e}}_r \mathrm{d}A_{r=\infty}. \end{aligned} \tag{5.10}$$

In the last step, the chemical potential for the dilute a and b solutes from Eq. (3.48) was employed. Note that $\Delta\mu_\infty$ is the chemical potential difference at the outer boundary of the system, not the local chemical potential difference at the reaction site. The power input, Eq. (5.10), equals the free energy exchange between the system and the apparatus. Due to the similarity of masses and sizes of the fluid constituents it does not make a difference whether we consider a fixed pressure at the outer boundaries of the system (Gibbs free energy) or a fixed system size (free energy).

5.2 Definition of the efficiency of swimming

In absence of a real power output, the efficiency of self-diffusiophoresis must be assessed by comparison with some other way of moving. A natural way to do this is to compare the energy dissipation of active swimming with the energy dissipation occurring when the same particle is dragged with constant speed through pure water. The swimming

efficiency is accordingly defined as

$$\begin{aligned}\epsilon \equiv \frac{6\pi\eta R\tilde{U}^2}{\tilde{P}_{\mathrm{in}}} &= \mathrm{Pe}\,\lambda^2 \frac{6\pi\, U^2}{\int \mathbf{J}_{\mathrm{b}}\Delta\mu_\infty\,\hat{\mathbf{e}}_r \mathrm{d}A_{r=\infty}} \\ &= \frac{\mathrm{Pe}}{\xi}\, k_{\mathrm{ba}} e^{-\psi(1)}\lambda^2 \frac{6\pi\, U^2}{\int \mathbf{J}_{\mathrm{b}}\hat{\mathbf{e}}_r \mathrm{d}A_{r=\infty}}.\end{aligned} \tag{5.11}$$

The Peclét number appears through nondimensionalization of the variables. Eq. (3.51) was used to produce the second line. The numerator of Eq. (5.11) is the hydrodynamic dissipation of a passively dragged sphere and the denominator is the power consumption of our external apparatus, providing the energy for active swimming. This definition is a natural extension to Lighthill's formula for hydrodynamic efficiency [73], where only hydrodynamic dissipation is considered in the denominator. The power consumption $\tilde{P}_{\mathrm{in}}$ is bounded from below by the hydrodynamic dissipation $2\eta\int \tilde{\mathbf{E}} : \nabla\tilde{\mathbf{u}}\,\mathrm{d}\tilde{V}$. This statement results formally from Eq. (4.2) with linear force-flux relationships. The hydrodynamic dissipation during active motion is always larger than the dissipation during the dragging of a passive particle in water

$$6\pi\eta R\tilde{U}^2 \leq 2\eta\int \tilde{\mathbf{E}} : \nabla\tilde{\mathbf{u}}\,\mathrm{d}\tilde{V}. \tag{5.12}$$

See Sec. 6.1.3 for a proof of this relation. We therefore always have $\epsilon \leq 1$ as long as no approximation is used to evaluate Eq. (5.11).

5.3 Analytical approximation

In the limit $\lambda \ll 1$ the lowest order boundary layer theory and speed $\tilde{U}_0$, Eq. (3.58), can be employed for the calculation of the efficiency from Eq. (5.11). The result is

$$\epsilon \approx \lambda^2\ \mathrm{Pe}\,\frac{6\pi}{4\pi\, A_b^0\Delta\mu_\infty}\left(\frac{2}{3}A_b^1 K_1\right)^2, \tag{5.13}$$

where the constants A_b^0 and A_b^1 reflect the effect of reaction induced concentration distortion and can be approximated with Eqns. (3.60). The efficiency can be rewritten into a somewhat more intuitive form by making use of the translational diffusion constant of the swimmer

$$D_{\mathrm{S}} \equiv \frac{kT}{6\pi\eta R}, \tag{5.14}$$

to yield from Eq. (5.13)

$$\epsilon \approx \lambda\,\mathcal{C}L^3\,\frac{D_{\mathrm{S}}}{D}\,\frac{kT}{\Delta\tilde{\mu}_\infty}\,\frac{4\pi\,\left(A_b^1 K_1\right)^2}{A_b^0}. \tag{5.15}$$

The first three dimensionless groups in Eq. (5.15) are inherently linked to the mechanism of self-diffusiophoresis and pose a fundamental limit on the magnitude of the efficiency. The

factor $\lambda \mathcal{C} L^3 = \mathcal{C}\, L^4/R$ reduces the efficiency of swimmers with a short interaction length L. It also indicates that increasing the solute concentration can lead to an increase in efficiency. The solute is usually much smaller than the swimmer and therefore $D_\mathrm{S}/D \ll 1$ also reduces the efficiency. The last two factors in Eq. (5.15) depend on the chemical reaction. Their contribution to the efficiency may be optimized by a smart choice of the reaction mechanism. We evaluate Eq. (5.15) by employing the parameters A_b^0, A_b^1 calculated from Eq. (3.56) with $n_\mathrm{max} = 70$. The results agree with numerical solutions for Eq. (5.11) when $\lambda \lesssim 0.01$ (see below). The asymptotic efficiency in Eq. (5.15) is not strictly bounded by unity since taking the limit $\lambda \to 0$ implies neglecting the convection of solutes in the denominator of Eq. (5.11).

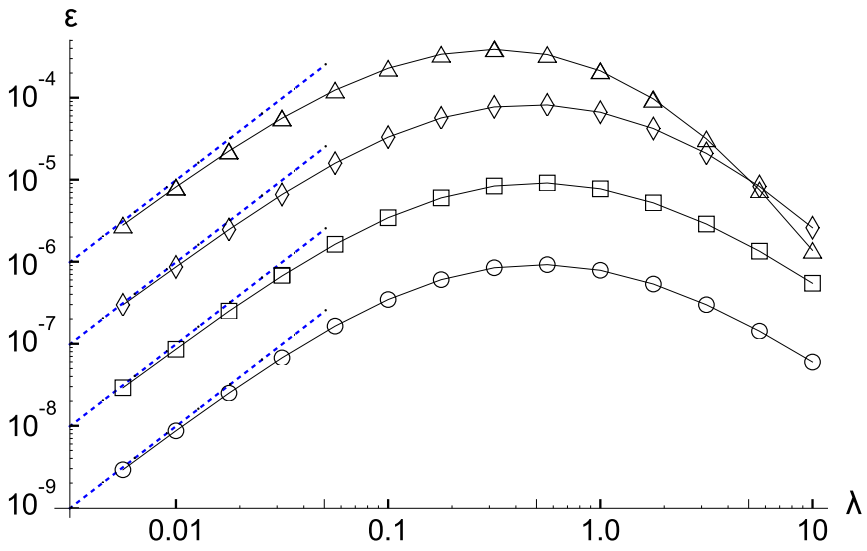

Figure 5.1: The swimming efficiency ϵ as a function of λ with constant Pe/ξ for $\psi(y) = \exp\left[-(r-1)/\lambda\right]$ and $k_\mathrm{ab} = k_\mathrm{ba} = 1$. (Dashed lines) Asymptotic results calculated from Eq. (5.15). ($\triangle$) $\mathrm{Pe}/\xi = 10$. ($\Diamond$) $\mathrm{Pe}/\xi = 1$. ($\square$) $\mathrm{Pe}/\xi = 0.1$. ($\circ$) $\mathrm{Pe}/\xi = 0.01$.

5.4 Numerical results

The full efficiency, Eq. (5.11), is evaluated numerically as done for the swimming speed in Sec. 3.3. An expansion in Legendre polynomials is truncated at $n_\mathrm{max} = 4$. In the linear response theory, numerator and denominator of Eq. (5.11) are both quadratic in $\Delta\mu_\infty$. Therefore, $\Delta\mu_\infty$ does not affect the efficiency in our framework.

The formula for the efficiency in the second line of Eq. (5.11) suggests that $\epsilon \sim \lambda^2\,\mathrm{Pe}/\xi \sim L^4$. As seen in Figs. 5.1 and 5.2, this scaling breaks down for $\lambda \gtrsim 1$. With a fixed Peclét number, $\mathrm{Pe}/\xi > 0$, the swimming efficiency even decreases for $\lambda \gtrsim 1$ (Fig. 5.1). Comparison with Fig. 3.2 shows that the reduction in efficiency is due to the re-

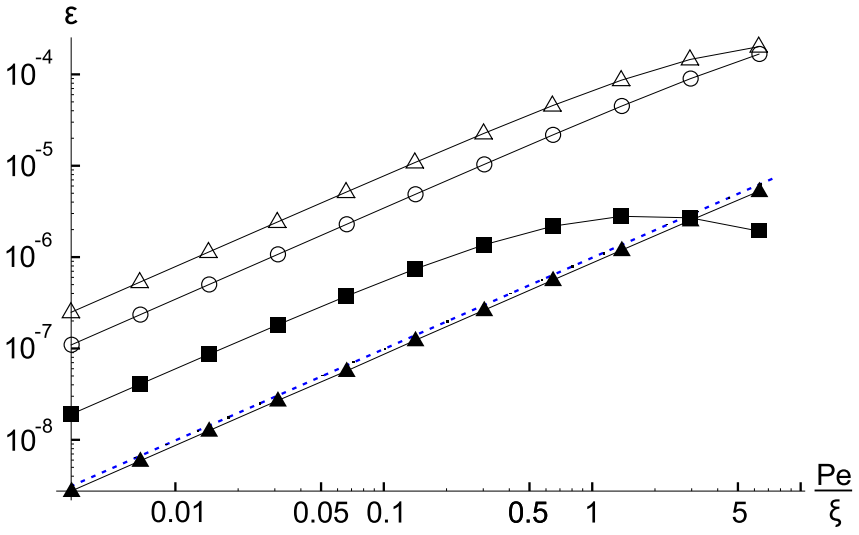

Figure 5.2: The swimming efficiency ϵ as a function of Pe/ξ with constant λ for $\psi(y) = \exp[-(r-1)/\lambda]$, $k_{\mathrm{ab}} = k_{\mathrm{ba}} = 1$. (Dashed line) Asymptotic result for $\lambda = 0.01$ calculated from Eq. (5.15). (■) $\lambda = 10$. (△) $\lambda = 1$. (○) $\lambda = 0.1$. (▲) $\lambda = 0.01$.

duction of swimming speed in this regime. When, for $\lambda \gtrsim 1$, the swimming speed does not increase $\sim \lambda^2$, fixing the Peclét number in Eq. (5.11) introduces a scaling of ϵ with a negative power of λ. As an alternative, one could remove the dependence of Pe on the interaction lengthscale L by setting $\mathrm{Pe}/(\xi\lambda^2) = \text{const}$ for Fig. 5.1. This way of plotting the data would render the decrease of ϵ for $\lambda \gtrsim 1$ less pronounced.

According to Eqns. (1.19, 3.51, 3.52), fixing Pe/ξ and λ implicitly sets an absolute equilibrium concentration scale. Therefore, Fig. 5.2 also suggests that the efficiency of diffusiophoretic swimming increases with the absolute concentration scale for $\lambda \lesssim 1$. Only the asymptotic analytical result for $\lambda = 0.01$ has been plotted in Fig. 5.2 because the curve for $\lambda = 0.1$ already showed significant deviations from the numerical data.

In Fig. 5.3, the dependence of the swimming efficiency on the strength of the interaction potential $\psi(1)$ is plotted. $\psi(1)$ influences both the reaction rate and the swimming speed and therefore it has a nonlinear effect on ϵ. Reaction induced concentration distortion plays an important role for the shape of the curve, in particular for $\psi(1) < 0$ when k_+ can become much larger than unity. For $\psi(1) \to 0$, the swimming efficiency vanishes.

Fig. 5.4 shows the swimming efficiency for fixed equilibrium constant $\tilde{c}_a^{\mathrm{eq}}(\infty)/\tilde{c}_b^{\mathrm{eq}}(\infty)$ and varying reaction rate k_{ba}. For simplicity, we consider here only $\lambda = 0.01 \ll 1$. Due to the truncation of the full numerical solution at Legendre polynomials of the order $n_{\max} = 4$ the error in the numerical data becomes large beyond the plotted range. The reaction induced concentration distortion again explains major features of the plotted curves. For $k_{\mathrm{ba}} \exp(-\psi(1)) \ll 1$ and $k_{\mathrm{ba}} \exp(-\psi(1)) \lesssim \tilde{c}_a^{\mathrm{eq}}(\infty)/\tilde{c}_b^{\mathrm{eq}}(\infty)$ the reaction induced concen-

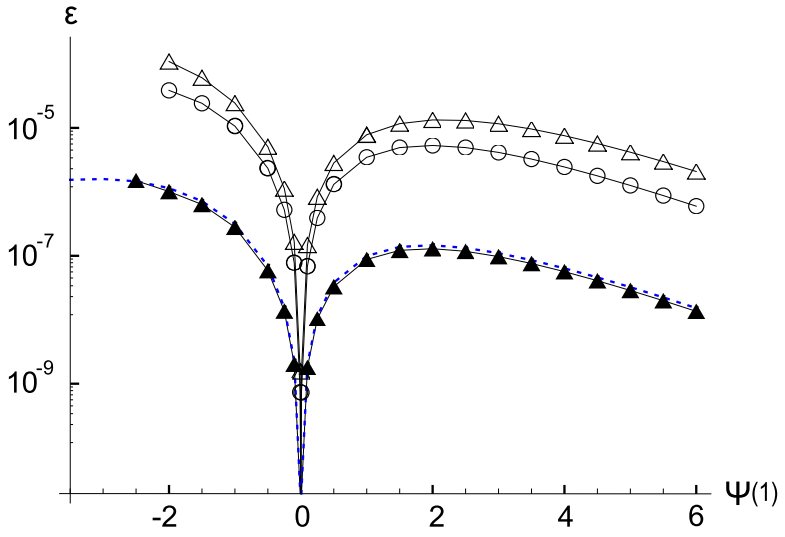

Figure 5.3: Swimming efficiency ϵ vs. the strength of the interaction potential $\psi(1)$, where $\psi(y) = \psi(1)\exp[-(r-1)/\lambda]$, $k_{\rm ab} = k_{\rm ba} = 1$ and $\mathrm{Pe}/\xi = 0.1$. (Dashed line) Asymptotic result for $\lambda = 0.01$ calculated from Eq. (5.15). ($\triangle$) $\lambda = 1$. ($\circ$) $\lambda = 0.1$. ($\blacktriangle$) $\lambda = 0.01$.

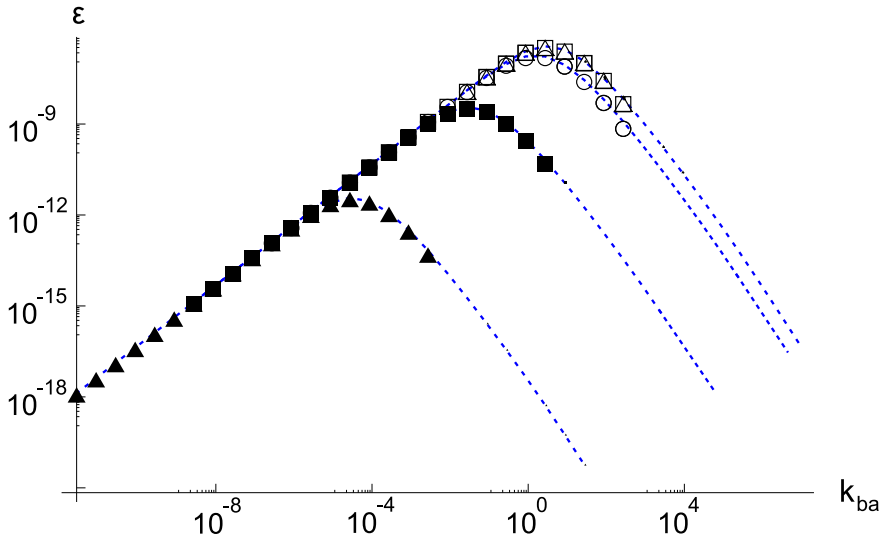

Figure 5.4: Dependence of the swimming efficiency ϵ on the reaction rate constant $k_{\rm ba}$ with fixed equilibrium constant $K_{\rm a} \equiv \tilde{c}_a^{\rm eq}(\infty)/\tilde{c}_b^{\rm eq}(\infty)$ and $\mathrm{Pe}/\xi = 0.1$, $\lambda = 0.01$, $\psi(y) = \exp[-(r-1)/\lambda]$. (Dashed lines) Asymptotic results calculated from Eq. (5.15). ($\blacktriangle$) $K_{\rm a} = 10^{-5}$. ($\blacksquare$) $K_{\rm a} = 10^{-2}$. ($\circ$) $K_{\rm a} = 1$. ($\square$) $K_{\rm a} = 10^{2}$. ($\triangle$) $K_{\rm a} = 10^{5}$.

tration distortion is negligible. Then ϵ rises linearly with $k_{\rm ba}$ and the curves fall onto each other. For larger equilibrium constants with $\tilde{c}_a^{\rm eq}(\infty)/\tilde{c}_b^{\rm eq}(\infty) \gg 10$ the location of the maximum of swimming efficiency becomes independent of the equilibrium constant. On employing Eq. (5.15) we here find the maximum of ϵ at $k_{\rm ba} \simeq 1.13\exp\psi(1)$.

5.5 Discussion

This chapter presents a systematic calculation of the efficiency of an active, phoretic swimmer. We analyze the model for self-diffusiophoresis from Chap. 3. The pertaining framework of irreversible thermodynamics is laid out in Chap. 4. Our model of self-diffusiophoresis comprises three modes of entropy production. Namely, hydrodynamic dissipation, dissipation in the chemical reaction and entropy production through diffusion of solutes. While the dissipative nature of the former two mechanisms is self-evident, the work equivalent of the entropy production through diffusion is not immediately clear. Diffusion only relates to an energetic contribution when considering an external apparatus that maintains the system in steady state. The external apparatus converts free energy change into work and thereby "pays" for the entropy production by diffusion. In Sec. 5.1, we identify the overall power consumption with the free energy exchange at the outer boundaries of the system. This finding contrasts somewhat with the commonly employed formalism for biomolecular motors [88], where the rate of local free energy change is identified with the power input. Our result can be seen as a natural extension of the former theories for a spatially extended driving mechanism.
From a conceptual viewpoint, one must stress the importance of solute convection for energy conservation in our system. For illustration, we picture a situation where the reaction rates are fully independent of the fluid motion. This would mean that the net exchange of solutes with the external apparatus is independent of the motion of the particle. Thus, according to Eq. (5.10), the power input would be independent of the hydrodynamic dissipation and energy conservation would be violated. Within this model, the only way how the particle speed may feed-back on the chemical reaction is via a convective modification of the concentrations.

In Sec. 5.2 we define the efficiency of swimming ϵ. This quantity compares the real power input with the power that would be necessary to drag a passive particle of the same size through water. In Eq. (5.15) we propose a scaling relation for the swimming efficiency as $\epsilon \sim D_\mathrm{S}/D \times L^4\mathcal{C}/R$, which holds for $L \ll R$. The efficiency of experimental catalytic swimmers can be estimated from this formula. For swimmers with size in the $1\,\mu m$ range and solute radii of about 1 Å, we have $D_\mathrm{S}/D \simeq 10^{-4}$ (see Eq. (5.14)). Given a concentration scale [54] of $\mathcal{C} \simeq 10^7\,1/\mu m^3$ and an interaction length of $L \simeq 1\,\mathrm{nm}$ we have $L^4\mathcal{C}/R = 10^{-5}$. Together we find $\epsilon \simeq 10^{-9}$. This number also corresponds to an estimate for the swimmers of Paxton et al. [91], although those are driven by self-electrophoresis. Sec. 5.4 provides detailed numerical results for the efficiency of self-diffusiophoresis. The efficiency has a maximum for $L/R \sim 1$. We also find a nonmonotonous dependence of ϵ on the magnitude of the interaction ψ and on the reaction rates.

In conclusion, we point out that this chapter details the first systematic assessment of

the energetics of active, phoretic motion [107]. We expect that the main relevance of this work lies in the scaling predictions and in the trends demonstrated in the numerical data. It would be highly desirable to compare these results with numerical simulations that go beyond the methodology employed in this thesis.

Chapter 6

General limits on the efficiency

6.1 Hydrodynamic efficiency

Hydrodynamic flow around a microparticle can be generated by a variety of mechanisms. Surface actuations can drive soft objects due to a no-slip boundary condition [73, 118]. In contrast, ciliated microorganisms produce a fluid flow near the surface, leading to an effective slip boundary condition [18]. The latter mechanism is similar to phoretic swimming of a microparticle inasmuch both exhibit a scale separation. In both cases, the lengthscale on which the fluid is driven is much shorter than a typical size of the swimmer. We refer here summarily to surface-near driving mechanisms. Surface-near driving mechanisms can rely on a variety of energy sources and differ accordingly in their thermodynamic description. In principle, their energy balance can be calculated, thus allowing for the computation of efficiencies. However, this approach is often not practical since the governing equations are either nonlinear or partly unknown. Seeking more general predictions for the efficiency of surface-near driving mechanisms, we now leave process-specific details aside. We consider only the hydrodynamic efficiency ϵ_h, which is a common upper bound for the true efficiency ϵ.

6.1.1 Definition of hydrodynamic efficiency

We assume that a constant, externally applied, force $\tilde{\mathbf{F}}_\mathrm{m}$ acts on the swimmer. When working against this force, the system's power output is given by

$$\tilde{P}_\mathrm{out} \equiv -\tilde{\mathbf{U}}\tilde{\mathbf{F}}_\mathrm{m}, \tag{6.1}$$

where the magnitude of the force is to be chosen such that $\tilde{P}_\mathrm{out} > 0$. The (positive) hydrodynamic power input $\tilde{P}_\mathrm{h,in}$ is defined as the sum of power output and hydrodynamic dissipation

$$\tilde{P}_\mathrm{h,in} \equiv -\tilde{\mathbf{U}}\tilde{\mathbf{F}}_\mathrm{m} + 2\eta \int \tilde{\mathbf{E}} : \nabla\tilde{\mathbf{u}}\, \mathrm{d}\tilde{V}. \tag{6.2}$$

Here we also use $\nabla \cdot \tilde{\mathbf{u}} = 0$, which implies, besides incompressibility, that the specific volumes of all fluid constituents are similar. We define the hydrodynamic efficiency as

$$\epsilon_{\mathrm{h}} \equiv \frac{\tilde{P}_{\mathrm{out}}}{\tilde{P}_{\mathrm{h,in}}} = \frac{-\tilde{\mathbf{U}}\tilde{\mathbf{F}}_{\mathrm{m}}}{-\tilde{\mathbf{U}}\tilde{\mathbf{F}}_{\mathrm{m}} + 2\eta \int \tilde{\mathbf{E}} : \nabla\tilde{\mathbf{u}}\, \mathrm{d}\tilde{V}}. \tag{6.3}$$

This efficiency depends on the external force $\tilde{\mathbf{F}}_{\mathrm{m}}$. In order to eliminate this dependence, we choose to use the force at maximum power output

$$\tilde{\mathbf{F}}^{*}_{\mathrm{m}} \equiv \arg\, \max_{\tilde{\mathbf{F}}_{\mathrm{m}}} \tilde{P}_{\mathrm{out}}. \tag{6.4}$$

The hydrodynamic efficiency at maximum power is then defined as

$$\epsilon^{*}_{\mathrm{h}} \equiv \epsilon_{\mathrm{h}}\big|_{\tilde{\mathbf{F}}_{\mathrm{m}}=\tilde{\mathbf{F}}^{*}_{\mathrm{m}}}. \tag{6.5}$$

6.1.2 Scaling of the efficiency of surface-near driving

A scaling argument for the efficiency can be given in line with the scaling argument for the speed in Sec. 1.1. The thickness of the boundary layer L is to be much smaller than R. First, we estimate the power output $\tilde{P}_{\mathrm{out}}$. The external force in the expression for the power output $-\tilde{\mathbf{U}}\tilde{\mathbf{F}}_{\mathrm{m}}$ demands for the presence of a long ranged Stokeslet [53] and therefore

$$\tilde{P}_{\mathrm{out}} \sim \eta R\, \tilde{U}^2. \tag{6.6}$$

The overall hydrodynamic work rate, $\tilde{P}_{\mathrm{h,in}}$, consists of the hydrodynamic work rate in the outer region and in the boundary layer. The dissipation rate in the outer region scales as $R^3 \times \eta\tilde{U}^2/R^2 \sim \eta R\tilde{U}^2$. The thinness of the boundary layer together with a no-slip condition at the surface of the particle leads to a drastic change of fluid velocity. This leads to large viscous dissipation near the particle. We write for the dissipation rate per volume in the boundary layer $2\eta\, \tilde{\mathbf{E}} : \nabla\tilde{\mathbf{u}} \sim \eta\tilde{U}^2/L^2$. The volume of the boundary layer is approximated with $R^2\, L$. Taken together, we have

$$\tilde{P}_{\mathrm{h,in}} \sim \eta\, \tilde{U}^2\, R^2/L. \tag{6.7}$$

Here, $\tilde{P}_{\mathrm{out}}$ and the dissipation outside the boundary region were dropped because their relative contribution $O(L/R)$. All together, the hydrodynamic efficiency scales to leading order in L/R as

$$\epsilon_{\mathrm{h}} \sim \epsilon^{*}_{\mathrm{h}} \sim L/R. \tag{6.8}$$

This results applies generically to any surface-near driving mechanism with $L \ll R$. Surface-near driving mechanisms are therefore quite inefficient.

6.1.3 Upper bounds on the hydrodynamic efficiency

Above estimate for the hydrodynamic efficiency loses its validity for swimmers where L is comparable to R. To derive a general upper limit for the hydrodynamic dissipation we employ an auxiliary fluid velocity $\tilde{\mathbf{u}}'$. The auxiliary fluid velocity obeys $\nabla \cdot \tilde{\mathbf{u}}' = 0$ and satisfies the Stokes equation as

$$\eta \nabla^2 \tilde{\mathbf{u}}' - \nabla \tilde{p}' = 0. \tag{6.9}$$

The true fluid velocity $\tilde{\mathbf{u}}$ obeys for arbitrary, nonzero body forces

$$\eta \nabla^2 \tilde{\mathbf{u}} - \nabla \tilde{p} \neq 0. \tag{6.10}$$

The boundary conditions for $\tilde{\mathbf{u}}'$ are to be the same as for $\tilde{\mathbf{u}}$, see Eq. (1.28). Starting from the inequality

$$\left(\tilde{\mathbf{E}}' - \tilde{\mathbf{E}}\right) : \left(\tilde{\mathbf{E}}' - \tilde{\mathbf{E}}\right) \geq 0, \tag{6.11}$$

we find that the hydrodynamic work rate is always bounded from below by the power that is necessary to drag a passive particle

$$2\eta \int \tilde{\mathbf{E}} : \nabla \tilde{\mathbf{u}} \, \mathrm{d}\tilde{V} \geq \int \nabla \cdot \left(\tilde{\mathbf{u}} \left[-\tilde{p}'\mathbf{I} + 2\eta \tilde{\mathbf{E}}'\right]\right) \, \mathrm{d}\tilde{V} = \tilde{\mathbf{U}}\mathbf{T}\tilde{\mathbf{U}}. \tag{6.12}$$

See below Eq. (1.32) for a definition of $\mathbf{T}$. Therefore we find from Eq. (6.2) that

$$\tilde{\mathbf{U}}\mathbf{T}\tilde{\mathbf{U}}/\tilde{P}_{\mathrm{h,in}} \leq 1. \tag{6.13}$$

Due to linearity of the Stokes equation, the power output working against an external force can be written as

$$\tilde{P}_{\mathrm{out}} = -\tilde{\mathbf{U}} \left[\mathbf{T}\tilde{\mathbf{U}} + \tilde{\mathcal{F}}\right], \tag{6.14}$$

where $\tilde{\mathcal{F}}$ is a function of the driving forces but independent of the fluid velocity. Explicit expressions for $\tilde{\mathcal{F}}$ are model-dependent. For diffusiophoretic swimming, one might refer, e.g., to Sec. 1.4.4 where Teubner's formula can provide an expression for $\tilde{\mathcal{F}}$. The particle velocity at maximum power output is

$$\tilde{\mathbf{U}}^* = -\mathbf{T}^{-1}\tilde{\mathcal{F}}/2. \tag{6.15}$$

Using $\tilde{\mathbf{U}}^*$ and Eq. (6.12) in Eq. (6.3) yields

$$\epsilon_{\mathrm{h}}^* \leq 1/2. \tag{6.16}$$

Remarkably, this is, in a quite general sense, an upper bound for the efficiency at maximum power of any hydrodynamic motor or swimmer in the Stokes regime. It is formally related to results for heat engines [124] but differs in the definition of efficiency and in that we are dealing with hydrodynamic systems. This bound, together with the scaling relation for the efficiency put forth in Sec. 6.1.2, capture the important features of the hydrodynamic efficiency at maximum power.

6.1.4 Hydrodynamic efficiency of passive phoresis

In order to illustrate the results from the preceding sections we now calculate the hydrodynamic efficiency of passive phoretic motion in externally maintained solute gradients. The model from the introductory part, Sec. 1.5, is directly used to accommodate ionic and nonionic solutes in one framework. Concentrations of ions are denoted by $\tilde{c}_{\mathrm{i},\pm}(r,\theta)$ with diffusion constants $D_\pm$. Due to charge neutrality in the bulk we have $\tilde{c}_{\mathrm{i}}^{\mathrm{bulk}} \equiv c_{\mathrm{i},+}^{\mathrm{bulk}} = c_{\mathrm{i},-}^{\mathrm{bulk}}$. As an alternative, we also consider one nonionic solute whose concentration is denoted by $\tilde{c}_{\mathrm{n}}(r,\theta)$. The externally maintained concentration gradient of ionic or nonionic solutes is modeled by the boundary conditions as

$$\begin{aligned} \hat{\mathbf{e}}_{\mathrm{r}}\,\tilde{\mathbf{j}}_{\{\mathrm{i,n}\}}|_{r=R} &= 0 \\ \left(\nabla\tilde{c}_{\{\mathrm{i,n}\}}\right)|_{r\to\infty} &= \nabla\tilde{c}_{\{\mathrm{i,n}\}}^{\mathrm{bulk}} = \text{const.} \times \hat{\mathbf{e}}_z. \end{aligned} \tag{6.17}$$

The concentration scale is chosen to be the concentration at the origin in absence of a swimmer $\tilde{c}_{\{\mathrm{i,n}\}}^{\mathrm{bulk}}(0)$. We limit our investigation to the linear response regime, where the equilibrium concentration is only slightly perturbed on the lengthscale of the particle

$$R|\nabla\tilde{c}_{\{\mathrm{i,n}\}}^{\mathrm{bulk}}|/\tilde{c}_{\{\mathrm{i,n}\}}^{\mathrm{bulk}}(0) \ll 1. \tag{6.18}$$

The interaction potential is denoted by $\tilde{\psi}$ in both the ionic and nonionic case. In equilibrium, $\tilde{\psi}$ is to be radially symmetric. As in the preceding chapters, we denote the lengthscale of the potental by L. The systems are described by the diffusion equation (1.18), the Stokes equation (1.27), and the boundary conditions (1.28, 1.29, 6.17).

In the case of ionic solutes, $\tilde{\psi}$ is determined by the Poisson-Boltzmann equation (2.10), which reads here

$$\nabla^2\tilde{\psi} = -\frac{4\pi(Ze)^2}{\varepsilon}\left(\tilde{c}_{\mathrm{i},+} - \tilde{c}_{\mathrm{i},-}\right). \tag{6.19}$$

The range of the ionic potential is determined by the Debye length

$$L = \sqrt{\varepsilon kT/\left[8\pi(Ze)^2 c_{\mathrm{i}}^{\mathrm{bulk}}(0)\right]}. \tag{6.20}$$

See the paragraph around Eq. (2.11) for the definition of the constants occurring in the Debye length. For electrolytes, the imposed concentration gradient can lead to an electric field in the bulk if the diffusion coefficients of the solutes are different. Since the electric current in the bulk vanishes, we require

$$0 = \tilde{\mathbf{j}}_{\mathrm{i},+}^{\mathrm{bulk}} - \tilde{\mathbf{j}}_{\mathrm{i},-}^{\mathrm{bulk}} = -D_+\left(\nabla\tilde{c}_{\mathrm{i},+}^{\mathrm{bulk}} + \frac{\tilde{c}_{\mathrm{i},+}^{\mathrm{bulk}}}{kT}\nabla\tilde{\psi}^{\mathrm{bulk}}\right) + D_-\left(\nabla\tilde{c}_{\mathrm{i},-}^{\mathrm{bulk}} - \frac{\tilde{c}_{\mathrm{i},-}^{\mathrm{bulk}}}{kT}\nabla\tilde{\psi}^{\mathrm{bulk}}\right). \tag{6.21}$$

The electric field in the bulk then follows as

$$\nabla\tilde{\psi}^{\mathrm{bulk}} = -kT\nu\nabla\ln\tilde{c}_{\mathrm{i}}^{\mathrm{bulk}}, \tag{6.22}$$

with reduced diffusion constant

$$\nu \equiv (D_+ - D_-)/(D_+ + D_-). \tag{6.23}$$

Boundary layer theory

As a prerequisite for the calculation of the efficiency, we first present the formula for the swimming speed put forth by Anderson and Prieve [6, 96]. The fluid velocity in the boundary layer is calculated in Sec. 1.5.1 to lowest order in L/R. We set $\Psi = (\tilde{\psi} - \tilde{\psi}^{\mathrm{bulk}})/kT$ and denote the concentrations at the outer periphery of the boundary layer with $\tilde{c}^{\infty}_{\{\mathrm{i,\,n}\}}(\theta)$. It follows from the assumption of linear response, Eq. (6.18), that Ψ is the equilibrium potential that is assumed to be radially symmetric. For nonionic solutes we define

$$f_{\mathrm{n}}(y) \equiv \left[e^{-\Psi} - 1\right], \tag{6.24}$$

while for ionic solutes

$$f_{\mathrm{i}}(y) \equiv \left[e^{-\Psi} + e^{\Psi} - 2\right] + \nu \left[e^{\Psi} - e^{-\Psi}\right]. \tag{6.25}$$

with $y = (\tilde{r} - R)/L$. Using these definitions along with Eq. (6.22) to rewrite the speed in the boundary layer given in Eq. (1.44) leads to

$$\tilde{u}_{\theta}(y,\theta) \approx -\frac{kTL^2}{\eta} \int_0^y \int_{y'}^{\infty} f_{\{\mathrm{i,\,n}\}}(y'')dy''dy' \frac{\partial_{\theta}\tilde{c}^{\infty}_{\{\mathrm{i,n}\}}(\theta)}{R}. \tag{6.26}$$

The slip velocity at the interface between the boundary layer and the outer flow was defined in Sec. 1.5.1 as $\tilde{\mathbf{u}}_{\mathrm{S}}(\theta) \equiv \hat{\mathbf{e}}_{\theta}\tilde{u}_{\theta}(y,\theta)|_{y\to\infty}$. The particle speed is

$$\tilde{U} \approx \frac{\tilde{F}_{\mathrm{m}}}{6\pi\eta R} + \frac{1}{2}\int_0^{\pi} \tilde{u}_{\mathrm{s}}(\theta)\sin^2\theta\,\mathrm{d}\theta = \frac{\tilde{F}_{\mathrm{m}}}{6\pi\eta R} + \frac{\tilde{\Xi}_1}{3}. \tag{6.27}$$

The expression $\tilde{\Xi}_1/3$ is simply the average of the slip velocity over the surface of the sphere. Upon maximizing the power output $\tilde{P}_{\mathrm{out}} = -\tilde{U}\tilde{F}_{\mathrm{m}}$ we find $\tilde{F}^{*}_{\mathrm{m}} = -\eta\pi R\tilde{\Xi}_1$. $\tilde{F}^{*}_{\mathrm{m}}$ is half the stall force at which no swimming occurs. The formula for the maximum power output is

$$\tilde{P}^{*}_{\mathrm{o}} = \frac{\pi\eta R\,\tilde{\Xi}_1^2}{6} = \frac{3\pi(kT)^2}{8R\eta}\left[L^2\int_0^{\infty} y f_{\{\mathrm{i,\,n}\}}(y)\mathrm{d}y\right]^2\left(\int_0^{\pi}\partial_{\theta}\tilde{c}^{\infty}_{\{\mathrm{i,n}\}}(\theta)\sin^2\theta\,\mathrm{d}\theta\right)^2. \tag{6.28}$$

We now calculate the hydrodynamic work rate $\tilde{P}_{\mathrm{h,in}}$. Inside the boundary layer we have

$$2\eta\int \tilde{\mathbf{E}}:\tilde{\mathbf{E}}\mathrm{d}\tilde{V}_{\mathrm{inner}} \approx 2\pi\eta\frac{R^2}{L}\int_0^{\infty}\int_0^{\pi}\left(\partial_y\tilde{u}_{\theta}(y)\right)^2\sin\theta\,\mathrm{d}\theta\,\mathrm{d}y \tag{6.29}$$

to lowest order in L/R. Insertion of the speed in the boundary layer (6.26) yields

$$2\eta\int \tilde{\mathbf{E}}:\tilde{\mathbf{E}}\mathrm{d}\tilde{V}_{\mathrm{inner}} \approx \frac{2\pi(kT)^2}{\eta}\int_0^{\pi}\left(\partial_{\theta}\tilde{c}^{\infty}_{\{\mathrm{i,n}\}}(\theta)\right)^2\sin\theta\,\mathrm{d}\theta\; I_{\mathrm{h}}, \tag{6.30}$$

where the integral I_{h} is defined as

$$I_{\mathrm{h}} \equiv L^3\int_0^{\infty}\left[\int_y^{\infty} f_{\{\mathrm{i,\,n}\}}(y')\mathrm{d}y'\right]^2\mathrm{d}y = L^3\,2\int_0^{\infty} f_{\{\mathrm{i,\,n}\}}(y)\int_0^{y} y' f_{\{\mathrm{i,\,n}\}}(y')\mathrm{d}y'\mathrm{d}y. \tag{6.31}$$

Partial integration was used to produce the latter formula. For the evaluation of the dissipation rate in the outer volume we use the identity $2\tilde{\mathbf{E}} : \tilde{\mathbf{E}} = (\nabla \times \tilde{\mathbf{u}})^2 + 2\,(\nabla\tilde{\mathbf{u}}) : (\nabla\tilde{\mathbf{u}})$, where $\nabla \times \tilde{\mathbf{u}}$ is the vorticity of the fluid. The dissipation in the outer region is given by

$$2\eta \int \tilde{\mathbf{E}} : \tilde{\mathbf{E}}\, \mathrm{d}\tilde{V}_{\mathrm{outer}} = \eta \int (\nabla \times \tilde{\mathbf{u}})^2\, \mathrm{d}\tilde{V}_{\mathrm{outer}} + 2\eta \int (\tilde{\mathbf{u}} \cdot \nabla\tilde{\mathbf{u}})\, \mathbf{n} \mathrm{d}\tilde{A}_{\tilde{r}=\infty}. \tag{6.32}$$

Any solution for the outer velocity field can be evaluated with this formula. In contrast to the power output, the second and higher moments of the slip velocity play a role for the overall dissipation. Explicit expressions for the outer fluid velocity can be found in Sec. 1.5.2. Upon inserting outer fields in Eq. (6.32), we find

$$2\eta \int \tilde{\mathbf{E}} : \tilde{\mathbf{E}}\, \mathrm{d}\tilde{V}_{\mathrm{outer}} \ll 2\eta \int \tilde{\mathbf{E}} : \tilde{\mathbf{E}}\, \mathrm{d}\tilde{V}_{\mathrm{inner}}, \tag{6.33}$$

since the left hand side is $\sim L^4/R$ while the right hand side is $\sim L^3$. We hence neglect the work in the outer region. The result for the hydrodynamic efficiency at maximum power, Eq. (6.5), becomes

$$\epsilon_{\mathrm{h}}^* \approx \frac{9\left[\int_0^\pi \partial_\theta \tilde{c}^{\infty}_{\{\mathrm{i,n}\}}(\theta) \sin^2\theta\, \mathrm{d}\theta\right]^2}{32 \int_0^\pi [\partial_\theta \tilde{c}^{\infty}_{\{\mathrm{i,n}\}}(\theta)]^2 \sin\theta\, \mathrm{d}\theta} \frac{L_{\mathrm{D}}}{R}, \tag{6.34}$$

where we have defined a dissipation length as

$$L_{\mathrm{D}} \equiv L \frac{\left[\int_0^\infty y f_{\{\mathrm{i,n}\}}(y) \mathrm{d}y\right]^2}{3 \int_0^\infty f_{\{\mathrm{i,n}\}}(y) \int_0^y y' f_{\{\mathrm{i,n}\}}(y') \mathrm{d}y' \mathrm{d}y}. \tag{6.35}$$

The dissipation length L_{D} is a measure for the radial extension of the layer where velocity gradients are strong. It is expected to be similar to the thickness of the layer where the fluid is driven by the body forces. For the considered ionic solution, L_{D} can be explicitly calculated with the boundary layer theory. We obtain here

$$L_{\mathrm{D}} \approx L\, \frac{\left[\ln(1-\gamma_w^2) + \frac{\nu\Psi(R)}{4}\right]^2}{3\left[\frac{\gamma_w^2 + \nu\gamma_w(2+\nu\gamma_w)}{(1-\gamma_w^2)} + \ln(1-\gamma_w^2) + \frac{\nu\Psi(R)}{4}\right]} \sim L, \tag{6.36}$$

where $\Psi(R) = (\tilde{\psi}(R,\theta) - \tilde{\psi}^{\mathrm{bulk}}(R,\theta))/kT$ is the constant equilibrium value of the potential on the surface of the particle and we define $\gamma_w \equiv \tanh(\Psi(R)/4)$.
In the case of nonionic solutes, the expression for L_{D} depends on the specific choice of $\tilde{\psi}$. We find for a hard-core repulsion $\Psi(y) = \Theta(L-y)$ as well as for $\Psi(y) = (L/y)^n$ with $n \to \infty$ and $L \ll R$ that $L_{\mathrm{D}} = L/2$. Together, the results from this section demonstrate that the boundary layer theory supports the scaling arguments for the hydrodynamic efficiency given in Eq. (6.8). In the following section we present numerical results that go beyond the boundary layer theory.

Numerical analysis

In order to extend our analysis to nanoparticles where $L \gtrsim R$ we solve the Eqns. (1.27, 1.18) with the boundary conditions Eqns. (1.28, 1.29, 6.17). For nonionic solutes we directly solve the equations after choosing a radially symmetric potential $\tilde{\psi}(r)$. Solute convection is fully neglected for simplicity.

In the case of ionic solutes we also solve the Poisson-Boltzmann equation (6.19). Here we employ a "Debye-Hückel" theory for concentration-gradient driven motion of weakly charged particles. Details of this theory can be found in [63]. The charge density on the particle $\tilde{q}$ is used as small parameter in the form $q \equiv 4\pi Ze\tilde{q}L\,(\varepsilon\, kT)^{-1} \ll 1$. Nonlinearities in the differential equations are avoided by a systematic expansion up to q^2. The results of this procedure are semi-analytical and can be directly employed to evaluate the formula (6.3) for the hydrodynamic efficiency.

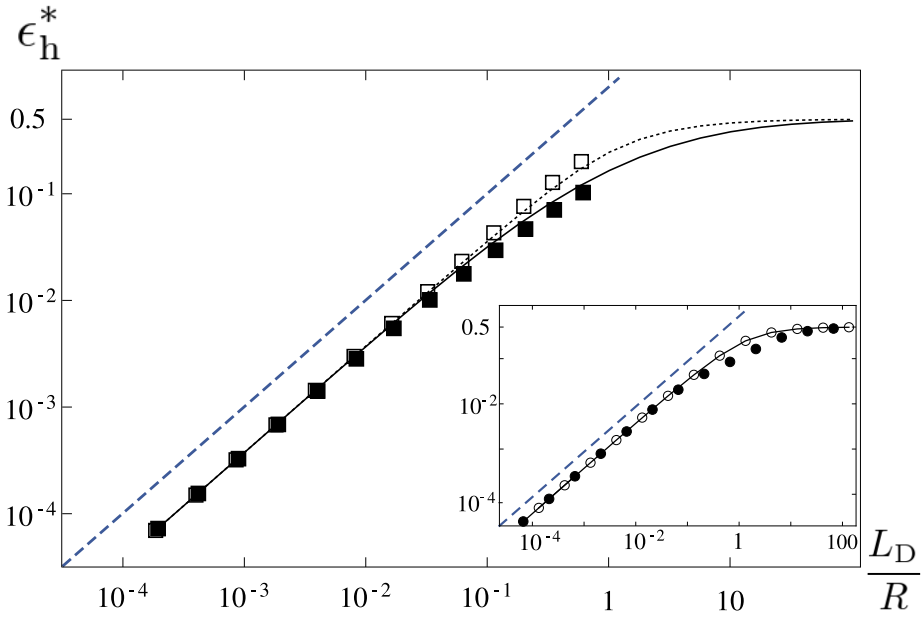

Figure 6.1: Efficiency at maximum power ϵ_h^* for diffusiophoresis in nonionic solutes. (□): Van der Waals attraction $\tilde{\psi}(y) = -16/9\ kT\, a^3R^3y^{-3}(y+2R)^{-3}$ where a is the solute radius. $a/R = [10^{-4}\ldots 1]$ and attraction is truncated at $y = a$. Concentration gradient is established externally. (■): Same potential as before but concentration gradient is produced by an active particle described in Sec. 3.2 with a solute emission rate $\sim (1+\cos\theta)$, Eq. (3.15). (· · · · · ·): Generic repulsion $\tilde{\psi}(y) = kT\,\exp(-y/l)$ with $l/R = [10^{-4}\ldots 10^2]$. Concentration gradient is established externally. (——): Same potential as before but concentration gradient is produced by the active particle from Sec. 3.2. Inset: diffusiophoresis in an externally established gradient of ionic solutes and $\kappa^{-1}/R = [10^{-4}\ldots 10^2]$. (• • •): $q = 0.1$, $\nu = 0$. (○ ○ ○): $q = -0.5$, $\nu = 10$. (——): $q = 0.1$, $\nu = 1$.

The calculated efficiency at maximum power $\epsilon_{\rm h}^*$ is displayed in Fig. 6.1. Note that $\epsilon_{\rm h}^*$ is independent of η and $(\nabla c_i)\,|_{r\to\infty}$. The absolute concentration level enters $\epsilon_{\rm h}^*$ only for ionic solutes via the Debye length. For $L_{\rm D} \lesssim R$ we find good agreement of the numerical results with the boundary layer theory where Eq. (6.34) predicts $\epsilon_{\rm h}^* = (3/8)\,L_{\rm D}$ since the concentrations are linear in $\cos\theta$. For $L_{\rm D} > R$ the efficiencies of nanoswimmers are actually in the range of the upper bound given by 1/2. The deviations from the analytical predictions are most pronounced in the intermediate regime of $L_{\rm D} \simeq R$. The results for ionic solutes are shown in the inset of Fig. 2.3. The results for ionic solutes are obviously quite similar to those for diffusiophoresis in a nonionic solute. However, it is interesting to note that the efficiency is larger when the two solutes have different mobilities $\nu \neq 0$. According to Eq. (6.22), we then have an electric field in the bulk. Thus, electrophoresis in the diffusion-generated electric field can enhance the hydrodynamic efficiency.

Hydrodynamic efficiency and slip boundary conditions

The boundary layer theory for the efficiency can be straightforwardly extended for finite hydrodynamic slip. We revert to the brief calculation in Sec. 1.5.3 for a single nonionic solute. The maximum power output is found to be

$$\tilde{P}_{\rm out}^* \approx \frac{3\pi\eta R}{8}\left(\frac{kT\,L^2}{\eta\,R}\left[\int_0^\infty y f_{\rm n}(y)dy + \frac{b}{L}\int_0^\infty f_{\rm n}(y)dy\right]\right)^2\left(\int_0^\pi \partial_\theta \tilde{c}_{\rm n}^\infty(\theta)\sin^2\theta\,{\rm d}\theta\right)^2. \tag{6.37}$$

Importantly, we now need to augment the hydrodynamic work rate $\tilde{P}_{\rm h,in}$ from Eq. (6.2) by an extra term taking the friction at the solid-liquid interface into account. The frictional force at the particle surface is $\sim -\Lambda\tilde{u}|_{y=0}$ with a friction coefficient $\Lambda = \eta/b$. This force causes a dissipation given by

$$\int \Lambda\tilde{\mathbf{u}}^2|_{y=0}{\rm d}\tilde{A}_{y=0} \approx b\frac{(kT)^2L^2}{\eta\,R^2}\left(\int_0^\infty y f_{\rm n}(y)dy\right)^2\int\left(\partial_\theta\tilde{c}_{\rm n}^\infty(\theta)\right)^2{\rm d}\tilde{A}_{y=0}. \tag{6.38}$$

The dissipation at the surface, Eq. (6.38), is added to the hydrodynamic work in the boundary layer given in Eq. (6.30). When calculating the hydrodynamic efficiency at maximum power, we again find Eq. (6.34) with a modified dissipation length. The new dissipation length includes the effect of surface slip and reads

$$L_{\rm D,\,slip} = \frac{L\left[\int_0^\infty y f_{\rm n}(y)dy + \frac{b}{L}\int_0^\infty f_{\rm n}(y)dy\right]^2}{3\int_0^\infty f_{\rm n}(y)\int_0^y y' f_{\rm n}(y')dy'dy + \frac{3\,b}{2\,L}\left(\int_0^\infty f_{\rm n}(y)dy\right)^2}. \tag{6.39}$$

Depending on the details of the surface interaction, slip lengths of $b \approx 30\,$nm are achievable [25]. For $b \gg L$, one can approximate $L_{\rm D,\,slip} \approx 2b/3$. Therefore, hydrodynamic slip can strongly affect the hydrodynamic efficiency. However, given that hydrodynamic efficiency is determined by $L_{\rm D,\,slip}/R$, it is hardly expected that one can reach a good hydrodynamic efficiency $\epsilon_{\rm h}$ only through a finite slip length.

In the previous sections of this chapter we have studied how Stokesian hydrodynamics imposes upper bounds on the overall efficiency of swimming. However, if the swimmers are to be employed for active transport of cargo, the randomness of motion of a free swimmer might also limit the efficiency in a very fundamental way. This subject shall be discussed in the following section.

6.2 Efficiency of transport

The notion of efficiency is only meaningful in the context of a well-defined task. The swimming efficiency in Eq. (5.11) is based on the comparison of two quanta of energy dissipation per unit time. In certain practical applications of diffusiophoresis one might prefer other efficiency measures. It is, e.g., interesting to have a measure for the energetic cost of using small swimmers for transport between two locations. In this case it may be appropriate to compare energy dissipation per transport distance, not per time. For concreteness, we think here of a slab geometry which the swimmers are to cross. Thereby, they move from one side at $\tilde{x} = 0$ to the other side at $\tilde{x} = \tilde{X} > 0$. Since the swimmers are

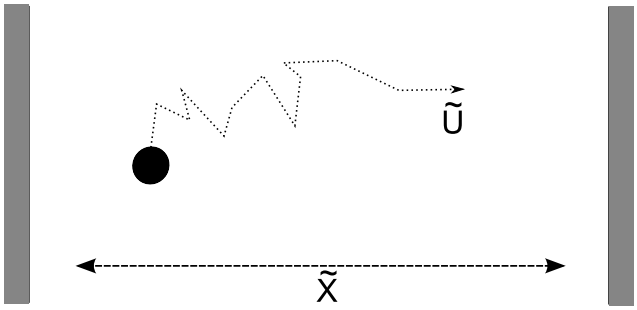

Figure 6.2: Model setup for undirected phoretic transport.

freely suspended, they will not swim straightly but Brownian, translational and rotational, diffusion comes into play. The translational diffusion has a constant $D_{\mathrm{S}} = kT/(6\pi\eta R)$ and the rotational diffusion happens on a timescale $\tau_{\mathrm{rot}} = 8\pi\eta R^3/kT$. For long times $\tilde{t} \gg \tau_{\mathrm{rot}}$, one can employ an effective translational diffusion constant [54, 46, 62, 86] where the effects of random diffusion and active, translational motion are incorporated as $D_{\mathrm{eff}} = D_{\mathrm{S}} + \tilde{U}^2\,\tau_{\mathrm{rot}}/6$. This approach neglects possible modifications of D_{S} and τ_{rot} due to the active processes. In our setup, we expect the transport distance $\tilde{X}$ to be much larger than a characteristic length of the random walk $\tilde{X} \gg D_{\mathrm{eff}}/|\tilde{U}|$. Employing reflecting boundary conditions at $\tilde{x} = 0$, the mean first passage time $\tilde{t}_{\mathrm{mf}}$ to reach $\tilde{x} = \tilde{X}$ is simply given by $\tilde{t}_{\mathrm{mf}} = \tilde{X}^2/(2D_{\mathrm{eff}})$. The energy consumed by the swimmer during the time $\tilde{t}_{\mathrm{mf}}$ can be estimated by $\tilde{P}_{\mathrm{in}}\,\tilde{t}_{\mathrm{mf}}$. For an energetic comparison, one might consider

dragging a passive particle directly across $\tilde{X}$. The corresponding dissipated work would be $6\pi\eta R|\tilde{U}|\,\tilde{X}$. Hence, we define a new efficiency of transport as

$$\epsilon_{\text{transp}} \equiv \frac{6\pi\eta R|\tilde{U}|\,\tilde{X}}{\tilde{P}_{\text{in}}\,\tilde{t}_{\text{mf}}} = \epsilon\,\frac{\tilde{X}}{|\tilde{U}|\,\tilde{t}_{\text{mf}}}, \tag{6.40}$$

which we relate on the right hand side to the efficiency of swimming ϵ through Eq. (5.11). Upon employing the result for the mean first passage time $\tilde{t}_{\text{mf}}$ given in the text above we find

$$\epsilon_{\text{transp}} = \frac{\epsilon}{\tilde{X}}\,\frac{2D_{\text{eff}}}{|\tilde{U}|} = \frac{\epsilon}{\tilde{X}}\left(\frac{2D_{\text{S}}}{|\tilde{U}|} + \frac{|\tilde{U}|\tau_{\text{rot}}}{3}\right). \tag{6.41}$$

This dependence $\sim 1/\tilde{X}$ of the relative energetic cost of direct transport compared to enhanced diffusion is a quite generic result. It emphasizes the necessity to impose a directionality on the active motion if the transport distance is to be of macroscopic size.

6.3 Discussion

The present chapter is dedicated to two mechanisms that generally limit the overall efficiency of active, phoretic transport. Namely, hydrodynamic dissipation and directional randomness of the motion. In Sec. 6.1 we suggest a generic scaling relation for the hydrodynamic efficiency of surface-near driving mechanisms as $\epsilon_{\text{h}} \sim L/R$ [106]. This scaling provides a widely applicable and simple concept to estimate the hydrodynamic efficiency without detailed knowledge of the system. The factor which limits the hydrodynamic efficiency also occurs in the formula for the full efficiency of a self-diffusiophoretic swimmer, Eq. (5.15) in Sec. 5.3. We exemplify the result with detailed analytical and numerical calculations for diffusiophoresis in an externally maintained solute gradient. Numerical calculations demonstrate that phoretic nanoswimmers with $R \gtrsim L$ offer energetic advantages compared to microswimmers. Hydrodynamic dissipation plays a negligible role for their efficiency and they asymptotically attain the maximum possible hydrodynamic efficiency. The concept of a nanoswimmer with $L \gtrsim R$ is much easier realized with ionic solutes where the Debye length can be tuned than with nonionic solutes whose surface interactions are quite complex. A further result of this chapter is a very general scaling prediction for the efficiency of undirected transport. We conclude here that autonomous swimmers can only transport micro-cargo efficiently if they are directed by some means.

Finally, one may ask the question whether the efficiency of small swimmers has a real-world relevance. Purcell famously argued that hydrodynamic efficiency is irrelevant for swimming microorganisms [99, 100]. The lower bound for the hydrodynamic dissipation rate of an organism with $R = 1\,\mu$m and $\tilde{U} = 1\,\mu$m/s is $6\pi\eta R\tilde{U}^2 \simeq 4.5\,kT$/s. This is less than the energy equivalent of a single molecule of ATP ($\simeq 23\,kT$) per second. Even with

a swimming efficiency that is somewhat below 10^{-3}, hydrodynamic dissipation is only a minute fraction of the overall metabolic energy throughput of a microorganism. However, with the emergence of technical applications for phoretic mechanisms, energetic aspects necessarily become relevant because of the sheer number of swimming particles. Furthermore, if a high swimming velocity is to be attained, the quadratic speed dependence of dissipation will also bring energetic viewpoints to attention. A particularly prominent example is the industrial application of electrophoretic or diffusiophoretic deposition [33, 8]. Further applications are displays for electronic devices that are based on the electrophoretic control of colored particles [84]. Since battery lifetime of portable devices, such a e-readers, is limited, the displays are designed to be as efficient as possible. Indeed, we found that genuine nanoparticles [57] or particles with thick Debye layers are employed here [26], which is in accordance with our quantitative results.

Perspectives

Many aspects of the theories presented in this thesis invite a deepened future investigation. A major limitation on predictions for self-electrophoresis (Chap. 2), as well as for self-diffusiophoresis (Chap. 3), is the assumption of dilute solutes. High densities of solutes near the swimmer may change the local viscosity, lead to modified diffusive transport and can cause educt or product inhibition of the chemical reaction. The model of self-electrophoresis studied in Chap. 2 could be improved here in two ways. First, analytical extensions of the boundary layer model could include the surface charge transport. Given that the electric potential of self-electrophoretic swimmers is higher than the thermal voltage, surface transport will almost certainly occur to some extent. In conjunction with this, the adsorption of salt or pollutants to the swimmer surface could be studied in greater detail. Second, a non-linear, Michaelis-Menten-like reaction kinetics can be studied. Usage of this kinetics for models of microswimmers can lead to more reliable predictions of the swimming speed at any concentration of H_2O_2. With regard to self-diffusiophoretic swimmers, it may be difficult to assess the importance of corrections for finite solute density since the solute-swimmer interactions are not well understood. In general, molecular dynamics simulations may offer a compelling alternative to increasingly complicated analytical corrections of the boundary layer theory.
The efficiency in Chap. 5 is calculated for the linear response regime. The assumption of small equilibrium perturbations limits the applicability of our theory. In future work, the condition of linear response could be relaxed in part of the processes, e.g., in the chemical reaction. The framework of irreversible thermodynamics presented in Chap. 4 might still be of use here [68].

Most promising perspectives lie however beyond increasingly detailed studies of the here established models. Active, phoretic motion can also be described in the framework of Langevin equations for the trajectory of the swimmer [110, 112]. Both, the particle position and the self-generated concentration field fluctuate. For small particles, these fluctuations may together influence the average swimming speed and lead to memory effects. An effective description could be derived from the standard framework for fluctuating hydrodynamics and concentrations [64, 46]. The coarse scale of a theory with

Langevin equations for the particle motion prohibits a calculation of the efficiency. However, questions related to the efficiency can still be addressed. For example, the efficiency of transport could be calculated for motion in complex environments. Neglecting some of the details of the phoretic mechanism could also allow to study the thermodynamics of several swimmers with interactions. Here, the long timescales introduced by the mutual interactions call for a modification of the local equilibrium theory.

Bibliography

[1] Website of U.S. Peroxide, LLC. http://www.h2o2.com/technical-library/physical-chemical-properties.

[2] B. Abécassis, C. Cottin-Bizonne, C. Ybert, A. Ajdari, and L. Bocquet. Boosting migration of large particles by solute contrasts. *Nature Mater.*, 7(10):785, 2008.

[3] A. Acrivos and T. D. Taylor. Heat and mass transfer from single spheres in Stokes flow. *Phys. Fluids*, 5:387, 1962.

[4] A. Ajdari and L. Bocquet. Giant amplification of interfacially driven transport by hydrodynamic slip: diffusio-osmosis and beyond. *Phys. Rev. Lett.*, 96(18):186102, 2006.

[5] J. L. Anderson. Transport mechanisms of biological colloids. *Ann. New York Acad. Sci.*, 469(1):166, 1986.

[6] J. L. Anderson. Colloid transport by interfacial forces. *Annu. Rev. Fluid Mech.*, 21(1):61, 1989.

[7] J. L. Anderson, M. E. Lowell, and D. C. Prieve. Motion of a particle generated by chemical gradients. Part 1. Non-electrolytes. *J. Fluid Mech.*, 117:107, 1982.

[8] J. L. Anderson and D. C. Prieve. Diffusiophoresis: migration of colloidal particles in gradients of solute concentration. *Sep. Purif. Methods*, 13(1):67, 1984.

[9] J. L. Anderson and D. C. Prieve. Diffusiophoresis caused by gradients of strongly adsorbing solutes. *Langmuir*, 7(2):403, 1991.

[10] J. E. Avron, O. Gat, and O. Kenneth. Optimal swimming at low Reynolds numbers. *Phys. Rev. Lett.*, 93(18):186001, 2004.

[11] S. Balasubramanian, D. Kagan, C.M. Jack Hu, S. Campuzano, M. J. Lobo-Castañon, N. Lim, D. Y. Kang, M. Zimmerman, L. Zhang, and J. Wang. Micromachine-enabled capture and isolation of cancer cells in complex media. *Angew. Chem. Int. Ed.*, 50(18):4161, 2011.

[12] L. Baraban, M. Tasinkevych, M. N. Popescu, S. Sanchez, S. Dietrich, and O. G. Schmidt. Transport of cargo by catalytic janus micro-motors. *Soft Matter*, 8:48, 2012.

[13] R. J. Bearman and J. G. Kirkwood. Statistical mechanics of transport processes. XI. equations of transport in multicomponent systems. *J. Chem. Phys.*, 28:136, 1958.

[14] J. Bialké, T. Speck, and H. Löwen. Crystallization in a dense suspension of self-propelled particles. *Phys. Rev. Lett.*, 108:168301, 2012.

[15] G. Bianchi, F. Mazza, and T. Mussini. Catalytic decomposition of acid hydrogen peroxide solutions on platinum, iridium, palladium and gold surfaces. *Electrochim. Acta*, 7(4):457, 1962.

[16] P. M. Biesheuvel, M. Van Soestbergen, and M. Z. Bazant. Imposed currents in galvanic cells. *Electrochim. Acta*, 54(21):4857, 2009.

[17] J. J. Bikerman. Electrokinetic equations and surface conductance. A survey of the diffuse double layer theory of colloidal solutions. *Trans. Faraday Soc.*, 35(0):154, 1940.

[18] J. R. Blake. A spherical envelope approach to ciliary propulsion. *J. Fluid Mech.*, 46(1):199, 1971.

[19] A. Bonnefont, F. Argoul, and M. Z. Bazant. Analysis of diffuse-layer effects on time-dependent interfacial kinetics. *J. Electroanal. Chem.*, 500(1-2):52, 2001.

[20] J. P. Boyd. *Chebyshev and Fourier spectral methods*. Dover publications, 2001.

[21] C. Brennen and H. Winet. Fluid mechanics of propulsion by cilia and flagella. *Annu. Rev. Fluid Mech.*, 9(1):339, 1977.

[22] W. R. Browne and B. L. Feringa. Making molecular machines work. *Nat. Nanotechnol.*, 1(1):25, 2006.

[23] F. Carrique and E. Ruiz-Reina. Effects of water dissociation and CO_2 contamination on the electrophoretic mobility of a spherical particle in aqueous salt-free concentrated suspensions. *J. Phys. Chem. B*, 113(25):8613, 2009.

[24] K. T. Chu and M. Z. Bazant. Nonlinear electrochemical relaxation around conductors. *Phys. Rev. E*, 74(1):011501, 2006.

[25] C. Cottin-Bizonne, B. Cross, A. Steinberger, and E. Charlaix. Boundary slip on smooth hydrophobic surfaces: intrinsic effects and possible artifacts. *Phys. Rev. Lett.*, 94(5):56102, 2005.

[26] A.L. Dalisa. Electrophoretic display technology. *IEEE Trans. Electron Devices*, 24(7):827, 1977.

[27] S. R. De Groot and P. Mazur. *Non-equilibrium thermodynamics*. Dover publications, 1984.

[28] A. V. Delgado, F. Gonzalez-Caballero, R. J. Hunter, L. K. Koopal, and J. Lyklema. Measurement and interpretation of electrokinetic phenomena. *Pure Appl. Chem.*, 77(10):1753, 2005.

[29] Y. Demirel and S. I. Sandler. Nonequilibrium thermodynamics in engineering and science. *J. Phys. Chem. B*, 108(1):31, 2004.

[30] U. K. Demirok, R. Laocharoensuk, K. M. Manesh, and J. Wang. Ultrafast catalytic alloy nanomotors. *Angew. Chem. Int. Ed.*, 47(48):9349, 2008.

[31] P. Dhar, T. M. Fischer, Y. Wang, T. E. Mallouk, W. F. Paxton, and A. Sen. Autonomously moving nanorods at a viscous interface. *Nano Lett.*, 6(1):66, 2006.

[32] J. K. G. Dhont. *An introduction to dynamics of colloids*. Elsevier Science, 1996.

[33] J. H. Dickerson and A. R. Boccaccini. *Electrophoretic deposition of nanomaterials*. Springer Verlag, 2011.

[34] S. S. Dukhin, E. Matijevic, and B. V. Derjaguin. *Surface and colloid science: electrokinetic phenomena*, volume 7. Wiley-Insterscience, 1974.

[35] S. Ebbens, R. A. L. Jones, A. J. Ryan, R. Golestanian, and J. R. Howse. Self-assembled autonomous runners and tumblers. *Phys. Rev. E*, 82(1):015304, 2010.

[36] S. Ebbens, A. Sadeghi, J. Howse, R. Golestanian, and R. Jones. Controlling phoretic swimmer trajectory. *MRS Proc.*, 1346:726, 2011.

[37] S. Ebbens, M. H. Tu, J. R. Howse, and R. Golestanian. Size dependence of the propulsion velocity for catalytic janus-sphere swimmers. *Phys. Rev. E*, 85(2):020401, 2012.

[38] S. J. Ebbens and J. R. Howse. In pursuit of propulsion at the nanoscale. *Soft Matter*, 6(4):726, 2010.

[39] S.J. Ebbens and J.R. Howse. Direct observation of the direction of motion for spherical catalytic swimmers. *Langmuir*, 27(20):12293, 2011.

[40] J. Elgeti and G. Gompper. Self-propelled rods near surfaces. *EPL*, 85:38002, 2009.

[41] A. Erbe, M. Zientara, L. Baraban, C. Kreidler, and P. Leiderer. Various driving mechanisms for generating motion of colloidal particles. *J. Phys.: Condens. Matter*, 20:404215, 2008.

[42] B. U. Felderhof. Dynamics of pressure propulsion of a sphere in a viscous compressible fluid. *J. Chem. Phys.*, 133:064903, 2010.

[43] S. Fournier-Bidoz, A. C. Arsenault, I. Manners, and G. A. Ozin. Synthetic self-propelled nanorotors. *Chem. Commun.*, 4:441, 2005.

[44] J. G. Gibbs and Y. P. Zhao. Autonomously motile catalytic nanomotors by bubble propulsion. *Appl. Phys. Lett.*, 94:163104, 2009.

[45] P. Glansdorff and I. Prigogine. *Thermodynamic theory of structure, stability and fluctuations*. Wiley-Interscience, 1971.

[46] R. Golestanian. Anomalous diffusion of symmetric and asymmetric active colloids. *Phys. Rev. Lett.*, 102(18):188305, 2009.

[47] R. Golestanian, T. B. Liverpool, and A. Ajdari. Propulsion of a molecular machine by asymmetric distribution of reaction products. *Phys. Rev. Lett.*, 94(22):220801, 2005.

[48] D. C. Grahame. Differential capacity of mercury in aqueous sodium fluoride solutions I. effect of concentration at 25°. *J. Am. Chem. Soc.*, 76(19):4819, 1954.

[49] I. Gyarmati, É. Gyarmati, and W. F. Heinz. *Non-equilibrium thermodynamics*. Springer Verlag, 1970.

[50] S. B. Hall, E. A. Khudaish, and A. L. Hart. Electrochemical oxidation of hydrogen peroxide at platinum electrodes. Part I. An adsorption-controlled mechanism. *Electrochim. Acta*, 43(5-6):579, 1997.

[51] S. B. Hall, E. A. Khudaish, and A. L. Hart. Electrochemical oxidation of hydrogen peroxide at platinum electrodes. Part II: effect of potential. *Electrochim. Acta*, 43(14-15):2015, 1998.

[52] M. M. Hanczyc, T. Toyota, T. Ikegami, N. Packard, and T. Sugawara. Fatty acid chemistry at the oil-water interface: self-propelled oil droplets. *J. Am. Chem. Soc.*, 129(30):9386, 2007.

[53] J. Happel and H. Brenner. *Low Reynolds number hydrodynamics*. Martinus Nijhoff, 1983.

[54] J. R. Howse, R. A. L. Jones, A. J. Ryan, T. Gough, R. Vafabakhsh, and R. Golestanian. Self-motile colloidal particles: from directed propulsion to random walk. *Phys. Rev. Lett.*, 99(4):48102, 2007.

[55] R. J. Hunter. *Foundations of colloid science*. Clarendon press, 1987.

[56] R. F. Ismagilov, A. Schwartz, N. Bowden, and G. M. Whitesides. Autonomous movement and self-assembly. *Angew. Chem. Int. Ed.*, 41(4):652, 2002.

[57] J. M. Jacobson, P. S. Drzaic, and I. D. Morrison. Electrophoretic displays using nanoparticles, 2001. US Patent 6,323,989.

[58] F. Jülicher, A. Ajdari, and J. Prost. Modeling molecular motors. *Rev. Mod. Phys.*, 69(4):1269, 1997.

[59] F. Jülicher and J. Prost. Generic theory of colloidal transport. *Eur. Phys. J. E*, 29(1):27, 2009.

[60] D. Kagan, S. Balasubramanian, and J. Wang. Chemically triggered swarming of gold microparticles. *Angew. Chem. Int. Ed.*, 50(2):503, 2011.

[61] E. R. Kay, D. A. Leigh, and F. Zerbetto. Synthetic molecular motors and mechanical machines. *Angew. Chem. Int. Ed.*, 46(1-2):72, 2007.

[62] H. Ke, S. Ye, R. L. Carroll, and K. Showalter. Motion analysis of self-propelled Pt-silica particles in hydrogen peroxide solutions. *J. Phys. Chem. A*, 114(17):5462, 2010.

[63] H. J. Keh and Y. K. Wei. Diffusiophoretic mobility of spherical particles at low potential and arbitrary double-layer thickness. *Langmuir*, 16(12):5289, 2000.

[64] J. Keizer. *Statistical thermodynamics of nonequilibrium processes*. Springer Verlag, 1987.

[65] M. J. Kim and K. S. Breuer. Use of bacterial carpets to enhance mixing in microfluidic systems. *J. Fluids Eng.*, 129:319, 2007.

[66] T. R. Kline, W. F. Paxton, T.E. Mallouk, and A. Sen. Catalytic nanomotors: remote-controlled autonomous movement of striped metallic nanorods. *Angew. Chem.*, 117(5):754, 2005.

[67] G. V. Kolmakov, V. V. Yashin, S. P. Levitan, and A. C. Balazs. Designing communicating colonies of biomimetic microcapsules. *Proc. Nat. Acad. Sci.*, 107(28):12417, 2010.

[68] D. K. Kondepudi and I. Prigogine. *From heat engines to dissipative structures*. John Wiley & Son, 2004.

[69] P. E. Lammert, J. Prost, and R. Bruinsma. Ion drive for vesicles and cells. *J. Theor. Biol.*, 178(4):387, 1996.

[70] R. Laocharoensuk, J. Burdick, and J. Wang. Carbon-nanotube-induced acceleration of catalytic nanomotors. *ACS nano*, 2(5):1069, 2008.

[71] E. Lauga and T. R. Powers. The hydrodynamics of swimming microorganisms. *Rep. Progr. Phys.*, 72:096601, 2009.

[72] A. Leewenhoeck. An abstract of a letter from Mr. Anthony Leewenhoeck at Delft, Dated Sep. 17. 1683. *Phil. Trans.*, 14(155-166):568.

[73] M. J. Lighthill. On the squirming motion of nearly spherical deformable bodies through liquids at very small Reynolds numbers. *Commun. Pure Appl. Math.*, 5(2):109, 1952.

[74] C. S. Mangelsdorf and L. R. White. Effects of stern-layer conductance on electrokinetic transport properties of colloidal particles. *J. Chem. Soc., Faraday Trans.*, 86(16):2859, 1990.

[75] N. Mano and A. Heller. Bioelectrochemical propulsion. *J. Am. Chem. Soc.*, 127(33):11574, 2005.

[76] G. Miño, T. E. Mallouk, T. Darnige, M. Hoyos, J. Dauchet, J. Dunstan, R. Soto, Y. Wang, A. Rousselet, and E. Clement. Enhanced diffusion due to active swimmers at a solid surface. *Phys. Rev. Lett.*, 106:048102, 2011.

[77] P. Mitchell. Hypothetical thermokinetic and electrokinetic mechanisms of locomotion in micro-organisms. 25:32, 1956.

[78] J. L. Moran and J. D. Posner. Electrokinetic locomotion due to reaction-induced charge auto-electrophoresis. *J. Fluid Mech.*, 680:31, 2011.

[79] J. L. Moran, P. M. Wheat, and J. D. Posner. Locomotion of electrocatalytic nanomotors due to reaction induced charge autoelectrophoresis. *Phys. Rev. E*, 81(6):065302, 2010.

[80] Y. Mukouyama, H. Hommura, S. Nakanishi, T. Nishimura, H. Konishi, and Y. Nakato. Mechanism and simulation of electrochemical current oscillations observed in the H_2O_2-reduction reaction on platinum electrodes in acidic solutions. *Bull. Chem. Soc. Jpn*, 72(6):1247, 1999.

[81] J. S. Newman and K. E. Thomas-Alyea. *Electrochemical systems*. Wiley-Interscience, 2004.

[82] R. W. O'Brien and L. R. White. Electrophoretic mobility of a spherical colloidal particle. *J. Chem. Soc. Faraday Trans. 2*, 74:1607, 1978.

[83] L. Onsager. Reciprocal relations in irreversible processes. i. *Phys. Rev.*, 37(4):405, 1931.

[84] I. Ota. Electrophoretic image reproduction process, 1975. US Patent 3,892,568.

[85] G. A. Ozin, I. Manners, S. Fournier-Bidoz, and A. Arsenault. Dream nanomachines. *Adv. Mater.*, 17(24):3011, 2005.

[86] J. Palacci, C. Cottin-Bizonne, C. Ybert, and L. Bocquet. Sedimentation and effective temperature of active colloidal suspensions. *Phys. Rev. Lett.*, 105(8):88304, 2010.

[87] D. Pantarotto, W. R. Browne, and B. L. Feringa. Autonomous propulsion of carbon nanotubes powered by a multienzyme ensemble. *Chemical Communications*, (13):1533, 2008.

[88] A. Parmeggiani, F. Jülicher, A. Ajdari, and J. Prost. Energy transduction of isothermal ratchets: generic aspects and specific examples close to and far from equilibrium. *Phys. Rev. E*, 60(2):2127, 1999.

[89] W. F. Paxton, P. T. Baker, T. R. Kline, Y. Wang, T. E. Mallouk, and A. Sen. Catalytically induced electrokinetics for motors and micropumps. *J. Am. Chem. Soc.*, 128(46):14881, 2006.

[90] W. F. Paxton, K. C. Kistler, C. C. Olmeda, A. Sen, S. K. St. Angelo, Y. Cao, T. E. Mallouk, P. E. Lammert, and V. H. Crespi. Catalytic nanomotors: autonomous movement of striped nanorods. *J. Am. Chem. Soc.*, 126(41):13424, 2004.

[91] W. F. Paxton, A. Sen, and T. E. Mallouk. Motility of catalytic nanoparticles through self-generated forces. *Chem. Eur. J.*, 11(22):6462, 2005.

[92] W. F. Paxton, S. Sundararajan, T. E. Mallouk, and A. Sen. Chemical locomotion. *Angew. Chem. Int. Ed.*, 45(33):5420, 2006.

[93] T. P. Pitta and H. C. Berg. Self-electrophoresis is not the mechanism for motility in swimming cyanobacteria. *J. Bacteriol.*, 177(19):5701, 1995.

[94] M. N. Popescu, S. Dietrich, and G. Oshanin. Confinement effects on diffusiophoretic self-propellers. *J. Chem. Phys.*, 130:194702, 2009.

[95] C. Pozrikidis. *Fluid dynamics: theory, computation, and numerical simulation.* Springer Verlag, 2009.

[96] D. C. Prieve, J. L. Anderson, J. P. Ebel, and M. E. Lowell. Motion of a particle generated by chemical gradients. Part 2. Electrolytes. *J. Fluid Mech.*, 148:247, 1984.

[97] D. C. Prieve and R. Roman. Diffusiophoresis of a rigid sphere through a viscous electrolyte solution. *J. Chem. Soc., Faraday Trans. 2*, 83(8):1287, 1987.

[98] I. Prigogine. Time, structure, and fluctuations. *Science*, 201(4358):777, 1978.

[99] E. M. Purcell. Life at low Reynolds number. *Am. J. Phys*, 45(1):3, 1977.

[100] E. M. Purcell. The efficiency of propulsion by a rotating flagellum. *Poc. Nat. Acad. Sci.*, 94(21):11307, 1997.

[101] M. Qian, X. Zhang, R. J. Wilson, and J. Feng. Efficiency of brownian motors in terms of entropy production rate. *Europhys. Lett.*, 84:10014, 2008.

[102] S. Qian and S. W. Joo. Analysis of self-electrophoretic motion of a spherical particle in a nanotube: effect of nonuniform surface charge density. *Langmuir*, 24(9):4778, 2008.

[103] S. Rafaï, L. Jibuti, and P. Peyla. Effective viscosity of microswimmer suspensions. *Phys. Rev. Lett.*, 104(9):98102, 2010.

[104] D. Rings, R. Schachoff, M. Selmke, F. Cichos, and K. Kroy. Hot brownian motion. *Phys. Rev. Lett.*, 105(9):90604, 2010.

[105] G. Rückner and R. Kapral. Chemically powered nanodimers. *Phys.Rev. Lett.*, 98(15):150603, 2007.

[106] B. Sabass and U. Seifert. Efficiency of surface-driven motion: nanoswimmers beat microswimmers. *Phys. Rev. Lett.*, 105(21):218103, 2010.

[107] B. Sabass and U. Seifert. Dynamics and efficiency of a self-propelled, diffusiophoretic swimmer. *J. Chem. Phys.*, 136(6):64508, 2012.

[108] B. Sabass and U. Seifert. Nonlinear, electrocatalytic swimming in the presence of salt. *To appear in J. Chem. Phys.*, 2012.

[109] D. A. Saville. Electrokinetic effects with small particles. *Annu. Rev. Fluid Mech.*, 9(1):321, 1977.

[110] M. Schienbein and H. Gruler. Langevin equation, Fokker-Planck equation and cell migration. *Bull. Math. Biol.*, 55(3):585, 1993.

[111] T. Schmiedl and U. Seifert. Efficiency of molecular motors at maximum power. *Europhys. Lett.*, 83:30005, 2008.

[112] F. Schweitzer. *Brownian agents and active particles: collective dynamics in the natural and social sciences*. Springer Verlag, 2007.

[113] U. Seifert. Stochastic thermodynamics: principles and perspectives. *Eur. Phys. J. B*, 64(3):423, 2008.

[114] K. Sekimoto. *Stochastic energetics*. Springer Verlag, 2010.

[115] A. Sen. Private communication.

[116] D. Shoup, G. Lipari, and A. Szabo. Diffusion-controlled bimolecular reaction rates. The effect of rotational diffusion and orientation constraints. *Biophys. J.*, 36(3):697, 1981.

[117] M. Smoluchowski. *Handbuch der Elektrizität und des Magnetismus. Band II*. Barth-Verlag, 1921.

[118] H. A. Stone and A. D. T. Samuel. Propulsion of microorganisms by surface distortions. *Phys. Rev. Lett.*, 77(19):4102, 1996.

[119] S. Sundararajan, P. E. Lammert, A. W. Zudans, V. H. Crespi, and A. Sen. Catalytic motors for transport of colloidal cargo. *Nano Lett.*, 8(5):1271, 2008.

[120] Y.G. Tao and R. Kapral. Swimming upstream: self-propelled nanodimer motors in a flow. *Soft Matter*, 6(4):756, 2009.

[121] M. Teubner. The motion of charged colloidal particles in electric fields. *J. Chem. Phys.*, 76:5564, 1982.

[122] S. Thakur and R. Kapral. Dynamics of self-propelled nanomotors in chemically active media. *J. Chem. Phys.*, 135:024509, 2011.

[123] S. Thutupalli, R. Seemann, and S. Herminghaus. Swarming behavior of simple model squirmers. *New J. Phys.*, 13:073021, 2011.

[124] C. Van den Broeck. Thermodynamic efficiency at maximum power. *Phys. Rev. Lett.*, 95(19):190602, 2005.

[125] M. Van Dyke. *Perturbation methods in fluid mechanics*. Parabolic press, 1975.

[126] J. Vicario, R. Eelkema, W. R. Browne, A. Meetsma, R. M. La Crois, and B. L. Feringa. Catalytic molecular motors: fuelling autonomous movement by a surface bound synthetic manganese catalase. *Chem. Commun.*, (31):3936, 2005.

[127] G. Volpe, I. Buttinoni, D. Vogt, H. J. Kümmerer, and C. Bechinger. Microswimmers in patterned environments. *Soft Matter*, 7(19):8810, 2011.

[128] K. Šolc and W. H. Stockmayer. Kinetics of diffusion-controlled reaction between chemically asymmetric molecules I. General theory. *J. Chem. Phys.*, 54(7):2981, 1971.

[129] H. Wang and L. Pilon. Accurate simulations of electric double layer capacitance of ultramicroelectrodes. *J. Phys. Chem. C*, 115(33):16711, 2011.

[130] Y. Wang, R. M. Hernandez, D. J. Bartlett Jr, J. M. Bingham, T. R. Kline, A. Sen, and T. E. Mallouk. Bipolar electrochemical mechanism for the propulsion of catalytic nanomotors in hydrogen peroxide solutions. *Langmuir*, 22(25):10451, 2006.

[131] J. B. Waterbury, J. M. Willey, D. G. Franks, F. W. Valois, and S. W. Watson. A cyanobacterium capable of swimming motility. *Science*, 230(4721):74, 1985.

[132] S. Wisniewski, B. Staniszewski, and R. Szymanik. *Thermodynamics of nonequilibrium processes*. D. Reidel Publishing Co., 1976.

[133] Y. Yang, V. Marceau, and G. Gompper. Swarm behavior of self-propelled rods and swimming flagella. *Phys. Rev. E*, 82(3):031904, 2010.

[134] E. Yariv. Electrokinetic self-propulsion by inhomogeneous surface kinetics. *Proc. R. Soc. A*, 467(2130):1645, 2011.

Danksagung

Allen die auf irgendeiner Weise zum Gelingen dieser Arbeit beigetragen haben möchte ich herzlich danken und alles Gute wünschen!

Zunächst gilt mein Dank Herrn Prof. Dr. Udo Seifert für die Aufnahme an seinem Institut zur Verfassung dieser Arbeit. Seine ganz persönliche Begeisterung für Physik und seine intensive Arbeit an theoretischen Fragen schaffen ein wunderbares Arbeitsklima. Ich möchte Udo Seifert auch für das schöne Thema und die Hilfe bei der Ausarbeitung danken.

Herrn Prof. Dr. Christian Holm danke ich für die Übernahme der zweiten Begutachtung der Arbeit trotz schwieriger Umstände.

Anja Steinhauser danke ich für ihre stets gut gelaunte, freundliche Hilfestellung bei administrativen Hürden.

David Abreu, Timo Bihr, Boris Lander, Daniel Schmid und Eva Zimmermann möchte ich für das liebevolle Korrekturlesen dieser Arbeit danken.

Schließlich möchte ich an dieser Stelle meiner Freundin HyoungJu Song mitteilen, wie sehr ich mich über die gemeinsam verbrachte, wunderbare Zeit freue.

Ehrenwörtliche Erklärung

Ich erkläre, dass ich diese Arbeit selbstständig verfasst und keine anderen als die angegebenen Quellen und Hilfmittel benutzt habe.

Stuttgart, 02.05.2012 Benedikt Sabaß